TECHNISCHE UNIVERSITÄT DARMSTADT

Identification and characterization of esterases involved in the conversion of oleosides in *Olea europaea*

Vom Fachbereich Biologie der Technischen Universität Darmstadt

zur Erlangung des akademischen Grades

eines *Doctor rerum naturalium*

genehmigte Dissertation von

M.Sc. Jascha Volk

aus Schwalbach am Taunus

1. Referent: Prof. Dr. Heribert Warzecha

2. Referent: Prof. Dr. Gerhard Thiel

Tag der Einreichung: 06.11.2018

Tag der mündlichen Prüfung: 11.01.2019

Darmstadt 2018

Volk, Jascha: Identification and characterization of esterases involved in the conversion of oleosides in *Olea europaea*

Darmstadt, Technische Universität Darmstadt

Jahr der Veröffentlichung der Dissertation auf TUprints: 2019

Tag der mündlichen Prüfung: 11.01.2019

Für Alessa

Summary

Since the epidemiological long-term survey of the 'Seven Countries Study', olive oil as a health-promoting food has gained increasing attention in pharmacological research. In this context, there was a particular interest in the so-called olive polyphenols, including the secoiridoid derivatives oleocanthal and oleacein, the regular intake of which has been associated with a protective effect against cancer as well as cardiovascular and neurodegenerative diseases. Both substances can be detected in relatively high concentrations in virgin olive oil, whereas they are usually not detectable in intact fruits or leaves. Only upon cell disruption, they are formed from the precursor molecules ligstroside and oleuropein by endogenous β-glucosidases and esterases. This mechanism is part of the plant defense against herbivores and pathogens by generating highly reactive intermediates and reaction products of dialdehydic structure that feature protein-crosslinking and denaturing activities. Despite an increasing interest in the research of these supposedly pharmaceutically active secondary metabolites, little is known about the endogenous enzymes involved in their production.

In addition to the already described oleuropein specific β-glucosidase, OeGLU, three esterases, OeEst030, OeEst228 and OeEst679, from *Olea europaea* acting on deglycosylated oleosides have been identified and characterized. Accordingly, for the first time the enzymatic biotransformation of ligstroside and oleuropein to oleocanthal and oleacein, respectively, was proven using an enzyme mixture. Moreover, two further esterases from *O. europeae*, OeEst391 and OeEst905, were identified which showed no activity against oleosides and their aglycones, but accepted methylated phytohormones as substrates. For all tested olive enzymes esterase activity against the plant hormones methyl jasmonate (MeJA) and methyl indoleacetic acid (MeIAA) was shown. Those results indicate a possible regulatory role of the enzymes in plant hormone signaling and their descent from respective esterases. Moreover, all tested olive esterases were also capable of catalyzing transesterification in the presence of ethanol yielding ethyl jasmonate (EtJA) and ethyl indole-3-acetate (EtIAA), a feature previously not known for plant esterases. The physiological relevance of this activity, however, has not been clarified.

Further investigations focused on the protein structures of OeEst030 and OeEst228. Thus, homology modeling studies suggested that the three-dimensional structures of both proteins show a high similarity to the crystal structure of PNAE and, therefore, supported an assignment to the α/β hydrolase superfamily. Accordingly, it can be assumed that in addition to a core domain consisting of five α helices and six β sheets, there is also a so-called cap domain which regulates the access of substrate to the active site. Furthermore, two of the three supposedly catalytic amino acids, namely serine and histidine, could be localized. The position of the acidic member of the catalytic triad, in

contrast, could not be determined. Initially assumed amino acids could be excluded by appropriate mutagenesis studies.

In summary, three novel esterases could be identified and characterized, expanding our knowledge of oleoside turnover in damaged tissue of *O. europaea*.

Zusammenfassung

Angestoßen durch die Ergebnisse der epidemiologischen Langzeituntersuchung der „Sieben Länder Studie“, ist Olivenöl als gesundheitsförderndes Nahrungsmittel immer mehr in den Fokus pharmakologischer Forschung gerückt. Ein besonderes Interesse galt hierbei den sogenannten Olivenpolyphenolen, darunter die Secoiridoid-Derivate Oleocanthal und Oleacein, deren regelmäßige Einnahme unter anderem mit einer protektiven Wirkung gegenüber Krebs sowie kardiovaskulären und neurodegenerativen Erkrankungen in Verbindung gebracht wird. Beide Substanzen konnten in vergleichsweise hohen Konzentrationen in nativem Olivenöl detektiert werden, während sie in intakten Früchten oder auch Blättern in der Regel nicht nachweisbar sind. Erst während dem Aufschluss der Zellen werden sie durch endogene β-Glukosidasen und Esterasen aus den Vorläufermolekülen Ligstrosid und Oleuropein gebildet. In der Natur dient dieser Mechanismus der Verteidigung der Olivenpflanze vor Fraßfeinden und Pathogenen, da entsprechende Intermediate und Reaktionsprodukte als reaktive Dialdehyde quervernetzende und denaturierende Aktivitäten gegenüber Proteinen aufweisen. Trotz eines steigenden Interesses an der Erforschung dieser vermeintlich pharmazeutisch aktiven Sekundärstoffe ist bisher allerdings wenig über die endogenen Enzyme bekannt, welche an deren Bildung beteiligt sind.

Zusätzlich zu der bereits beschriebenen Oleuropein-spezifischen β-Glukosidase, OeGLU, konnten nun drei Esterasen, OeEst030, OeEst228 und OeEst679, aus *Olea europaea* identifiziert und charakterisiert werden, welche deglykosylierte Oleoside als Substrat akzeptieren. Damit konnte erstmals die enzymatische Biotransformation von Ligstrosid zu Oleocanthal und Oleuropein zu Oleacein mittels eines Enzymgemisches erreicht werden. Ferner konnten zwei weitere Esterasen, OeEst391 und OeEst905, aus *O. europaea* identifiziert werden, welche zwar keine Aktivität gegenüber Oleoside und deren Aglykone zeigten, jedoch methylierte Phytohormone als Substrat akzeptieren. So konnte für alle getesteten Oliven-Enzyme Esterase-Aktivität gegenüber den Pflanzenhormonen Methyljasmonat (MeJA) und Methylindolessigsäure (MeIAA) gezeigt werden. Dies lässt auf eine mögliche regulatorische Rolle der Esterasen in der Pflanzenhormon-Signalkaskade und auf eine evolutionäre Beziehung zu Phytohormon-Esterasen schließen. Weiterhin konnte für alle getesteten Oliven-Esterasen Transesterifizierungsaktivität nachgewiesen werden, wodurch in Anwesenheit Ethanol Ethyljasmonat (EtJA) und Ethylindolessigsäure (EtIAA) gebildet wurden. Hierbei handelt es sich um eine bisher noch nicht für pflanzliche Esterasen beschriebene Eigenschaft, deren physiologische Bedeutung nicht geklärt ist.

Der letzte Abschnitt der Studie widmete sich der Aufklärung der Proteinstrukturen von OeEst030 und OeEst228. So konnten Homologie-Modellierungs-Studien nahelegen, dass die dreidimensionalen

Strukturen beider Proteine eine sehr hohe Ähnlichkeit zur Kristallstruktur von PNAE aufweisen und ermöglichten somit eine Zuordnung zur α/β Hydrolase Superfamilie. Entsprechend kann davon ausgegangen werde, dass neben einer Kerndomäne, bestehend aus fünf α-Helices und sechs β-Faltblättern ebenfalls eine sogenannte „Cap“-Domäne vorhanden ist, welche den Zugang von Substrat zur Bindetasche reguliert. Ferner konnten zwei der drei vermeintlich katalytischen Aminosäuren, nämlich Serin und Histidin, lokalisiert werden. Die Position der sauren Aminosäure der katalytischen Triade konnte trotz umfangreicher Mutagenesestudien hingegen nicht abschließend bestimmt werden.

Insgesamt konnten drei neue Esterasen identifiziert und charakterisiert werden, welche unser Wissen über den Umsatz von Oleosiden in beschädigten Gewebe von *O. europaea* erweitert.

Table of Contents

List of Abbreviations

µg	microgram
µM	mikromolar
µL	microliter
aa	amino acids
AD	Alzheimer's disease
API-ESI	atmospheric pressure ionization - electrospray ionization
BCE	before current era
bp	base pairs
BSA	bovine serum albumin
cDNA	complementary deoxyribonucleic acid
CDS	DNA coding sequence
CHD	coronary heart disease
CI	confidence interval
Cq	quantification cycle
ddH_2O	double distilled water
DMSO	dimethyl sulfoxide
DNA	deoxyribonucleic acid
dNTP	deoxyribonucleoside triphosphate
DW	dry weight
EDTA	ethylenediaminetetraacetic acid
EtIAA	ethyl indole-3-acetic acid
EtJA	ethyl jasmonate
EtOH	ethanol
g	gravitational force
g	gram
GC	gas chromatography
gDNA	genomic deoxyribonucleic acid
h	hours
HPLC	high-performance liquid chromatography
IAA	indole-3-acetic acid
JA	jasmonic acid
Kbp	kilobase pairs
kDa	kilodalton
kg	kilogram
kV	kilovolt

L	liter
LC	liquid chromatography
M	molar
MeIAA	methyl indole-3-acetate
MeJA	methyl jasmonate
MeOH	methanol
MeSA	methyl salicylate
MIA	monoterpene indole alkaloid
mg	miligram
min	minute
mL	mililiter
mM	milimolar
MS	mass spectrometry
MSA	multiple sequence alignment
MUFA	mono-unsaturated fatty acid
nm	nanometer
no	number
NRQ	normalized relative quantity
nt	nucleotide
OD	optical density
OME	oleoside 11-methyl ester
PCR	polymerase chain reaction
pNPA	para-nitrophenyl acetate
pNPB	para-nitrophenyl butyrate
pNPB	para-nitrophenol
Rf	retention factor
RNA	ribonucleic acid
ROO	refined olive oil
RQ	relative quantity
Rt	retention time
RT	room temperature
SA	salicylic acid
SD	standard deviation
sdm	site-directed mutagenesis
SDS-PAGE	sodium dodecyl sulfate - polyacrylamide gel electrophoresis
sec	seconds

seq.	sequence
TLC	thin-layer chromatography
U	unit
V	volt
VOO	virgin olive oil

List of Figures

List of Tables

1. Introduction

1.1. *Olea europaea* – a symbol of the Mediterranean culture

The olive (*Olea europaea* ssp. *europaea* var. *europaea*) is one of the oldest agricultural tree crops worldwide [1]. Even though the onset of its domestication is still controversially debated, a widely accepted view is that the initial habituation took place during the Chalcolithic in the 4th millennium BCE in the northeastern Levant. This single cultivation event was followed by human-mediated spread throughout the Mediterranean Basin and multiple secondary diversifications [2, 3]. The main progenitor of the cultivated olive (*Olea europaea* ssp. *europaea* var. *europaea*), on the other hand, is indisputably the wild Mediterranean olive (*Olea europaea* ssp. *europaea* var. *sylvestris*). However, also the subspecies *laperrinei*, *cuspidata*, *guanchica*, *maroccana* and *cerasiformis* are considered genetic sources in the cultivation process [4]. Nowadays, more than 1,200 different cultivars are described, with the highest diversity found in Italy (538 varieties) [5, 6]. However, the cited number is expected to be a strong underestimation of the actual quantity due to lack of information on minor local cultivars and ecotypes [6, 7].

For thousands of years, the olive has been an important part of the Mediterranean culture. Historically, olive trees have been cultivated both for their wood and fruits used for production of olive oil. Even though the latter was primarily employed as lamp fuel, a wide variety of applications has been documented. Amongst others, the oil was used as an ointment for treating diseases, for the care of skin and hair, to anoint of royalty and warriors and in religious rituals [4, 8]. Its exploitation as a source of food, in contrast, was not the initial motivation of olive oil production. It was not until the beginning of the ancient Roman age that the oil gained in importance from a nutritional point of view [4, 9]. Still, its status as an indispensable staple of the Mediterranean diet has been established only in recent centuries. Although the Mediterranean countries remain the main consumers of olive oil today, a trend towards increased demand worldwide has been observed: between 1995/1996 and 2015/2016, its consumption in Germany and the USA, for example, increased from 16,400 to 62,700 tons per year (+ 382.3 %) and from 101,000 to 321,000 tons per year (+ 317.8 %), respectively. Thus, the global consumption of olive oil grew from 1,888,500 to 2,979,500 tons per year (+ 157.8 %) within the same time span [10].

1.2. The Seven Countries Study – promotion of the Mediterranean diet

In recent decades, the Mediterranean diet, and thus also olive oil as one of its central components, has gained global interest. A cornerstone of this development was the Seven Countries Study initiated in 1947 by the American physiologist Ancel Keys. At the time, a significant increase in

mortality of middle-aged men was observed in the USA, with barely any information as to the reasons. In this context, a prospective study involving 300 subjects (men in executive positions) was initiated. Its long-term objective was to associate differences in lifestyle and behavior with the span of life, or rather, with the risk of mortality. In the following years, Keys and his colleagues managed to establish international collaborations in order to extend the study to other countries [11]. In 1958, the Seven Countries Study was officially launched, with nearly 13,000 male participants aged 40–59 living in the USA, the Netherlands, Finland, Italy, the former Yugoslavia, Greece and Japan [12, 13]. In course of this epidemiological investigation, it emerged that the populations surveyed in the Mediterranean countries, namely Italy and Greece, showed comparably low occurrence of coronary heart diseases (CHD), certain types of cancer and dementia resulting in increased lifespan [14, 15]. It soon became evident that the prevailing dietary habits had to be one of the main reasons for these observations.

The so-called Mediterranean diet is rich in cereal products, legumes, fruits and vegetables with a moderate content of fish. Dairy and meat products, in contrast, represent only its minor part [16, 17]. However, the most outstanding feature of this diet is the use of virgin olive oil (VOO) as the primary source of fat resulting in an increased intake of monounsaturated fatty acids (MUFAs) [18]. The latter characteristic purred the assumption that high consumption of MUFAs, particularly oleic acid, which makes up to 84 % of total fatty acids in VOO [19], was the primary factor contributing to the observed health promoting effects. More recent studies questioned this concept by testing VOO, refined olive oil (ROO) as well as other seed derived oils featuring similar MUFA contents for their protective function against, amongst others, CHD in various clinical examinations. Interestingly, positive effects could be demonstrated only for VOO, while even ROO supplementation did not lead to similar results [20-22]. Thus, the focus of the following research shifted from MUFAs to other components present exclusively in VOO, an unrefined olive oil produced using the cold-pressing method. The crucial minor constituents, which represent up to 2 % of the total VOO weight, encompass more than 230 chemical compounds including, e.g., aliphatic and triterpenic alcohols, sterols, hydrocarbons and phenols [23]. Especially metabolites representative of the latter group have recently been examined for their health-promoting effects.

1.3. Health-promoting effects of olive oil phenols

The array of phenols present in olive oil comprises at least 36 structurally distinct compounds including simple phenols (e.g., tyrosol, hydroxytyrosol and p-coumaric acid), polyphenols (e.g., lignans and flavonols) and secoiridoids [24, 25]. Most of the described health-promoting effects have

been thus far associated with the simple olive phenolic compounds: tyrosol (p-HPEA) and hydroxytyrosol (3,4-DHPEA) as well as their secoiridoid derivatives (e.g., ligstroside and oleuropein).

Positive impact on the cardiovascular system was proven, amongst others, in *in vivo* human studies showing that the consumption of 25-50 mL of phenol-rich VOO per day led to an increase in high-density lipoproteins (HDL) cholesterol levels [20, 26] and a decline of those characteristic of circulating oxidized cholesterol [26, 27]. Both observations were associated with reduction of CHD risk [28, 29]. Furthermore, decreased systolic and diastolic blood pressure values were determined in hypertensive patients after implementation of an olive phenol-enriched diet [20]. Considering the boost in risk of CHD due to high blood pressure, these results suggest a preventive function of VOO [30].

Evidence for anticarcinogenic properties of olive phenols has mainly been supplied by *in vitro* studies, whereas conclusive *in vivo* studies are only available in a limited number. In the latter, however, significant inhibitory effects on the initiation and progression phase of carcinogenesis were proven in various mice models. Hashim *et al.*, for example, showed reduced tumor growth and metastatic deposit in BALB7c scid (SCID, severe combined immunodeficiency) mice harbouring HT115 cells (human adenocarcinoma cells) after treatment with 25 mg of olive phenol extract per kg per day during several weeks [31]. Another experimental set-up demonstrated oleuropein-induced tumor regression in mice with soft tissue sarcomas [32]. In human intervention studies, in contrast, cancer-prevention effects of olive oil phenols could only be indicated so far by reduction of oxidative DNA damage, e.g., in lymphocytes [33] and mitochondrial DNA of mononuclear cells [27].

Furthermore, potential neuroprotective functions of olive oil phenols against several neurodegenerative diseases were demonstrated in *in vivo* experiments focusing on isolated compounds. Feeding the APP/PS1 transgenic mice, representatives of a common Alzheimer's disease (AD) mouse model, with 5 mg of hydroxytyrosol per kg per day over six months, for example, led to improved electroencephalographic (EEG) activity as well as reduced brain inflammation and mitochondrial oxidative stress. Therefore, the authors concluded that hydroxytyrosol could be a functional dietary ingredient in the prevention of AD [34]. Feeding experiments with its derivative, oleuropein aglycone were performed by Grossi *et al.* using another AD mouse model strain, namely TgCRND8. After eight weeks of oleuropein aglycone administration, the transgenic mice showed significantly improved cognitive performance, comparable with that of wild type mice. Analysis of the corresponding brain tissue indicated that the secoiridoid interfered with the *de novo* amyloid-β (Aβ) deposition and, remarkably, assisted disaggregation of existing plaques, thus counteracting one of the main factors of AD pathogenesis [35]. Similar results were obtained when testing the activity of oleocanthal, which represents one of the most abundant secoiridoid derivatives in VOO. Its

administration to a wild-type strain of laboratory mice, for example, resulted in up-regulation of Aβ-degrading enzymes. The metabolite is therefore assumed to exert supporting activity in Aβ clearance from the brain [36].

1.4. Phenols and secoridoids of *O. europaea*

Among secondary plant metabolites, phenols constitute probably the largest and most ubiquitous group of compounds. Even though they encompass a broad variety of chemical structures, all phenols are characterized by the presence of at least one benzene ring with one or more hydroxyl groups. Their physiological functions are diverse, ranging from plant defense mechanisms against pathogens and herbivores through protection against abiotic stress factors (e.g., UV light, drought, etc.) to attracting pollinators and other mutualistic or beneficial organisms. Thus, phenols are compounds that play a key role in any plant's survival in its environment [37, 38].

The most prominent phenols in *O. europaea* are oleoside-type secoiridoids, a class of compounds that is not only abundant but also exclusive to members of the Oleaceae family. Their molecular structure is characterized by the presence of an oleosidic skeleton, particularly represented by oleoside 11-methyl ester and its aglycone, elenolic acid. Complex phenolic compounds, like ligstroside, oleuropein and corresponding aglycones, are derived from those core structures *via* an ester linkage with a phenylethyl alcohol derivative, tyrosol or hydroxytyrosol [39, 40].

Unfortunately, despite the increasing interest in biological activities of the enumerated secoiridoid metabolites, only little is known about their biosynthesis. According to early studies, the biosynthetic pathway leading to oleoside-type secoiridoids is similar to that resulting in their secologanin-derived counterparts [40]. The latter has recently been completely elucidated in *Catharanthus roseus* [41].

1.4.1. Biosynthesis of oleoside-type secoiridoids

Generation of the iridoid scaffold is initiated from geranyl diphosphate *via* synthesis of geraniol by the corresponding enzyme, geraniol synthase (GES; Figure 1) [42]. Further steps include hydroxylation at C8 (carbon in position 8) by geraniol 10-hydroxylase/8-oxidase (G8O) leading to 8-hydroxygeraniol [43], which is then converted by 8-hydroxygeraniol oxidoreductase (8-HGO) to 8-oxogeranial [41], a direct precursor of nepetalactol and its dialdehyde, iridodial. The latter step is accomplished through cyclization of 8-oxogeranial by iridoid synthase (IS) [44]. Both products are further converted by iridoid oxidase (IO) *via* iridotrial into 7-deoxyloganetic acid [42, 45], subsequently glycosylated by glucosyltransferase 7-DLGT (7-deoxylogentic acid-O-glucosyltransferase) [41, 46]. The resulting compound, 7-deoxyloganic acid, constitutes the last

common intermediate in the biosynthesis of various types of secoiridoids. In *O. europaea*, only two of the aforementioned enzymes, OeGES1 [47] and OeISY [48], have been identified so far. However, on the basis of homology studies, candidate genes potentially encoding the remaining catalysts have been proposed [48, 49].

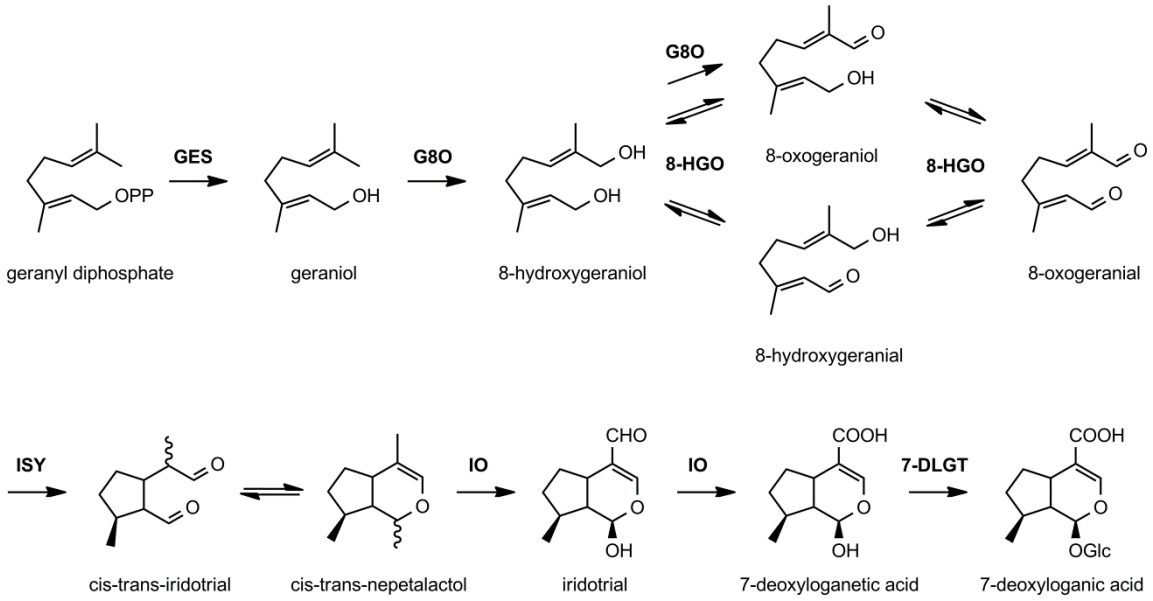

Figure 1: Biosynthesis of 7-deoxyloganic acid in *C. roseus*. The iridoid 7-deoxyloganic acid represents the last common precursor of the biosynthetic routes leading to oleoside-type and secologanin-type secoiridoids. GES, geraniol synthase; G8O, geraniol 10-hydroxylase/8-oxidase; 8-HGO, 8-hydroxygeraniol oxidoreductase; ISY, iridoid synthase; IO, iridoid oxidase; 7-DLGT, 7-deoxyloganetic acid glucosyl transferase.

Even though after generation of 7-deoxyloganic acid the biosynthetic route branches into two different trails leading to either secologanin or oleoside 11-methyl ester (Figure 2), both seem to be analogous. The basis for this conclusion was established in course of hydroponic feeding experiments with labelled precursors in two species of Oleaceae, namely *Syringa josikaea* and *Fraxinus excelsior*. Incorporation studies of the supplemented substrates revealed downstream intermediates in the biosynthesis of the oleoside-type secoiridoid, oleuropein. Consequently, hydroxylation of 7-deoxyloganic acid at C7 was postulated as the consecutive biosynthetic step yielding 7-epi-loganic acid; its subsequent oxidation generating 7-ketologanic acid. The following metabolic reaction, methylation of 7-ketologanic acid, results in 7-ketologanin, a direct precursor of oleoside 11-methyl ester. Conversions of either loganin into secologanin or 7-ketologanin into oleoside 11-methyl ester are expected to be accomplished *via* a similar mechanism. The oxidative ring fissure of 7-ketologanin, however, starts at a higher oxidation level, therefore generating a more oxidized product [40, 50].

Although enzymes acting on the aforementioned substrates have not been characterized yet, corresponding candidate genes were recently identified [48, 49].

Furthermore, the hydroponic feeding studies of Damtoft *et al.* indicated that oleoside 11-methyl ester was first glucosylated, yielding 7-β-1-D-glucosyl-11-methyl oleoside, and then linked to tyrosol *via* esterification. The resulting heterosidic ester of oleoside 11-methyl ester and tyrosol (p-hydroxyphenylethanol; p-DHPEA), known as ligstroside, is consequently the first derivative in the biosynthetic route of oleosides featuring phenolic properties. The assumption that oleuropein, as an ester of oleoside 11-methyl ester and hydroxytyrosol, is generated in course of a similar reaction, however, could not be supported by the aforementioned experiments. Instead, oleuropein was characterized as a hydroxylation product of ligstroside, as indicated by incorporation patterns of the labelled substrate [40, 50].

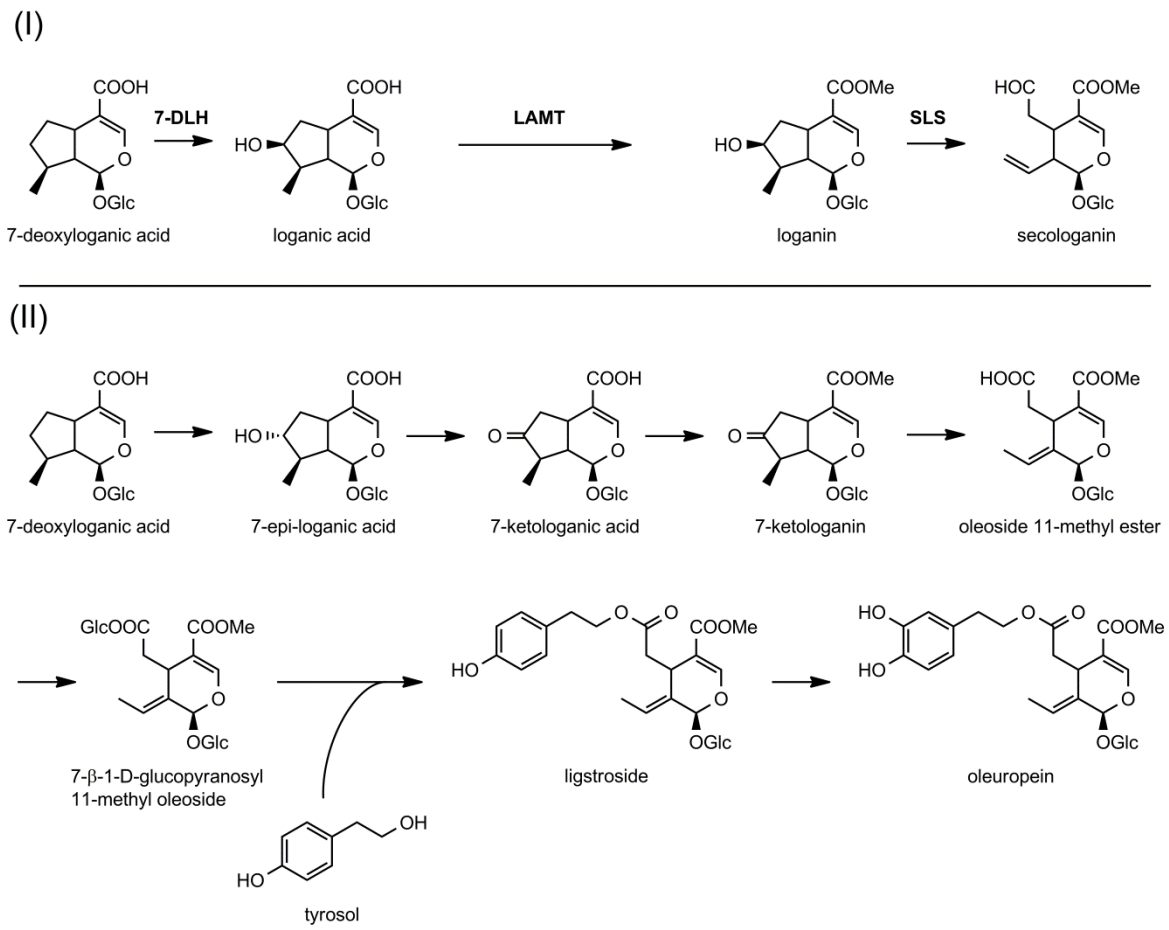

Figure 2: Biosynthesis of secologanin in *C. roseus* (I) in comparison to the proposed oleoside biosynthetic pathway (II). Intermediates in the biosynthesis of oleoside 11-methyl ester as well as oleuropein have been identified in *Fraxinus excelsior* and *Syringa josikaea* by means of hydroponic feeding studies with labelled substrates [40, 50]. 7-DLH, 7-deoxyloganic acid hydrolase; LAMT, loganic acid O-methyltransferase; SLS, secologanin synthase.

1.4.2. Mechanisms of ligstroside and oleuropein degradation

Oleuropein is the most prominent secoiridoid derivative in *O. europaea*, detectable in all types of its tissues. Its concentrations can reach up to 140 mg per g dry weight (DW) in unripe olive fruits [51, 52], 90 mg per g DW in leaves [53], 58 mg per g DW in stems and 6 mg per g DW in roots [54]. While the content of oleuropein declines significantly during fruit maturation, an opposite trend is characteristic of its precursor; ligstroside accumulates in olive fruits reaching its highest concentrations (up to 11.4 mg per g DW) before the drupe color changes to purple-black [55]. Both secoiridoids represent precursors of a series of different degradation products mainly detectable in mature or damaged tissue of *O. europaea*, for example in fruits and accordingly in VOO. In the chemical structure of both metabolites, three bonds that are prone to hydrolytic cleavage can be discerned: the ester bonds, both between the oleoside moiety and the phenylethyl alcohol and between the carboxyl and the methyl group, as well as the glucosidic bond. It, therefore, can be assumed that the endogenous olive enzymes responsible for the degradation of oleuropein and ligstroside belong to the class of esterases and β-glucosidases [56, 57]. Depending on the sequence of the catalysis, the process leads to a wide range of alternative intermediates, or rather hydrolysis products, which differ significantly in their chemical stability (Figure 3) [58, 59].

For some cultivars of *O. europaea*, it has been shown that the decrease in oleuropein content during fruit ripening coincided, amongst others, with accumulation of demethyloleuropein; this led to the hypothesis of demethyloleuropein being a direct degradation product [49, 51]. Also demethylligstroside was detected in ripe fruits of some cultivars; however, measured concentrations were comparably low relative to demethyloleuropein levels (up to 2.5 mg per g DW) and not clearly associated with a decrease in the quantity of ligstroside [55]. In addition to the demethylation, hydrolysis of the ester bond between hydroxytyrosol and oleoside 11-methyl ester is expected to occur in course of oleuropein degradation. Accordingly, the levels of hydroxytyrosol during fruit maturation were observed to follow the trend of accumulation analogous to that of demethyloleuropein [49]. The boost in content of both compounds is further accompanied by a significant increase in total esterase activity within the corresponding tissue, supporting the postulated coexistence of both aforementioned pathways of oleuropein degradation [60, 61].

The most extensively described and well-documented route of oleuropein and ligstroside disintegration, however, starts with their deglycosylation leading to the corresponding aglycones, also known as 3,4-DHPEA-EA and p-HPEA-EA , respectively. Also in this case, the relevant metabolite concentrations in olive fruit tissue were shown to increase during maturation, with their accumulation accompanied by a simultaneous escalation of β-glucosidase activity [62, 63]. The specific β-glucosidase capable of hydrolyzing oleuropein has recently been identified and

characterized [1, 64]. In contrast to the aforementioned degradation products, the aglycones represent highly reactive compounds. Namely, detachment of the stabilizing glucose molecule exposes the labile hemiacetal C1, leading to the opening of the elenolic ring. In case of the oleuropein aglycone, this results in formation of oleuropeindial with its enol and keto (dialdehyde) forms in tautomeric equilibrium [58, 65, 66]. Protein-crosslinking activity of the latter derivatives as well as their relevance in plant defense has been extensively described in literature [64, 66, 67]. Although not explicitly reported, a similar keto-enol tautomerism can be expected of the ligstroside aglycone upon ring opening.

Subjecting ligstroside and oleuropein to a combination of methyl esterase and β-glucosidase activities followed by non-enzymatic decarboxylation yields dialdehydic forms of the respective decarboxymethyl aglycones, oleocanthal and oleacein. Even though degradation products of ligstroside generally appear to amass in significantly lower concentrations compared to those of oleuropein, oleocanthal accumulation is particularly unique in this context. In fruit tissue of *O. europaea* L. cv. Arbequina, for example, oleocanthal concentrations were below 0.6 µmol per g DW (corresponding to around 0.183 mg per g DW) with no significant level changes in samples from a single location in Seville; even lower quantities of the metabolite were recorded in samples from Lleida during fruit maturation. Oleacein, on the other hand, was shown to accumulate in a similar fashion as oleuropein aglycone [62]. Interestingly, the enumerated observations reflect the complete opposite of what Alagna *et al.* have reported for 12 Italian cultivars, wherein a decrease in oleacein levels was recorded during fruit development in all cases [49].

Finally, it should be mentioned that, despite the accumulation of specific phenolic secoiridoid derivatives, total content of phenols declines during olive fruit development. Furthermore, biosynthesis of the enumerated secoiridoid compounds in different tissues of *O. europaea* was shown to strongly depend on several factors, such as the cultivar, region of cultivation, agricultural techniques and maturation phase [24, 68]. The amount of the metabolites of interest in olive oil is also heavily influenced by the method of extraction and processing as well as storage time [24]. In case of VOO, fruits are crushed by mechanical means without refining and application of chemicals. During this procedure, cell compartments are destroyed, resulting in mixing of metabolites and enzymes present in the cells. Since heat and chemicals are not used, the endogenous enzymes remain mostly active, producing a large number of degradation products, including the aforementioned compounds [69]. Interestingly, even though oleocanthal is hardly detectable in intact cells of *O. europaea* it represents together with oleacein one of the most abundant secoiridoid derivatives in VOO, followed by the aglycones of ligstroside and oleuropein. This observation was corroborated by Karkoula *et al.* who analyzed 340 monovarietal Greek and Californian olive oils for

their content of phenols, revealing concentrations of up to 711 mg per kg and 588 mg per kg for oleocanthal and oleacein, respectively [70].

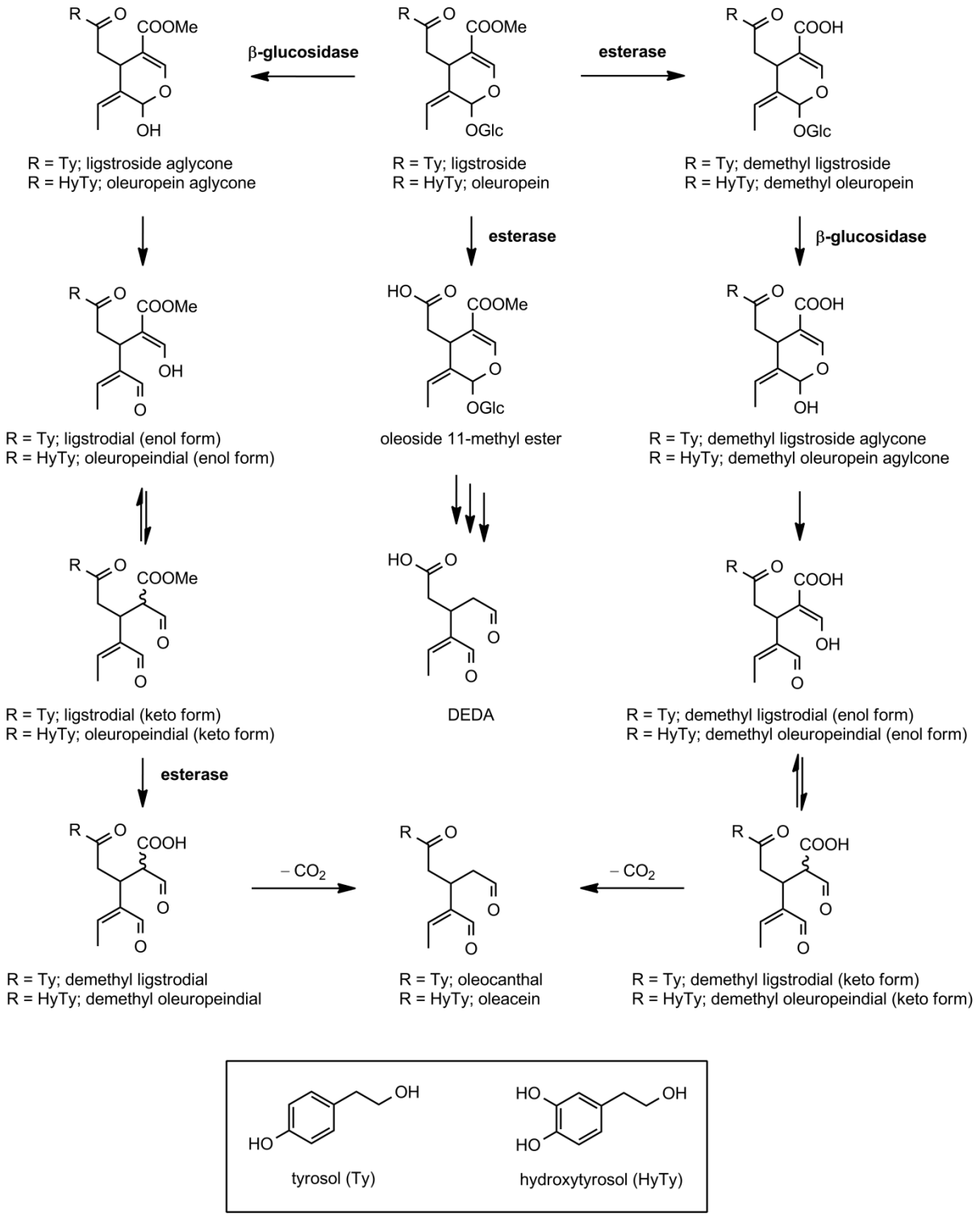

Figure 3: Proposed routes of ligstroside and oleuropein degradation in plants of the Oleaceae family. The scheme illustrates those intermediates that are generated by enzymatic hydrolysis leading to the degradation products oleocanthal, oleacein as well as decarboxymethyl elenolic acid dialdehyde (DEDA).

1.5. Superfamily of α/β hydrolases

The α/β hydrolase superfamily, first described in 1992 [71], represents one of the largest groups of structurally related enzymes featuring a broad range of functions. Even though members of this family are predominantly simple hydrolases, like those esterases expected to be involved in oleoside degradation, it also comprises more unusual hydrolytic enzymes, such as epoxide hydrolases, haloalkane dehalogenases and dienelactone hydrolases, as well as non-catalytic proteins. And yet, all these enzymes, despite divergent evolutionary origins and functionalities, appear to be related, sharing the core α/β fold structure encompassing their catalytic machinery [72].

The initially described, basic canonical fold is composed of an eight-stranded β-sheet with an α-helical connection between each of the six rear strands (Figure 4). The corresponding β-strand order of 1-2-4-3-5-6-7-8 exhibits a left-handed super-helical twist resulting in orthogonal positioning of the first and last β-elements. With the exception of strand β2, all are in parallel orientation. Since its original publication, however, a large number of variations of the basic fold have been documented, leading to the definition of the minimum α/β fold criterion: the presence of at least five β-strands. The plasticity of this superfamily furthermore results from the fact that insertions of a few amino acids up to complete domains can be tolerated while the functionality of the catalytic machinery remains maintained [73].

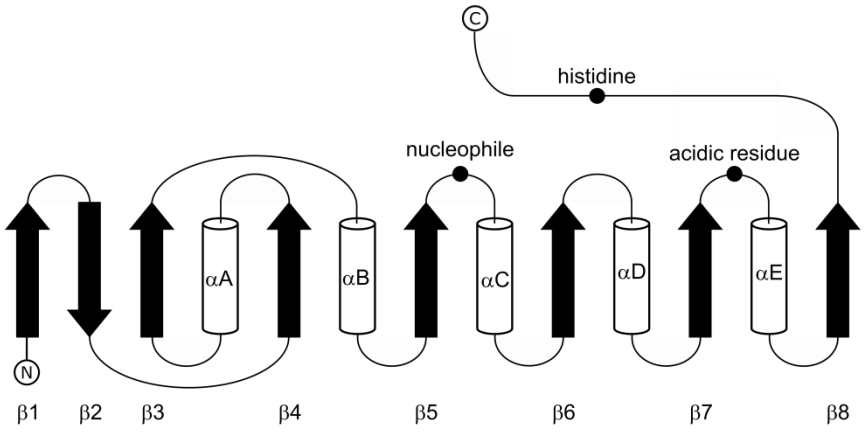

Figure 4: Topology diagram of the two dimensional structure of the canonical α/β hydrolase fold [71]. α-helices and β-strands are illustrated as black arrows and white cylinders, respectively. The relative position of amino acids forming the catalytic triad is highlighted with black dots.

Another key feature of the α/β hydrolase enzymes is the catalytic triad consisting of a nucleophile (usually serine, S), an acid (aspartic, D or glutamic acid, E) and histidine (H). The nucleophile is always located at the top of a very sharp turn (γ-turn) following strand β5, the so-called 'nucleophile elbow', representing the most conserved feature within the superfamily. To sustain the geometry of this turn, it is required that the nucleophile be flanked in positions -2 and +2 by amino acids exhibiting small side-chains, such as glycine (G), often resulting in the consensus sequence G-X-S-X-G (X, any amino acid) [72, 73]. Additionally, Carr *et al.* proposed that the third amino acid following the nucleophile needs to be 'small' to avoid steric hindrance with strand β4 [72]. The nucleophile elbow not only enables positioning of the nucleophile close to the substrate, but also contributes to the formation of the oxy-anion binding hole, which stabilizes the negatively charged transition state that occurs during hydrolysis. The oxy-anion binding site is formed by virtue of hydrogen bonds of two backbone nitrogen atoms, one derived from the amino acid immediately following the nucleophile and the other usually provided by an amino acid positioned between strand β3 and helix αA [72]. The acidic member of the catalytic triad is usually located downstream of strand β7. However, studies on specific bacterial dehalogenases, for example, demonstrated that its positioning following strand β6 is also possible [74-76]. The functional histidine, in contrast, represents a strictly conserved member of the catalytic machinery and is, therefore, always located downstream of strand β8 [72, 73].

1.6. Polyneuridine aldehyde esterase (PNAE)

The biosynthetic pathway leading to ajmaline in *Rauvolfia serpentina* is one of the most studied metabolic trails involving monoterpenoid indole alkaloids (MIAs). This multi-step biosynthesis is particularly interesting due to the structural complexity of ajmaline, generated by an array of enzymes of various classes starting from the precursor molecules, tryptamine and secologanin [77]. A key step in this pathway is the conversion of the monoterpenoid (C10) indole alkaloid, polyneuridine aldehyde into its C9 derivative, 16-epivellosimine (Figure 5). This is accomplished through demethylation of the former into polyneuridine β-aldehydoacid facilitated by the corresponding esterase, polyneuridine aldehyde esterase (PNAE), followed by non-enzymatic decarboxylation yielding 16-epivellosimine [78]. In-depth studies on the catalytic machinery and the crystal structure of PNAE from *R. serpentina* led to its classification as a member of the α/β hydrolase superfamily. Thus, it was shown that its core domain consists of six β-sheets and five flanking α-helices [79], while two additional β-strands and three helices form a 'cap domain' [77]. As common for most representatives of the enzyme family, the catalytic triad is composed of serine, aspartic acid and histidine located at amino acid positions 87, 216 and 244, respectively [79, 80].

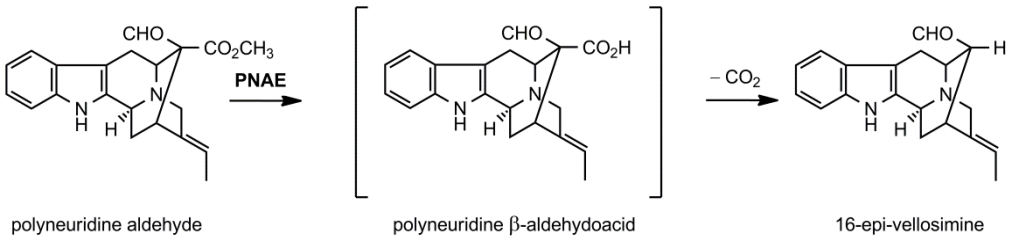

Figure 5: Conversion of polyneuridine aldehyde into epi-vellosimine by PNAE. The enzymatic demethylation yields polyneuridine aldehyde acid, which undergoes spontaneous decarboxylation resulting in 16-epi-vellosimine.

1.7. Aim of the study

In course of the past two decades, many of the health-promoting properties of VOO have been linked to its content of phenols, particularly oleoside-type secoiridoids. Amongst these, the degradation products of ligstroside and oleuropein were identified as target compounds of special interest. The ligstroside-derived oleocantal, for example, is currently being investigated in various model systems of AD for its neuroprotective properties [36, 81]. Despite the increasing number of studies focusing on beneficial activities of these compounds, little is known about the enzymes involved in their production. Neither the pathway of oleuropein biosynthesis nor the degradation routes leading to its derivatives, abundantly present in VOO, are sufficiently elucidated. So far, only one specific β-glucosidase acting on oleuropein has been described in *O. europaea* [64], while enzymes hydrolyzing the ester bonds within the structure remain unknown. Consequently, identification of the relevant olive catalysts is the key to a better understanding of the degradation processes occurring in course of fruit development or during production of VOO.

In this context, the Federal Ministry of Education and Research (BMBF)-funded project, NeurOliv was initiated in 2015. Its aims were: delineation of the metabolite degradation routes, improvement of secoiridoid isolation procedures and evaluation of the biofunctional and metabolic properties of the target compounds in model systems of AD. As part of this overarching project, the hereby presented study was focused on the identification and characterization of esterases involved in the degradation of ligstroside and oleuropein in *O. europaea* leading to the valuable compounds, oleocanthal and oleacein, respectively.

For this purpose, the first step in the undertaken experimental process was screening of the transcriptome of *O. europaea* for candidate esterase genes relying on homology studies using the well-characterized polyneuridine aldehyde esterase (PNAE) as a model enzyme. The identified coding sequences were then to be amplified with gene-specific primers from a cDNA pool of available olive cultivars and introduced into a bacterial cloning system for subsequent expression in *Escherichia coli*.

Resulting protein preparations were to be tested for their esterase activity towards selected oleosides as well as phytohormones. A further characterization of the identified enzymes was to be accomplished by means of homology modelling as well as mutagenesis studies revealing information about corresponding three-dimensional structures and catalytic amino acids. Finally, expression levels of the corresponding genes in callus culture cells and in leaf and fruit tissues of *O. europaea* L. cv. Canino should be analyzed using quantitative polymerase chain reaction (qPCR).

2. Materials and Methods

2.1. Materials

2.1.1. Substrates and analytical standards

substance	supplier	purity	concentration	solvent
ethyl indole-3-acetate	Sigma-Aldrich	99 %	200 mM	EtOH or DMSO
indole-3-acetic acid	Sigma-Aldrich	98 %	200 mM	EtOH or DMSO
jasmonic acid	Duchefa	≥ 95 %	200 mM	EtOH or DMSO
ligstroside	N-Zyme BioTec	≥ 90 %	9.6 mM	ddH_2O
methyl indole-3-acetate	Sigma-Aldrich	≥ 99 %	200 mM	EtOH or DMSO
methyl jasmonate	Sigma-Aldrich	95 %	200 mM	EtOH or DMSO
methyl salicylate	Sigma-Aldrich	≥ 95 %	200 mM	EtOH or DMSO
oleacein	N-Zyme BioTec	81 %	1.25 mM	MeOH
oleocanthal	N-Zyme BioTec	79 %	1.64 mM	30 % (v/v) EtOH
oleuropein	Sigma-Aldrich	≥ 95 %	25 mM	MeOH
oleoside 11-methyl ester	Sigma-Aldrich	> 98 %	25 mM	MeOH
para-nitrophenol	Carl Roth	≥ 95 %	50 mM	DMSO
para-nitrophenyl acetate	Merck	≥ 95 %	50 mM	DMSO
para-nitrophenyl butyrate	Sigma-Aldrich	≥ 95 %	50 mM	DMSO
salicylic acid	Carl Roth	≥ 95 %	200 mM	EtOH
strictosidine	purified from *R. serpentina*	n.d.	15 mM	MeOH

2.1.2. Oligonucleotides

All oligonucleotides were purchased from Eurofins Genomics GmbH (Ebersberg, DE).

no	name	nucleotide sequence 5'-3'
1.	OeEst030_fw	ATGGGAGATAACCAAAAACAGCATCTTGTTC
2.	OeEst030_rv	TTATTTTCCAACAATCTCCAATATATATTTGTAAAGCTCT
3.	OeEst228_fw	ATGGAAGCAAAGCAACAAATGCATTTTGTTCTC
4.	OeEst228_rv	TTATTTTCCAACAATATCCAATATATATTGGCAAAGAGTGTTGG
5.	OeEst391_fw	ATGGAAGAAAAGCAACAGAGGCATTTTGTTC
6.	OeEst391_rv	TTATTTTGCTATATCCAATAAATATTGGCAAAGTGCATGA
7.	OeEst905_fw	ATGGAAGGTGAAAAGAAGCAAATACATTTT
8.	OeEst905_rv	TTAGTTTGCTATTATATCCAATAAACATTGATAAAGTTTT
9.	OeEst030NcoI_fw	CGAGCCATGGGAGATAACCAAAAACAGCATCTTGTTC
10.	OeEst030XhoI_rv	ATACCTCGAGTTATTTTCCAACAATCTCCAATATATATTTGTAAAGCTCT
11.	OeEst228NcoI_fw	TCACCATGGAAGCAAAGCAACAAATGCATTTTG
12.	OeEst228XhoI_rv	ATACCTCGAGTTATTTTCCAACAATATCCAATATATATTGGCAAAGAGTGTTGG GAT
13.	OeEst391NcoI_fw	TTCACCATGGAAGAAAAGCAACAGAGGCATTTTGTTCTCGTGCA
14.	OeEst391HindIII_rv	GCGGTAAGCTTTTATTTTGCTATATCCAATAAATATTGGCAAAGTGCAT
15.	OeEst905NcoI_fw	CGAGCCATGGAAGGTGAAAAGAAGCAAATACATTTT
16.	OeEst905XhoI_rv	ATACCTCGAGTTAGTTTGCTATTATATCCAATAAACATTGATAAAGTTTT
17.	OeEst030sdm_fw	GTATATGCCACGGAGCTTGGTG
18.	OeEst030sdm_rv	CATGTATGAGAACAAGATGCTG
19.	OeEst228sdm_fw	ATGGTATATGCCACGGAGCTTGGTGC
20.	OeEst228sdm_rv	GTACGAGAACAAAGTGCCTTTGTTG
21.	OeEst905sdm_fw	GTGCATGCCACGGATCTTGGT
22.	OeEst905sdm_rv	CATGAACTAGGACAAAATGTATTTG
23.	OeEst030sdmS211A_fw	AGCTGGTGCAGATGAAGCCGAAAATG
24.	OeEst030sdmS211A_rv	ATAATGAAAGCACGCTTTAC
25.	OeEst030sdmE212A_fw	GGTGCATCTGCAGCCGAAAATG
26.	OeEst030sdmE212A_rv	AGCTATAATGAAAGCACGC
27.	OeEst030sdmE214A_fw	TCTGAAGCCGCAAATGATTC
28.	OeEst030sdmE214A_rv	TGCACCAGCTATAATGAAAG
29.	OeEst030sdmD216A_fw	GCCGAAAATGCTTTCTATCGTTG

30.	OeEst030sdmD216A_rv	TTCAGATGCACCAGCTATAATG
31.	predEF1-α_fw	CTTGAGGCCCTTGACCAGATTTC
32.	predEF1-α_rev	TCACTTGACACCCTTCTTGGC
33.	predPP2A_fw	GGTGAAAGTCCTCCATGCAAACAG
34.	predPP2A_rev	CGATATCCATGGCCAGTTCTACGA
35.	qPCREF1-α_fw	AATTTGCCGAGCTCCTGACC
36.	qPCREF1-α_rv	AACACCAACGGCAACAGTCT
37.	qPCR-PP2A_fw	GGATAGGAGGCAACGCTC
38.	qPCR-PP2A_rv	CAGTCTCCACAGAGTAGTATC
39.	qPCROeEst030_fw	GCCTGACACTACAAATCCGC
40.	qPCROeEst030_rv	TGGCCCCTGATAAGTACCGA
41.	qPCROeEst228_fw	TTCGAACACTCAAACCGCAC
42.	qPCROeEst228_rv	GAGCCTGGCCTCACTAAAGT
43.	qPCROeEst905_fw	TTGTTGAGGCCAGGCTCTCT
44.	qPCROeEst905_rv	CCATGTGGTCGGCATCTTCT
45.	OeEst679_fw	ATGGGAGATAACCAAAAACAGCATCTTGTTCTCGTACATGGTATATGCCA
46.	OeEst679_rv	TTAATTTGGTTTATTTTCCACAATATCCAATATATATCGGCAAAGAGTTTTAGGA TTTGAAATCA
47.	OeEst679NcoI_fw	CGAGCCATGGGAGATAACCAAAAACAGCATCTTG
48.	OeEst679HindIII_rv	GCTCAAGCTTTTAATTTGGTTTATTTTCCACAATATCCAATATATATCGG
49.	OeEst679sdm_fw	GTATATGCCACGGAGCTTGGTG
50.	OeEst679sdm_rv	CATGTACGAGAACAAGATGC

2.1.3. Bacterial strains

The following two strains of *Escherichia coli* were used in course of this study:

strain	supplier	genotype
TOP10	Thermo Fisher Scientific Inc. (Waltham, MA, USA)	F- *mcrA*, Δ(*mrr-hsd*RMS-*mcr*BC), Φ80*lac*ZΔM15, Δ*lac*X74, *rec*A1, *ara*D139, Δ(*araleu*)7697, *gal*U, *gal*K, *rps*L(StrR), *end*A1, *nup*G
BL21 pLysS	New England Biolabs (Ipswich, MA, USA)	F–, *omp*T, *hsd*S_B (r_B–, m_B–), *dcm*, *gal*, λ(DE3), pLysS, Cam^r

2.2. Cultivation of biological material

2.2.1. Generation of sterile *O. europaea* seedlings

Olive fruits of *O. europaea* L. cv. Koroneiki and Chemlali were obtained from N-Zyme BioTec GmbH, while fruits of the variety Canino were harvested in Viterbo, Italy. The exocarp was removed, the endocarp was cracked carefully and the embryo was sterilized for 15 min with 5 % (v/v) sodium hypochlorite containing 0.05 % (v/v) Tween-20. After several aseptic rinses with sterile ddH_2O seeds were placed on Rugini Olive solid medium (Duchefa Biochemie, Haarlem, NL) containing 30 g/L of sucrose and 7 % (w/v) phyto agar (Duchefa Biochemie, Haarlem, NL) and incubated at 26°C with a 16h-light photoperiod. After germination, seedlings were transferred to fresh solid medium and further cultivated for approximately four weeks. Afterwards, plantlets were used for the generation of callus cultures or transferred to soil for subsequent cultivation in a greenhouse at 23°C, 60 % humidity and with a daily photoperiod of 16 h.

2.2.2. Generation of callus cultures

For the generation of callus cultures, leaf tissue from sterile *O. europaea* seedlings was cut down into approximately 0.25 cm^2 pieces and placed onto callus-inducing medium (CIM) [82]. The medium composition was: 3,163 mg/L of Gamborg B5 medium including vitamins (Duchefa Biochemie, Haarlem, NL), 2 % (w/v) sucrose, 0.5 g/L of 2-(N-morpholino)ethaneseulfonic acid (MES), 0.5 mg/L of 2,4-dichlorophenoxyacetic acid (2,4-D), 0.05 mg/L of kinetin and 7.0 g/L of phyto agar (Duchefa Biochemie, Haarlem, NL). Incubation conditions were the same as applied for the cultivation of sterile seedlings (2.2.1). After 10-13 days, callus cells were separated from leaf tissue and transferred to fresh medium. Established callus cultures were subcultured every 14-17 days.

2.2.3. Cultivation of *E. coli*

Overnight cultures of *E. coli* strain TOP10 and BL21(DE3) pLysS were grown in LB liquid medium [83] supplemented with antibiotics at 37°C and 160 rpm for 16-18 h. For cultivation of TOP10 *E. coli* cells harboring pCR-Blunt (Thermo Fisher Scientific Inc., Waltham, USA) or pET-32a(+) plasmids (Merck KGaA, Darmstadt, DE) either 50 µg/mL of kanamycin or 100 µg/mL of carbenicillin, respectively, were added. Cultivation of BL21(DE3) pLysS cells transformed with aforementioned plasmids required the additional supplementation with 25 µg/mL of chloramphenicol.

2.3. Molecular cloning methods

2.3.1. Isolation of nucleic acid

2.3.1.1. Isolation of total RNA

Tissue of *O. europaea* was flash frozen in liquid nitrogen and subsequently ground using mortar and pestle. Aliquots of 100 mg were stored at -80°C until further use. The isolation of total RNA was performed on basis of the peqGOLD TriFast protocol (VWR International GmbH, Darmstadt, DE). Therefore, 1 mL of TriFast was added to each aliquot of ground tissue. Samples were vortexed and incubated for 5 min at RT. Afterwards, 200 µL of chloroform were added, samples were shaken by hand for 15 sec and incubated for 3 min at RT. Centrifugation at 12,000 ×*g* and 4°C for 15 min resulted in phase separation. The upper, aqueous phase was transferred to a new reaction tube and the extraction procedure was repeated using 500 µL of chloroform. Precipitation of RNA was then accomplished by adding 500 µL of isopropanol in combination with a 10 min incubation step on ice. After 15 min at 12,000 ×*g* and 4°C, the supernatant was removed and the pellet was washed twice with 1 mL of 75 % (v/v) ethanol by vortexing and subsequent centrifugation. In a final step, the ethanol was removed and the RNA pellet was dried for several min at 55°C, dissolved in 50-100 µL nuclease-free water and incubated for further 3 min at 55°C in order to enhance solubility. Remaining precipitations were removed by centrifugation under the aforementioned conditions. Quantification was accomplished by photometric measurements (2.3.2) and determination of the quality or rather the degradation grade of the samples was carried out by agarose gel electrophoresis (2.3.3.2). For further use of the total RNA in qPCR experiments, samples were cleaned from remaining gDNA by means of the TURBO DNA-free Kit (Thermo Fisher Scientific Inc., Waltham, MA, USA) according to the manufacturer's protocol. Total RNA preparations were stored at -80°C.

2.3.1.2. Isolation of plasmid DNA

The isolation of plasmid DNA from *E. coli* cells was performed using the Plasmid Miniprep Kit I (VWR International GmbH, Darmstadt, DE) according to the manufacturer's protocol.

2.3.2. Quantification of nucleic acid

Samples containing nucleic acids were quantified by photometric measurements using the NanoDrop ND-1000-spectrometer device (VWR International GmbH, Darmstadt, DE).

2.3.3. Electrophoretic separation of nucleic acids

2.3.3.1. Electrophoresis of DNA

DNA fragments were separated on a 1.0-1.5 % (w/v) agarose gel according to their size. Therefore, agarose was melted in 1× TAE buffer (40 mM tris, 20 mM acetic acid and 1 mM EDTA), cooled down to approximately 65°C and supplemented with 5 µL of the DNA gel stain Nancy-520 (Sigma-Aldrich, Darmstadt, DE). DNA samples were mixed 6 to 1 with 6× DNA loading dye (Thermo Fisher Scientific Inc., Waltham, MA, USA) before applying to the gel. Separation was performed for around 40-60 min in 1× TAE buffer using a voltage of 120 V. Afterwards, DNA fragments were visualized under UV light by means of the Gel iX Imager (INTAS Science Imaging Instruments GmbH, Göttingen, DE).

2.3.3.2. Electrophoresis of RNA

Integrity of the total RNA preparations was analyzed by gel electrophoresis on a formaldehyde agarose gel. Prior to analysis, all required instruments were soaked in 3 % (v/v) H_2O_2 for several hours or treated with RNase-ExitusPlus (AppliChem GmbH, Darmstadt, DE). Preparation of the gel was accomplished by adding 1 g of agarose to 10 mL of 10× MOPS buffer (200 mM MOPS, 50 mM sodium acetate, 20 mM EDTA; pH 7.0) and 87.2 mL of double autoclaved ddH_2O. The suspension was boiled and then, after cooling to around 65°C, supplemented with 2.7 mL of formaldehyde (37 %). The solidified gel was equilibrated for 30 min in respective running buffer (1× MOPS buffer containing 1 % (v/v) formaldehyde (37 %)). RNA samples were mixed with 2× RNA Gel Loading Dye (Thermo Fisher Scientific Inc., Waltham, MA, USA), heated to 70°C for 10 min and subsequently placed on ice for at least 2 min. The electrophoretic separation took place at 100 V for around 1.5 h, while subsequent visualization was performed as described before (2.3.3.1.).

2.3.4. Extraction of DNA fragments from agarose gels

DNA fragments of interest were extracted and purified from agarose gels using the Wizard SV Gel and PCR Clean-Up System (Promega Corporation, Madison, WI, USA) according to the manufacturer's protocol.

2.3.5. First strand cDNA synthesis

Synthesis of first strand cDNA was performed using the SuperScript IV Reverse Transcriptase (Thermo Fisher Scientific Inc., Waltham, MA, USA) according to the manufacturer's recommendations. The 20 µL reaction mixture contained 1× SSIV Buffer, 2 mM dNTP Mix (0.5 mM each), 5 mM DTT, 40 U of

RiboLock RNase Inhibitor (Thermo Fisher Scientific Inc., Waltham, MA, USA), 200 U of SuperScript IV Reverse Transcriptase and around 500 ng of total RNA in combination with either 0.1 µM gene-specific primer or 2.5 µM oligo(dT)$_{20}$ primer. The reaction took place at 50°C for 10 min and was determined by incubation at 80°C for 10 min. For use in qPCR experiments, the mix was then supplemented with 5 U of RNase H (New England Biolabs, Ipswich, MA, USA) and incubated at 37°C for 20 min. In order to minimize cDNA synthesis-related variations, two independent reaction approaches were subsequently combined.

2.3.6. Polymerase chain reaction (PCR)

Polymerase chain reaction for amplification of target sequences from cDNA and plasmid DNA was performed using Phusion (Thermo Fisher Scientific Inc., Waltham, MA, USA) and Pfu DNA polymerase (Promega, Madison, WI, USA), respectively. Resulting PCR products were analyzed by agarose gel electrophoresis and the DNA fragments of the expected size were extracted from gel (2.3.4.).

Pfu PCR set-up (100 µL)

10 µL	10× Pfu Buffer with $MgSO_4$
10 µL	dNTPs (2 mM each)
2 µL	forward primer (10 µM)
2 µL	reverse primer (10 µM)
2 µL	Pfu DNA polymerase (2.5 U)
1 µL	plasmid DNA (75 ng)
73 µL	nuclease-free water

Phusion PCR set-up (100 µL)

10 µL	10× Pfu Buffer with $MgSO_4$
8 µL	dNTP Mix (2 mM each)
5 µL	forward primer (10 µM)
5 µL	reverse primer (10 µM)
1 µL	Phusion DNA polymerase (2 U)
10 µL	cDNA (250 ng*[1])
63 µL	nuclease-free water

*[1]equivalent to 250 ng of total RNA applied to the cDNA synthesis reaction before

	Pfu PCR		Phusion PCR		
step	**temperature**	**duration**	**temperature**	**duration**	
initial denaturation	95°C	3 min	98°C	30 sec	
denaturation	95°C	40 sec	98°C	10 sec	35 cycles
annealing	variable*[2]	30 sec	variable*[2]	30 sec	
elongation	72°C	1 min 15 sec	72°C	40 sec	
final elongation	72°C	10 min	72°C	10 min	

*[2]according to the recommendations of the oligonucleotide manufacturer

2.3.7. Blunt-end ligation

Purified DNA fragments of unknown sequence were cloned into the blunt DNA cloning vector pCR-Blunt derived from the Zero Blunt PCR Cloning Kit (Thermo Fisher Scientific Inc, Waltham, MA, USA). A 10 µL reaction mix contained 5 U of ExpressLink T4 DNA Ligase, 1× ExpressLink T4 DNA Ligase Buffer, 25 ng of linearized vector and the amount of insert DNA required to achieve a molar ratio of approximately 1 to 3 (vector to insert). After an incubation step for 1.5-2 h at 25°C, plasmid amplification was accomplished in *E. coli* TOP10 cells.

2.3.8. Transformation of competent *E. coli* cells

Chemically competent cells of *E. coli* strain TOP10 or BL21(DE3) pLysS were transformed *via* heat shock. Therefore, a 50 µl aliquot of bacterial cells was thawed on ice for around 5 min. Then, either 5 µL of ligation product or 75 ng of purified plasmid DNA were added to the aliquot. The suspension was gently stirred with the pipet tip and afterwards incubated for 20 min on ice. The heat shock was applied by placing the reaction tube for 1 min in a 42°C water bath followed by additional 3 min on ice. The cell suspension was then supplemented with 500 µL of LB-medium without antibiotics and regenerated for 1 h at 37°C and 750 rpm and afterwards transferred to LB-medium plates amended with appropriate antibiotics (2.2.3) and 40 µg/mL of X-Gal (5-bromo-4-chloro-3-indolyl-β-D-galactopyranoside). Cultures were then incubated for 16-18 h at 37°C and stored afterwards at 4°C.

2.3.9. Colony screening PCR

Colonies of *E. coli* grown after transformation on selection medium were analyzed for the presence of the introduced gene of interest. Therefore, several colonies of each transformation approach were picked and dispersed in 30 µL of sterile water. 10 µL of this bacterial solution were mixed with 10 µL of Taq PCR mix resulting in a final reaction composition of 1× Taq buffer, 0.2 mM of each dNTP, 1.5 mM $MgCl_2$, 0.1 µM forward and reverse primer and 0.5 U of recombinant Taq DNA Polymerase (Thermo Fisher Scientific Inc, Waltham, MA, USA). Applied PCR conditions are described below.

Resulting DNA amplicons were analyzed by agarose gel electrophoresis (2.3.3.1). Colonies proven to harbor the gene of interest were subsequently used to inoculate 4 mL overnight cultures (2.2.3.).

step	temperature	duration	
initial denaturation	95°C	3 min	
denaturation	95°C	40 sec	35 cycles
annealing	variable*	30 sec	
elongation	72°C	1 min 15 sec	
final elongation	72°C	10 min	

*according to the recommendations of the oligonucleotide manufacturer

2.3.10. DNA sequencing

Sequencing of genes of interest within pCR-Blunt or pET-32a(+) vectors was carried out by Eurofins Genomics GmbH (Ebersberg, DE).

2.3.11. Site-directed mutagenesis

Substitution of single nucleotides within a gene of interest was accomplished through site-directed mutagenesis (SDM) by means of the Q5 Site-Directed Mutagenesis Kit (New England Biolabs, Ipswich, MA, USA). In the first part of this study, SDM was applied in order to remove an internal NcoI restriction sites within the sequences *OeEst030* (pos. 48-53), *OeEst228* (pos. 48-53) and *OeEst905* (pos. 51-56). This was accomplished by introducing a silent mutation into the motif 5'-CCATGG-3' leading to the sequence 5'-CCACGG-3'.

Furthermore, site-directed mutagenesis was applied for the modification of the coding sequence *OeEst030* in order to obtain the amino acid exchanges S211D, E212A, E214A and D216A in corresponding proteins. All SDM experiments were performed using the construct pCR-Blunt_*OeEst030* in combination with the oligonucleotides no 17-30 (2.1.2.). Verification of successfully manipulated DNA sequences was accomplished by DNA sequencing (2.3.10.).

2.3.12. Restriction and ligation of DNA fragments

For the introduction of genes of interest into the bacterial expression vector pET-32a(+), corresponding sequences and the destination vector had to be linearized featuring complementary overhangs. Therefore, pCR-Blunt vectors harboring the relevant coding sequences flanked by NcoI and XhoI or HindIII restriction sites as well as the expression vector were digested with the same combination of restriction enzymes. A standard 20 µL reaction mix consisted of 1× FastDigest buffer,

1.0-1.5 µg of plasmid DNA, 1 µL of FastDigest NcoI and 1 µL of either FastDigest XhoI or FastDigest HindIII. After 15 min of incubation at 37°C, enzymes were heat-inactivated at 80°C for 10 min. Restriction products were separated by agarose gel electrophoresis (2.3.3.1) and purified from gel (2.3.4.). All aforementioned restriction enzymes including appropriate buffers were purchased from Thermo Fisher Scientific Inc. (Waltham, MA, USA).

Ligation of linearized genes of interest into the pET-32a(+) vector was accomplished using the T4 DNA Ligase (Promega, Madison, WI, USA). The 10 µL ligation mix was composed of 1× ligase buffer, 1 U of T4 DNA ligase, 20 ng of digested pET-32a(+) vector and around 10 ng of digested gene of interest resulting in a molar ratio of approximately 1 to 3 (vector to insert). The reaction was performed at 25°C for 2.0-2.5 h and resulting ligation products were amplified in cells of *E. coli* TOP10 (2.3.8.).

2.3.13. Quantitative real-time PCR (qPCR)

Real-time PCR is a method used to monitor the amplification of target DNA sequences during each cycle of a PCR *via* fluorescent dyes [84]. The principal is based on the fact that the fluorescence signal increases in proportion to the generated number of PCR product molecules. The measured signal intensity is then plotted against the cycle number resulting in a sigmoid curve. Generally, there are two different kinds of fluorescent reporters used: dsDNA-binding dyes and target-specific fluorescent dyes that are attached to PCR primers or probes. Experiments described in this study were conducted with the former.

During the initial cycles of the qPCR, cycles 3 to 15, usually no significant change in the fluorescence intensity can be detected. This signal level, the so-called baseline, provides information about the background noise of the reaction and is therefore subtracted from the results. The threshold is then set above the baseline within the exponential growth region, usually at 10 times of the standard deviation of the average fluorescence signal of the baseline. The intersection of the threshold with the amplification plot defines the Cq (quantification cycle, previously known as threshold cycle (Ct)) of a sample. By comparison of this value with the results of a standard curve or the Cq of an internal reference gene, it is possible to calculate the initial DNA copy number or to compare the quantity of templates within different samples, respectively [85].

The 20 µL qPCR reaction mixture consisted of PowerUp SYBR Green Master Mix (Thermo Fisher Scientific, Waltham, MA, USA), 0.5 µM forward and reverse qPCR primer (2.1.2., oligonucleotides no 31-44) and approximately 5 ng of RNase-treated cDNA (2.3.5.). In order to screen for remaining gDNA contaminations within the cDNA samples, so-called no-amplification controls (NACs) were set up. Therefore, DNase-treated total RNA (2.3.1.1.) was used for a reverse transcription reaction (2.3.5)

lacking reverse transcriptase. Afterwards, RNase-treatment was performed followed by qPCR. Additionally, qPCR samples containing ddH_2O instead of template served as negative controls (no template controls (NTCs)).

All samples were analyzed in triplets using MicroAmp Optical 96-Well Reaction Plates (Thermo Fisher Scientific, Waltham, MA, USA) and the OneStepPlus Real-Time PCR System (Applied Biosystems Inc, Foster City, CA, USA) under the following conditions: an initial denaturation at 95°C for 2 min was followed by 40 cycles consisting of 3 sec denaturation at 95°C and 30 sec annealing and elongation at 63°C for amplification of the reference targets, *EF1-α* and *PP2A*, and 60°C when gene-specific primers for *OeEst030*, *OeEst228* and *OeEst905* were used. To verify the formation of one specific amplicon, melting curve analysis was performed for each PCR sample according to the manufacturer's protocol.

2.4. Protein biochemical methods

2.4.1. Induction of gene expression and cell lysis

For gene expression experiments, 600 mL of TB-medium amended with carbenicillin (100 µg/mL) and chloramphenicol (25 µg/mL) were inoculated with 10 mL of overnight culture (2.2.3.) of *E. coli* strain BL21(DE3) pLysS harboring the desired expression vector. The cell suspension was cultivated for several hours at 37°C and 160 rpm until reaching an OD_{600} of around 0.8. Expression of the gene of interest was then induced by addition of 0.4 mM isopropyl β-D-1-thiogalactopyranoside (IPTG). Further cultivation of the expression culture took place at 26°C for 16-18 h.

Afterwards, bacterial cells were harvested by centrifugation at 5,000 ×*g* and 4°C for 10 min. The resulting pellet was resuspended in 3 volumes of Lysis-Equilibration-Wash (LEW) buffer (50 mM NaH_2PO_4, 300 mM NaCl, pH 8.0) supplemented with 1 mM 4-(2-aminoethyl)benzenesulfonyl fluoride hydrochloride (AEBSF), 6 mM 3-((3-cholamidopropyl) dimethylammonio)-1-propanesulfonate (CHAPS) and 1 mg/mL of lysozyme (equates to around 35,000 FIP/mL) followed by incubation for 30 min on ice. Cells were then mechanically disrupted by sonication (6 × 10 s bursts with a 15 s cooling period between each step), mixed with 2 U of DNase I per mL and incubated for further 20 min on ice. Afterwards, the crude lysate was centrifuged twice at 10,000 ×*g* and 4°C for 45 min and the resulting supernatant was immediately used for protein purification *via* affinity chromatography.

2.4.2. Purification of recombinant proteins *via* affinity chromatography

Recombinant proteins produced within this study were linked to a polyhistidine-tag enabling the purification *via* immobilized metal ion affinity chromatography (IMAC). Therefore, cleared bacterial lysate (2.4.1.) was applied to a Protino Column 14 mL (Macherey-Nagel, Düren, DE) packed with 1.2 g of Protino Ni-TED Resin (Macherey-Nagel, Düren, DE), which was pre-equilibrated with 9.6 mL of LEW buffer. Unbound or only weakly bound proteins were then removed in two consecutive washing steps with 9.6 mL of LEW buffer containing 2 mM imidazole. Subsequent elution of the polyhistidine-tagged proteins was achieved in three fractions using 7.2 mL LEW-buffer containing increasing concentrations of imidazole (50 mM, 150 mM and 250 mM). All collected fractions were stored at 4°C until analysis by SDS-PAGE in combination with Coomassie Brilliant Blue staining.

2.4.3. Desalting and concentrating

Affinity chromatography fractions containing the protein of interest, as indicated by SDS-PAGE and subsequent Coomassie Brilliant Blue staining, were combined and applied onto a Vivaspin Turbo 15 ultrafiltration unit (Sartorius AG, Göttingen, DE). The protein solution was concentrated to a total volume of 2.0 mL and washed thrice with 7.0 mL of sodium phosphate buffer (100 mM, pH 7.4). After the final concentration of the sample to around 1.5 mL, protein quantity was determined by means of the bicinchoninic acid assay. If the calculated concentration exceeded a value of 2 mg/mL, the sample was diluted to this value using the aforementioned buffer. In order to store protein preparations at -20°C, one volume of 50 % (v/v) glycerol was added resulting in the following buffer composition: 50 mM sodium phosphate (pH 7.4) and 25 % (v/v) glycerol. Final protein preparations were analyzed again by BCA as well as SDS-PAGE followed by silver nitrate staining.

2.4.4. Bicinchoninic acid assay (BCA)

Determination of protein concentration was accomplished by means of the Pierce BCA Protein Assay Kit (Thermo Fisher Scientific Inc., Waltham, MA, USA). The procedure was performed according to the manufacturer's protocol using bovine serum albumin (BSA) as a protein standard. For the quantification of protein solutions right after desalting and concentrating (2.4.3.) dilutions of 1:2, 1:5 and 1:10 in 100 mM sodium phosphate (pH 7.4) were measured in duplets. Protein preparations including glycerol were analyzed in triplets after diluting the sample 2:5, 1:5 and 1:10.

2.4.5. Sodium dodecyl sulfate-polyacrylamide gel electrophoresis (SDS-PAGE)

Protein samples were analyzed by sodium dodecyl sulfate-polyacrylamide gel electrophoresis (SDS-PAGE) using a discontinuous buffer system. The polyacrylamide gel was casted in two steps: first the resolving gel solution was poured into the gel cassette, overlaid with 5 mm of isopropanol and polymerized for around 30 min. Afterwards isopropanol was discarded and the stacking gel solution was filled on top of the resolving gel. An appropriate comb was inserted and the gel was allowed to polymerize for at least 40 min. The polyacrylamide gel was then overlaid with SDS-PAGE running buffer (192 mM glycine, 25 mM tris, 10 % (w/v) SDS) and loaded with protein samples. Electrophoretic separation was performed for 1 h at 40 V and further 2.5 h at 100 V. Afterwards, the gel was stained with either Coomassie Brilliant Blue (2.4.6.1) or silver nitrate (2.4.6.2).

Sample preparation

Protein samples were mixed with an equal volume of 2× SDS-loading dye (100 mM Tris-HCl (pH 8.3), 20 % (v/v) glycerol, 4 % (w/v) SDS, 0.2 % (w/v) bromphenol blue) boiled at 95°C for 10 min and afterwards placed on ice for at least 2 min. If the sample was a pellet, 200 µL of 2× SDS loading dye were added and a centrifugation step at 17,000 ×*g* and RT for 10 min was included right after the heating step. Unless otherwise stated, 25 µL of each protein sample was then applied together with 5 µL of the protein size marker 'PageRuler Prestained Protein Ladder, 10 to 180 kDa' (Thermo Fisher Scientific Inc., Waltham, MA, USA) to the polyacrylamide gel.

Resolving gel (13 %)

2.17 mL	acrylamide solution (30 %)
1.25 mL	Tris-HCl (1.5 M, pH 8.8)
1.47 mL	ddH_2O
50 µL	SDS (10 % (w/v))
50 µL	ammonium persulfate
10 µL	tetramethylethylendiamin

Stacking gel (3.75 %)

0.40 mL	acrylamide solution (30 %)
0.94 mL	Tris-HCl (0.5 M, pH 6.8)
1.70 mL	ddH_2O
30 µL	SDS (10 % (w/v))
30 µL	ammonium persulfate
5 µL	tetramethylethylendiamin

2.4.6. Visualization of proteins separated *via* SDS-PAGE

2.4.6.1. Coomassie Brilliant Blue staining

Samples taken during gene expression and protein purification procedures were analyzed by SDS-PAGE with subsequent visualization by Coomassie Brilliant Blue staining. Therefore, polyacrylamide gels were soaked in Coomassie staining solution (50 % (v/v) methanol, 10 % (v/v) acetic acid, 0.5 %

(w/v) Coomassie Brilliant Blue G 250) and incubated for 15 min on an orbital shaker followed by 20 min incubation in destaining solution (30 % (v/v) ethanol, 10 % (v/v) acetic acid). A final destaining step was performed overnight. In order to document the results, the polyacrylamide gel was wrapped in plastic foil and scanned.

2.4.6.2. Silver nitrate staining

Visualization of proteins on polyacrylamide gels using silver nitrate is approximately 50-100 times more sensitive compared to classical Coomassie Brillant Blue staining [86]. Therefore, this method is particularly suitable for detecting minor contaminants within a protein preparation.

After SDS-PAGE, the polyacrylamide gel was incubated on an orbital shaker for 30 min in fixing solution (50 % (v/v) methanol, 12 % (v/v) acetic acid, 0.02 % (v/v) formaldehyde) followed by two washing steps in 50 % (v/v) ethanol for 10 min. To enhance sensitivity of the coloration, the gel was pre-treated for 1 min in 0.8 mM sodium thiosulfate solution. Two washing steps with ddH_2O were performed (around 20 sec per step) before the coloration solution (15 mM silver nitrate, 0.028 % (v/v) formaldehyde) was applied for 10 min. After two further washing steps in ddH_2O, the gel was incubated in development solution (0.56 M sodium carbonate, 5.65 µM sodium thiosulfate, 0.02 % (v/v) formaldehyde) until the desired signal intensity was reached. Subsequently, development solution was discarded, two washing steps were performed and the gel was fixed in stop solution (50 % (v/v) methanol, 12 % (v/v) acetic acid) for around 5 min. For documentation of the results, the gel was sealed in plastic wrap and scanned.

2.5. Characterization of recombinant proteins

2.5.1. Unspecific esterase activity assays

Purified recombinant enzymes were initially analyzed for their activity against the chromogenic substrates para-nitrophenyl acetate (pNPA) and para-nitrophenyl butyrate (pNPB). Both compounds are characterized by their broad acceptance as substrates for enzymes featuring esterase or lipase activity and are therefore commonly used for the initial verification of those activities in unknown proteins. Furthermore, hydrolysis of those substrates releases para-nitrophenol (pNP), which can be spectrophotometrically detected at a wavelength of 405 nm.

A standard assay mix consisted of 10 µg/mL of recombinant protein, 0.5 mM of pNPA or pNPB and 50 mM sodium phosphate (pH 7.4) in a total volume of 200 µL. Increase of the absorption at 405 nm corresponding to the release of pNP was determined in intervals of 30 sec for 10 min at 25°C using

the Epoch 2 Microplate Spectrophotometer (BioTek Instruments, Winooski, VT, USA). Additionally, in order to calculate the reaction rates, autohydrolysis of the substrates was determined and a standard curve of pNP was produced applying the same conditions. All reaction samples were set up in triplets and resulting reaction rates were specified in units with one unit of esterase activity being the amount of enzyme required to release 1 µmol of pNP per min under the aforementioned conditions

2.5.2. Esterase activity assays towards olive secoiridoids

In order to identify endogenous substrates of the described olive enzymes, recombinant proteins were incubated with different secoiridoids from *O. europaea*. While oleuropein and oleoside 11-methyl ester were purchased from Sigma Aldrich (St. Louis, MO, USA), ligstroside was kindly provided by N-Zyme BioTec GmbH (Darmstadt, DE). Reaction mixtures were composed of 0.5 mM substrate and 100 µg/mL of recombinant enzyme in a total volume of 100 µL buffered either in 50 mM sodium acetate (pH 5.0) or 50 mM sodium phosphate (pH 7.4). After 1 h of incubation at 30°C, enzymes were precipitated by addition of two volumes of ice-cold methanol followed by centrifugation at 4°C and 17,000 ×*g* for 20 min. Resulting supernatant was analyzed by LC-MS using the conditions described in chapter 2.6.1.1.

Furthermore, corresponding aglycones, namely ligstroside aglycone, oleuropein aglycone and elenolic acid, were tested as substrates for the recombinant esterases. Therefore, the aforementioned assay mixtures buffered in sodium acetate were supplemented with 1 mg/mL (corresponding to ≥ 2 U/mL) β-glucosidase from almonds (Sigma-Aldrich, St. Louis, MO, USA). Samples containing only substrate and β-glucosidase served as negative control.

2.5.3. Activity towards strictosidine and its aglycone

Strictosidine assays were composed of 75 µM strictosidine and 100 µg/mL of recombinant protein buffered either in 50 mM sodium acetate (pH 5.0) or 50 mM sodium phosphate (pH 7.4). After 1 h of incubation at 30°C, reactions were stopped by addition of one volume of ice-cold acetonitrile. Precipitated proteins were separated by centrifugation at 4°C and 17,000 ×*g* for 20 min and resulting supernatant was analyzed by LC-MS (2.6.1.3.).

For activity assays towards strictosidine aglycone, reaction mixtures were further supplemented with 2.5 µg/mL of strictosidine glucosidase (SG) kindly provided by Dr. Iryna Gerasimenko.

2.5.4. Activity towards methylated plant hormones

The recombinant esterases were also tested for their ability to demethylate the plant hormones methyl jasmonate (MeJA), methyl salicylate (MeSA) and methyl indole-3-acetate (MeIAA). Appropriate reaction mixtures consisted of 2 mM of substrate and 100 µg/mL of protein buffered in 50 mM sodium phosphate (pH 7.4) in a total volume of 100 µL. The enzymatic conversion took place at 30°C for 1 h and was stopped by addition of 20 µL of 1 M HCl. Precipitated proteins were removed by centrifugation at 17,000 ×*g* for 20 min, followed by an extraction with 800 µL of diethyl ether. The resulting organic layer was either evaporated at RT to 30-40 µL for further analysis by TLC or evaporated completely for analysis by GC-MS. In the latter case, silylation was then performed by addition of 150 µL of BSTFA + 1 % TMCS (Sigma-Aldrich, St. Louis, MO, USA) and subsequent incubation for 30 min at 70°C.

In contrast to enzyme activity assays with MeJA and MeSA, those using MeIAA as substrate could be analyzed by LC-MS. For this purpose, however, assay conditions were modified: a 200 µL reaction mix was composed of 100 µg/mL of recombinant protein and 0.5 mM of MeIAA buffered in 50 mM sodium phosphate (pH 7.4). Samples were incubated for 1 h at 30°C and afterwards supplemented with 200 µL of ice-cold acetonitrile in order to precipitate all proteins. After centrifugation at 17,000 ×*g* and 4°C for 20 min, supernatant was transferred to HPLC vials and subsequently analyzed (2.6.2.).

2.6. Analytical methods

2.6.1. Reverse-phased liquid chromatography (LC) and mass spectrometry (MS)

Analysis of enzyme activity assays was performed using liquid chromatography (LC) coupled with mass spectrometry (MS). The LC device was a 1260 Infinity System (Agilent Technologies, Santa Clara, CA, USA) consisting of the following components: G4225A high performance degasser, G1313B binary pump, G1329B autosampler, G1316C column thermostat, G4212B diode array detector. For subsequent mass spectrometry analysis of compounds separated by LC, the 6120 Single Quadrupole (Agilent Technologies, Santa Clara, CA, USA) was used applying the following parameters: atmospheric pressure ionization-electrospray ionization (API-ESI), positive and negative ion mode, N_2 as nebulizing gas at a flow rate of 12 L/min under a pressure of 35 psig, drying gas temperature of 350°C and capillary voltage of 3 kV.

2.6.1.1. Analysis of oleoside-type secoiridoids

Enzyme assays containing oleoside-type secoiridoids were analyzed by LC-MS using the analytical C18 column 'ZORBAX Eclipse Plus C18 (4.6 × 250 mm, 5 µm)' (Agilent Technologies, Santa Clara, CA, USA) and a solvent system consisting of 0.1 % formic acid in ddH_2O (solvent A) and methanol (solvent B). Samples (20 µL) were injected onto the column and separated at 30°C and a flow rate of 0.5 mL/min. Photometric detection of relevant substances was accomplished at a wavelength of 240 and 280 nm.

time (min)	solvent A (%)	solvent B (%)	
0.0-10.0	90	10	isocratic
10.0-70.0	10	90	gradient
70.0-80.0	0	100	isocratic
80.0-90.0	90	10	isocratic

2.6.1.2. Analysis of indole-3-acetic acid and derivatives

Enzyme assays containing the plant hormone MeIAA and its derivatives were analyzed by LC-MS using the analytical C18 column 'Poroshell 120 SB-C18 (3.0 × 150 mm, 2.7 µm)' (Agilent Technologies, Santa Clara, CA, USA) and a solvent system consisting of 0.1 % formic acid in ddH_2O (solvent A) and methanol (solvent B). Samples (5 µL) were injected onto the column and separated at 30°C and a flow rate of 0.5 mL/min. Photometric detection of relevant substances was accomplished at a wavelength of 278 nm.

time (min)	solvent A (%)	solvent B (%)	
0.0-2.0	70	30	isocratic
2.0-12.0	10	90	gradient
12.0-15.0	0	100	isocratic
15.0-20.0	70	30	isocratic

2.6.1.3. Analysis of secologanin-type secoiridoids

Enzyme assays containing secologanin-type secoiridoids were analyzed by LC-MS using the analytical C18 column 'Poroshell 120 SB-C18 (3.0 × 150 mm, 2.7 µm)' (Agilent Technologies, Santa Clara, CA, USA) and a solvent system consisting of 0.1 % formic acid in ddH_2O (solvent A) and acetonitrile (solvent B). Samples (10 µL) were injected onto the column and separated at 30°C and a flow rate of

0.5 mL/min. Photometric detection of relevant substances was accomplished at a wavelength of 250 nm.

time (min)	solvent A (%)	solvent B (%)	
0.0-2.0	90	10	isocratic
2.0-17.0	30	70	gradient
17.0-22.0	0	100	isocratic
22.0-28.0	90	10	isocratic

2.6.2. Gas chromatography (GC)

Gas chromatography (GC) analysis was performed using a QP 2010 Ultra gas chromatography-mass spectrometry system (Shimadzu, Duisburg, Germany). Samples (1µL) were injected onto a DB-5MS column (30 m × 0.25 mm × 0.25 µm, Phenomenex, Aschaffenburg, DE) with an initial oven temperature of 40°C. After 1 min at constant temperature, the column was heated by 15°C per min to 250°C at which it stayed for 5 min. Hydrogen was used as carrier gas with a flow rate of 3.07 mL/min. Measurements were made through electron-impact ionization (GC-EI-MS) at 70 eV. The ion source and transfer line were kept at 230°C. Obtained data were analyzed by means of the software OpenChrome 1.0.0.

2.6.3. Thin-layer chromatography

First analyses of assays with plant hormones as substrates were accomplished by means of thin-layer chromatography (TLC). Enzyme assay extracts (2.5.4.) were separated on a TLC silica gel 60 F254 plate (Merck KGaA, Darmstadt, DE) using a mobile phase consisting of n-hexane, ethyl acetate and acetic acid in a ratio of 70:30:1. MeSA and its demethylation product were detected under UV light as fluorescence depleting spots. For the visualization of MeJA, MeSA and their derivatives, the silica gel was sprayed with a coloration solution composed of 2.5 % (v/v) p-anisaldehyde, 3.5 % (v/v) sulfuric acid and 1.0 % (v/v) acetic acid. Subsequently, plates were ‘burned’ for 7 min at 105°C and immediately sprayed with ddH_2O in order to brighten the background [87].

2.7. Software-based analysis

2.7.1. Sequence alignments

Sequence alignments were performed with the Basic Local Alignment Search Tool (BLAST) [88] from the National Center for Biotechnology Information (NCBI). For generation of multiple sequence alignments the Clustal Omega software [89] was used.

2.7.2. Primer design for qPCR experiments

Oligonucleotides for qPCR experiments were designed by means of the Online Tool Primer3web Version 4.1.0 [90] using default settings. Potential primer pairs were aligned against a transcriptome data base of *O. europaea* [91] in order to verify target specificity.

2.7.3. Analysis of qPCR raw data

First analysis of the qPCR data was performed using the StepOne Software v2.3 (Thermo Fisher Scientific, Waltham, MA, USA). In this context, NTC and -RT samples were checked for the absence of amplicons and potential outliers were removed. Non-baseline corrected amplification data (normalized reporter; Rn) was then exported and further processed with the software LinRegPCR [92, 93]. Baseline determination was accomplished using the windows-of-linearity option 'amplification groups' and a 'common' Cq-threshold for each gene of interest (goi) and corresponding endogenous controls. Resulting Cq values and mean PCR efficiencies of each target were exported to excel and used for the following calculations. According to the 'error minimization' approach for the calculation of normalized relative quantities (NRQs) [94], the Cq value of each sample (mean of three technical replicates) was calibrated against the arithmetic mean quantification cycle value across all samples for the same gene. Afterwards, relative quantity (RQ) of each sample was calculated using the gene specific PCR efficiency, followed by normalization of the target RQs against the geometrical mean of corresponding reference RQs. Then all normalized relative quantities (NRQ) of the same target were divided by the lowest calculated value. All further calculations were performed on the log2 transformed values. The mean NRQ value of each biological group was calculated from the arithmetic mean of the three biological replicates. Deviations within each group were determined as 95 % confidence interval (CI). Significant differences in expression levels between biological groups were investigated by means of the two-tailed Student's t-test applying a cut-off value of $p = 0.05$. Results were then back-transformed into linear NRQs and presented in three independent bar charts.

2.7.4. Homology modelling of protein structures

Modelling of three dimensional structures of OeEst030 and OeEst228 was performed using the fully automated protein homology modelling server SWISS-MODEL [95]. Therefore, amino acid sequences were submitted to the server and aligned with the sequence of PNAE (pdb entry 1wfl.1.A). Based on the available crystal structure of the reference protein, comparative modelling was performed using the implemented engine ProMod3. Expected total accuracy of resulting model was presented as QMEAN score [96], while the local quality estimate provided information about the accuracy of regions within sequence of the model. Model quality was also assessed by a Ramachandran plot which is based on the evaluation of the two torsion angles phi and psi for each amino acid within the modelled 3D structure. A high percentage of amino acids featuring 'allowed', also referred to as 'Ramachandran favored', values is an indicator for a good reliability of the model.

Visualization of the protein models was accomplished by means of the Discovery Studio Visualizer software (Biovia, San Diego, CA, USA).

3. Results

3.1. Identification of potential carboxylesterase encoding genes

The initial step of the project was the identification of candidate genes encoding carboxylesterases that are involved in the degradation of ligstroside and oleuropein leading to oleocanthal and oleacein, respectively. This was accomplished by screening an available olive genome data base [91] for candidate sequences showing a significant homology to the well-characterized polyneuridine aldehyde esterase (PNAE) from *R. serpentina* [78, 97]. PNAE cleaves the methyl ester of an intermediate MIA in the biosynthetic route leading to ajmaline and is, therefore, acting on a substrate that, like the oleosides described here, originates from the iridoid pathway. Hence, it was assumed that a similar enzyme was recruited for the demethylation of oleuropein and its derivatives.

From a large number of protein sequences with a homology of more than 50 % to PNAE, data base entries OE6A025905P1, OE6A065391P1, OE6A038228P1 and OE6A059030P1 were selected for further investigation. All four candidates not only shared high sequence similarities of more than 68 % with PNAE (Table 1), but also showed significant homology with other well characterized members of the class II carboxylesterases, namely the hydroxynitril lyase (HNL) from *Hevea brasilienses* [98], the methyl jasmonate esterase (MJE) from *Solanum lycopersicum* [99] and the salicylic acid binding protein 2 (SABP2) from *Nicotiana tabacum* [100].

Table 1: Putative esterases identified on basis of homology studies using PNAE as reference protein. Temporary denotations were assigned to the data base entry numbers (DB entry no) [91]. Corresponding protein sequences were compared to the sequence of PNAE, which is consisting of 264 amino acids (aa).

DB entry no	seq. length (aa)	denotation	seq. identity (%)	seq. similarity (%)
OE6A059030P1	260	OeEst030	42.6	68.4
OE6A038228P1	261	OeEst228	51.4	70.2
OE6A065391P1	259	OeEst391	54.5	73.3
OE6A025905P1	261	OeEst905	58.7	77.6

As indicated by a multiple sequence alignment (MSA) (Figure 6), the catalytic triad typical for proteins of the α/β hydrolase fold superfamily is present in all four candidates. This motif is consisting of a nucleophile and a strictly conserved histidine (H) positioned after strand β5 at the top of the 'nucleophile elbow' and the last β strand, respectively, as well as an acidic residue usually positioned after strand β7 [73]. As shown in Figure 6, aforementioned histidine is located at amino acid position 240 for OeEst030 and OeEst391 and position 241 for OeEst228 and OeEst905. The nucleophile, here

serine (S), is located at position 83 in all candidates except for OeEst905, where its position shifted by one position towards the C-terminus. As required for the geometry of the 'nucleophile elbow', in all candidate sequences corresponding serine is flanked by amino acids featuring small residues, such as glycine (G) and alanine (A), leading to the sequence motif G-X-S-X-G/A-G (X, any amino acid). The acidic member of the proposed catalytic triad is represented by aspartate at position 212 and 213 for OeEst391 and OeEst905, respectively. OeEst030 and OeEst228, however, differ in case of the location of this acidic residue. Although they do not possess the corresponding amino acid at the expected position as indicated by the MSA, their protein sequence contains several acidic residues in close proximity.

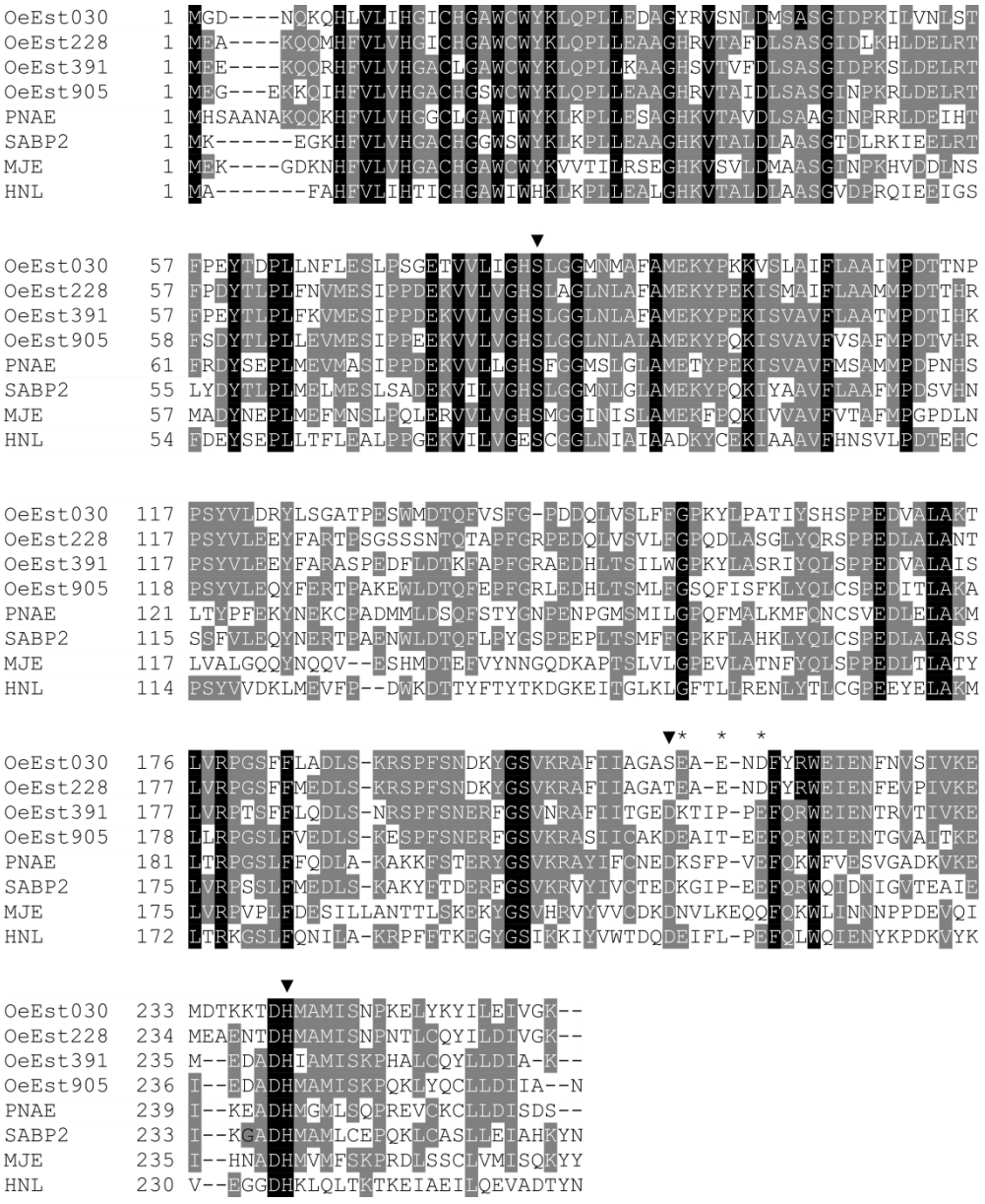

Figure 6: MSA of amino acid sequences of the putative esterases OeEst030, OeEst228, OeEst391 and OeEst905 with well characterized plant esterases including polyneuridine aldehyde esterase (PNAE) from *Rauvolfia serpentina* (accession no. Q9SE93.1), salicylic binding protein 2 (SABP2) from *Nicotiana tabacum* (NP_001312442.1), methyl jasmonate esterase (MJE)

from *Solanum lycopersicum* (NP_001233813.3) and hydroxynitril lyase (HNL) from *Hevea brasilienses* (P52704). Amino acids identical in all or at least four sequences are shown in white letters on black background or shaded in grey, respectively. Amino acid positions expected to form the catalytic triad consisting of serine (S), aspartate (A) and histidine (H) are marked with black arrows. Alternative positions potentially providing the acidic member of the catalytic triad in the amino acid sequence of OeEst030 and OeEst228 are highlighted with asterisks.

3.2. Isolation of the identified coding sequences

The procedure of isolating the desired DNA coding sequences from tissue of *O. europaea* started with the extraction of total RNA. Therefore, leaf material was harvested from plants of the cultivars Chemlali and Koroneiki and pulverized by mortar and pestle. Total RNA was then isolated (2.3.1.1) and subsequently used for reverse transcription (2.3.5.). In a next step, the desired target sequences were amplified from the generated cDNA *via* Pfu PCR (2.3.6.) with gene-specific primers (2.1.2.; oligonucleotides no 1-8). Resulting PCR products were then analyzed by agarose gel electrophoresis (2.3.3.1.) for the presence of a specific amplicon with the size of around 780 bp.

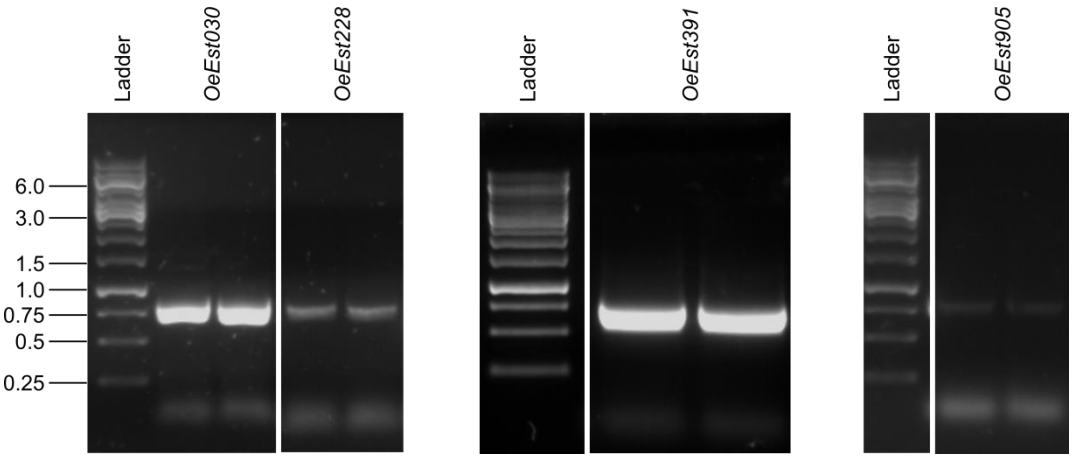

Figure 7: Agarose gel electrophoresis of DNA fragments generated in course of the CDS isolation procedure. Candidate sequences *OeEst030*, *OeEst228*, *OeEst391* and *OeEst905* were amplified from cDNA of *O. europaea* using gene-specific primers. Each sample was analyzed on two lanes. Numbers to the left indicate the size (kbp) of marker DNA fragments (Ladder). For the unprocessed version of the gel pictures see Supporting Figure 1 (Appendix).

The bands of the expected size (Figure 7) were extracted and purified from gel (2.3.4.). Afterwards, DNA fragments were cloned into the pCR-Blunt vector *via* blunt-end ligation (2.3.7.) followed by heat shock transformation of competent cells of *E. coli* TOP10 (2.3.8.). After incubation for 16-18 h at 37°C, colony screening PCR (2.3.9.) using gene-specific primers was performed for the verification of successfully transformed cells. From each transformation approach several positives candidates were

used to set up overnight cultures. Plasmid DNA was then isolated from those by means of the plasmid mini prep kit (2.3.1.2.) and subsequently sequenced (2.3.10.). An alignment of the isolated DNA sequences against the corresponding transcriptome data base entries [91] revealed high sequence identities (Table 2) confirming the successful isolation of the desired candidate sequences.

Table 2: Comparison of the isolated DNA coding sequences with those retrieved from the transcriptome data base of *O. europaea* L. cv. Farga [91]. The table column 'origin' refers to the cultivar from which the corresponding coding sequence was isolated.

isolate	origin	seq. identity (%)	reference seq.
OeEst030	*O. europaea* L. cv. Koroneiki	100.0	OE6A059030P1
OeEst228	*O. europaea* L. cv. Chemlali	99.87	OE6A038228P1
OeEst391	*O. europaea* L. cv. Chemlali	97.18	OE6A065391P1
OeEst905	*O. europaea* L. cv. Chemlali	99.11	OE6A025905P1

3.3. Introduction of the genes of interest into a bacterial expression system

For expression of the genes of interest using a bacterial expression system, coding sequences had to be introduced into an appropriate expression vector. For this purpose, the pET-32a(+) vector was chosen as destination vector enabling the production of recombinant protein fused at the N-terminus with a solubility enhancing thioredoxin tag (TRX tag) as well as a polyhistidine tag. In order to subclone the genes of interest into the multiple cloning site of this expression vector, it was necessary to add appropriate restriction sites to the coding sequences. Therefore, the constructed plasmids pCR-Blunt_*OeEst030*, pCR-Blunt_*OeEst228*, pCR-Blunt_*OeEst391* and pCR-Blunt_*OeEst905* were used as templates for Pfu PCRs (2.3.6.) using modified versions of the gene-specific primers (2.1.2.; oligonucleotides no 9-16). Thereby, amplicons of *OeEst030*, *OeEst228* and *OeEst905* were generated featuring NcoI and XhoI restriction sites at the 5' and 3' terminus, respectively. Due to an internal XhoI restriction site within the sequence of *OeEst391*, it was decided to add a HindIII restriction site at the 3' terminus instead. Again, PCR products were analyzed by agarose gel electrophoresis (2.3.3.1.), extracted from gel (2.3.4.) and cloned into the pCR-Blunt vector *via* blunt-end ligation (2.3.7.). Competent cells of *E. coli* TOP10 were then transformed with the ligation products and the screening procedure for successfully transformed cells was carried out as described previously. Resulting plasmids were isolated from overnight cultures and verified by sequencing.

In a next step, it was necessary to remove an internal NcoI restriction site within the gene sequences *OeEst030*, *OeEst228* and *OeEst905*. This was accomplished by site directed mutagenesis (2.3.11.)

introducing a silent mutation at position 51 within the nucleotide sequences of *OeEst030* and *OeEst228* and at position 54 within the sequence of *OeEst905*. After amplification in *E. coli* TOP10 cells, the modified plasmids were checked by sequencing for the presence of the nucleotide substitution.

Following this, the modified constructs as well as the destination vector pET-32a(+) were digested with appropriate restriction enzymes (2.3.12.). Resulting DNA molecules were separated by agarose gel electrophoresis and the fragments of approximately 780 bp and 5,850 bp corresponding to the genes of interest and the pET-32a(+) backbone, respectively, were extracted from gel. Ligation of the coding sequences into the destination vector was then accomplished by means of the T4 DNA ligase in a reaction mix containing insert DNA and linearized plasmid DNA in a molar ratio of 3 to 1 (2.3.12.). Selection and amplification of selected constructs was again accomplished in cells of *E. coli* strain TOP10. For gene expression purposes, competent cells of *E. coli* BL21(DE3) pLysS were transformed with the constructs pET-32a(+)_*OeEst030sdm*, pET-32a(+)_*OeEst228sdm*, pET-32a(+)_*OeEst391* and pET-32a(+)_*OeEst905sdm*, as well as an unmodified pET-32a(+) vector.

3.4. Production of putative olive esterases in cells of *E. coli*

Expression cultures with a volume of 600 mL were set up (2.4.1.) and grown until an OD_{600} of around 0.8. Gene expression was induced by addition of IPTG, followed by further incubation overnight. Afterwards, cells were harvested by centrifugation and disrupted by enzymatic and mechanical means (2.4.1.). Recombinant proteins were then isolated from the crude bacterial lysate by immobilized metal ion affinity chromatography (IMAC) using a column matrix pre-charged with Ni^{2+} ions (2.4.2.). Resulting chromatography fractions were analyzed by SDS-PAGE (2.4.5.) followed by Coomassie Brillant Blue staining (2.4.6.1.) for the presence of the proteins of interest as well as for contaminations through endogenous *E. coli* proteins. In all purification approaches, elution fractions 1, 2 and 3 showed the presence of the desired proteins featuring sizes of around 46 to 47 kDa, while lacking any significant contaminations. Therefore, those fractions were combined and concentrated. Salts as well as imidazole derived from the elution buffer were replaced by sodium phosphate (100 mM, pH 7.4) (2.4.3.). Samples were then quantified by BCA assay (2.4.4.), diluted using the aforementioned buffer and supplemented with glycerol. The concentration of the final protein preparations buffered in 50 mM sodium phosphate (pH 7.4) was again determined by means of the BCA assay, while the quality was analyzed by SDS-PAGE (2.4.5.) combined with silver nitrate staining (2.4.6.2.). As shown in Figure 8, preparations of OeEst030, OeEst228, OeEst391 and OeEst905 contained the desired protein of approximately 46-47 kDa. The sample OeEst391, however, showed higher concentration of background proteins as indicated by clearly visible bands of various sizes.

Analysis of the reference protein preparation of PNAE produced using the expression vector pQE2 resulted in the detection of a large band of around 30 kDa representing the protein of interest equipped only with a C-terminal polyhistidine tag. A slightly visible smear below this band, however, indicated a small amount of degraded protein. The protein preparation produced using an unmodified pET-32a(+) vector contained the expected TRX tag protein in its monomeric (size of approx. 20 kDa) as well as in multimeric forms (sizes of around 40 and 80 kDa).

Table 3: Concentrations of recombinant protein preparations produced in course of this study. Calculations were done on basis of three dilutions with three technical replicates each. SD, standard deviation.

protein sample	concentration (µg/mL)	SD (%)
OeEst030	825	± 1.9
OeEst228	1,091	± 5.5
OeEst391	750	± 1.6
OeEst905	1,321	± 1.1
PNAE	4,207	± 8.6
TRX fusion protein	1,384	± 1.4

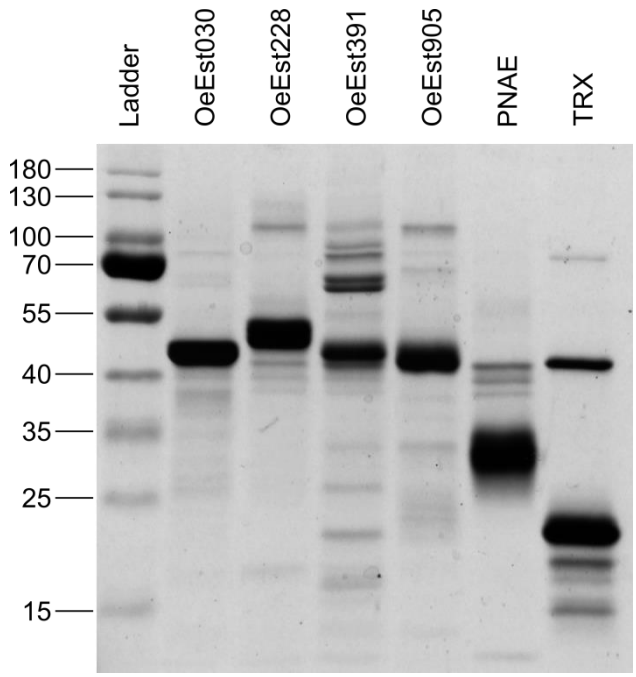

Figure 8: SDS-PAGE analysis of recombinant protein preparations produced in course of this study. Visualization was accomplished by subsequent staining of the gel with silver nitrate. Approximately one µg of each sample was applied to the gel. Numbers to the left indicate molecular mass of marker proteins in kDa (Ladder).

3.5. Characterization of newly identified candidates

3.5.1. Determination of unspecific esterase activity

In a first set of enzyme activity assays, the newly identified proteins were tested for their ability to hydrolyze the carboxylic esters of p-nitrophenyl acetate (pNPA) and p-nitrophenyl butyrate (pNPB). Both substrates are commonly used for the initial verification of general esterase activities of putative members of the α/β hydrolase fold superfamily. The proteins OeEst030, OeEst228, OeEst391, OeEst905 and PNAE as well as the TRX fusion protein were incubated with 0.5 mM of substrates and resulting release of p-nitrophenol (pNP) was monitored at 405 nm (2.5.1.). In order to calculate respective turnover rates, first the extinction coefficient of pNP under the applied conditions had to be determined. Therefore, a standard curve with different concentrations of the chromogenic compound was generated, resulting in an extinction of 30.215 per µmol. Additionally, autohydrolysis rates of pNPA and pNPB were determined and subtracted from the results of the kinetic measurements.

As shown in Table 4, all candidates as well as the PNAE showed detectable activity towards the tested substrates. The TRX fusion protein, in contrast, did not lead to conversion rates significantly higher than autohydrolsis, neither with pNPA nor with pNPB.

Table 4: Enzyme activity of recombinant proteins against the substrates p-nitrophenyl acetate (pNPA) and p-nitrophenyl butyrate (pNPB). One unit of esterase activity was defined as the amount of protein releasing one µmol of p-nitrophenol per minute.

	specific activity (U per g)	
protein sample	**pNPA**	**pNPB**
OeEst030	234.6 ± 1.4	675.1 ± 7.3
OeEst228	147.4 ± 2.7	1,121.9 ± 2.3
OeEst391	302.5 ± 5.3	404.1 ± 5.9
OeEst905	1,915.6 ± 42.9	1,700.5 ± 26.4
PNAE	98.1 ± 1.0	35.5 ± 0.7
TRX fusion protein	3.0 ± 2.1	1.5 ± 2.0

3.5.2. Enzyme activity assays towards olive secoiridoids and derivatives

The aim of this study was the identification of methyl esterases with catalytic activity towards specific oleoside-type secoiridoids from *O. europaea*. Therefore, first assays with olive endogenous compounds were performed using ligstroside, oleuropein and oleoside 11-methyl ester (OME) as

substrates (2.5.2.). A standard reaction mixture consisted of 0.5 mM of substrate and 100 µg/mL of recombinant protein. After one hour of incubation at 30°C, reactions were stopped and subsequently analyzed by LC-MS (2.6.1.1.). However, no enzymatic activity of the recombinant proteins against the tested secoiridoids could be detected. Thus, only peaks corresponding to the substrates ligstroside (Rt of 45.11 min), oleuropein (Rt of 41.68 min) or oleoside 11-methyl ester (Rt of 30.34 min) were visible (Figure 9).

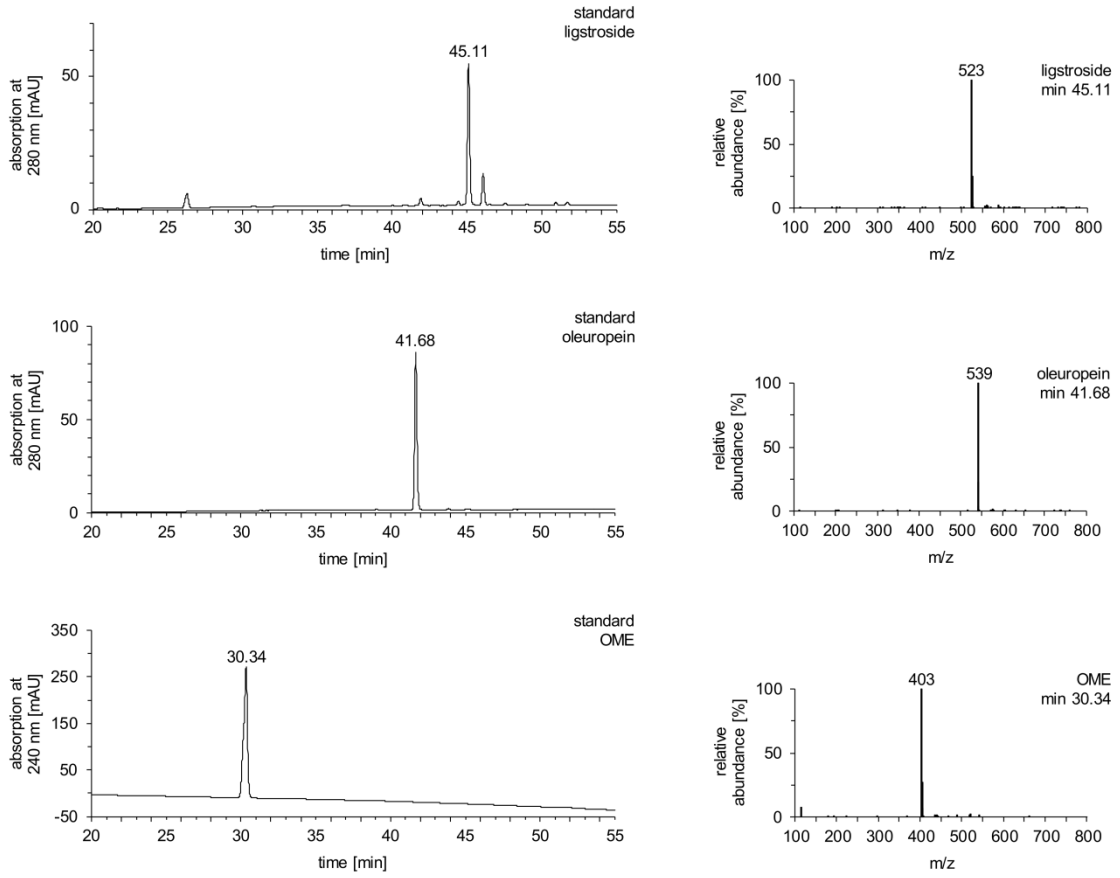

Figure 9: LC-MS analysis of ligstroside, oleuropein and oleoside 11-methyl ester standards. Separation was performed using the LC-MS method described in chapter 2.6.1. Chromatograms on the left show HPLC analysis of authentic standards, while chromatograms on the right provide information on corresponding mass spectrum. Under the applied conditions, ligstroside features a retention time of 45.11 min with an m/z value of 523 $[M-H]^-$, while oleuropein elutes after 41.68 min showing an m/z value of 539 $[M-H]^-$. Oleoside 11-methyl ester (OME) elutes after 30.34 min featuring an m/z value of 403 $[M-H]^-$.

Based on the proposed degradation routes described earlier (1.4.2.), it can be assumed that not only secoiridoid glycosides, but also corresponding aglycones could undergo demethylation by specific endogenous esterases. Hence, the deglycosylated forms of ligstroside, oleuropein and

oleoside 11-methyl ester were also tested as substrates for the recombinant enzymes. However, those aglycones are unstable and highly reactive compounds known to feature strong protein cross-linking activity as demonstrated by Konno et al. exemplarily for oleuropein aglycone [67]. This led to the assumption that instead of directly supplementing respective compounds as substrates to the reaction mix, a constant generation of these during the incubation time could be preferred. Therefore, the secoiridoids ligstroside, oleuropein and oleoside 11-methyl ester were applied to a reaction mixture containing recombinant esterase and β-glucosidase from almond (2.5.3.). The concentration of β-glucosidase has been adjusted to generate less than 1 mM of deglycosylation product during one hour of incubation, ensuring constant release of minute amounts of substrate for the determination of specific esterase activity. As depicted in Figure 10, hydrolysis of the glucosidic bond within ligstroside led to the formation of four new peaks detectable with the applied LC-MS method at min 44.27, 44.74, 45.25 and 45.66. With the major ion being 361 $[M-H]^-$ as determined by means of negative ion mode, those peaks corresponded to different derivatives of ligstroside aglycone. Similarly, deglycosylation of oleuropein led to four peaks (Rt of 40.59, 41.00, 41.45 and 41.86 min) representing different isomeres of oleuropein aglycone as indicated by a major ion of 377 $[M-H]^-$. Analysis of the conversion products of oleoside 11-methyl ester revealed the presence of two peaks representing substances eluting at min 26.15 and 26.63 as well as a third peak at min 38.87 showing distinctive 'tailing'. All three peaks shared the same major ion of 241 $[M-H]^-$ leading to the assumption that corresponding substances were isomeres of elenolic acid. Furthermore, a peak featuring an elution time of 30.33 and the m/z of 403 $[M-H]^-$ was detectable indicating remaining amounts of oleoside 11-methyl ester.

The two-step assays including β-glucosidase and OeEst030 or OeEst228, in contrast, resulted in the generation of new compounds when applying the substrates ligstroside, oleuropein and oleoside 11-methyl ester respectively. The substance produced from ligstroside eluted at min 44.4 featuring a major m/z peak of 303 in negative ion mode (Figure 11), while the assays containing oleuropein yielded a compound with a retention time of 40.3 min and a major ion of 319 (Figure 12). A comparison with authentic standards could confirm that those peaks corresponded to oleocanthal (Rt of 44.38 min) and oleacein (Rt of 40.28 min). The conversion of oleoside 11-methyl ester through β-glucosidase and esterase activity generated a product eluting at min 23.3 (Figure 13). Corresponding MS analysis revealed an ion of 183 as major m/z peak, when negative ion mode was applied. Lacking an appropriate standard, however, it was not possible to confirm that the newly generated peak corresponded to the expected product, namely decarboxymethyl elenolic acid dialdehyde, which would result from demethylation of elenolic acid followed by non-enzymatic decarboxylation. Two-step assays containing β-glucosidase and OeEst391, OeEst905 or PNAE, in

contrast, did not led to the generation of compounds other than the products generated through deglycosylation (see Appendix, Supporting Figures 2-4).

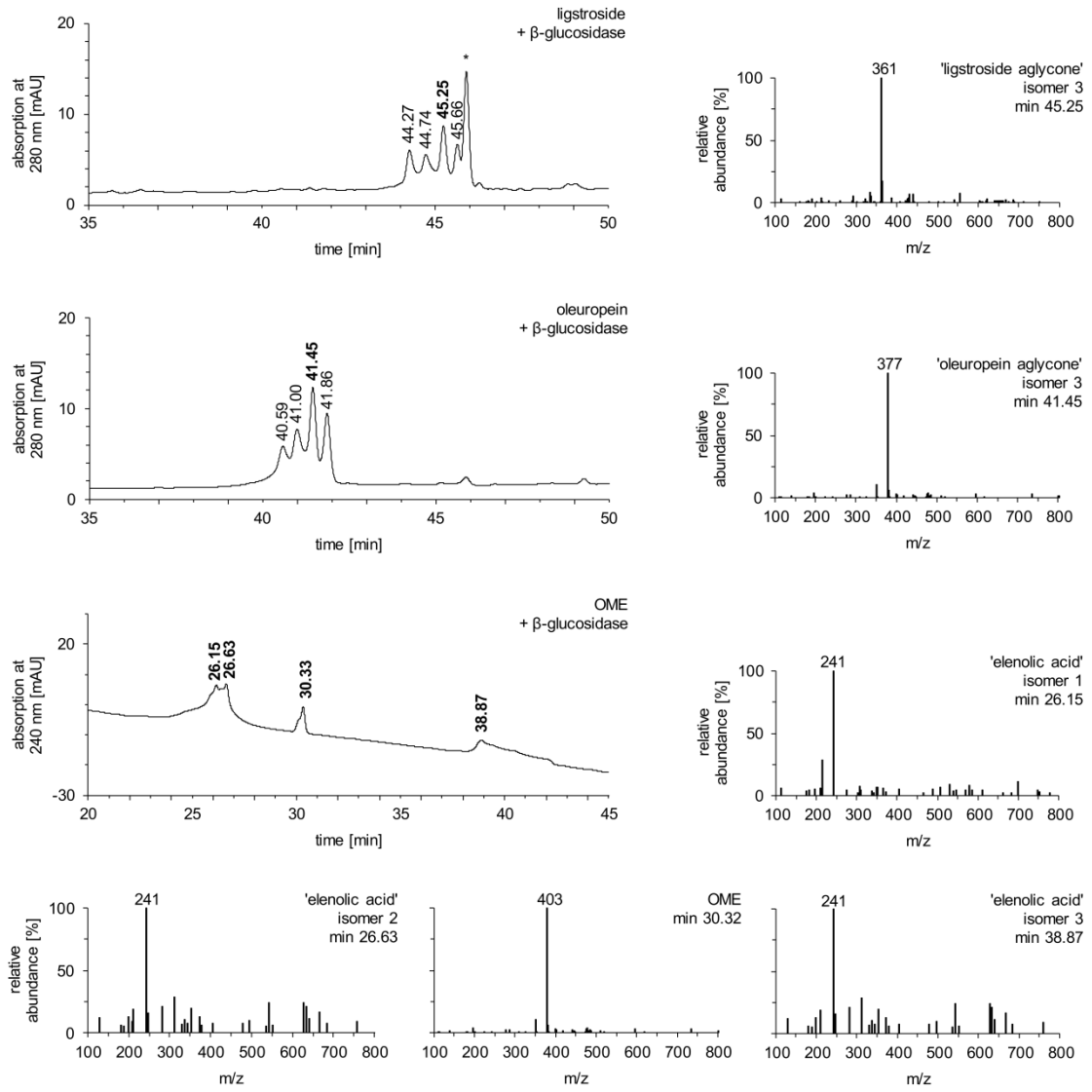

Figure 10: LC-MS analysis of deglycosylation products derived from ligstroside, oleuropein and oleoside 11-methyl ester. All three substances were incubated together with β-glucosidase from almonds for 1 h at 30°C. Reaction products were analyzed using the LC-MS method described in chapter 2.6.1. Deglycosylation of ligstroside and oleuropein led to the formation of four derivatives featuring differing elution times, while showing highly similar mass spectra when compared to each other. The peak marked with an asterisk, however, represents an impurity within the ligstroside preparation, which was not converted in any of the tested reaction approaches. Analysis of the conversion products derived from oleoside 11-methyl ester (OME) resulted in the detection of three aglycone isomers, eluting at min 26.15, 26.63 and 38.87, as well as remaining amounts of OME (min 30.33) as indicated by corresponding m/z values.

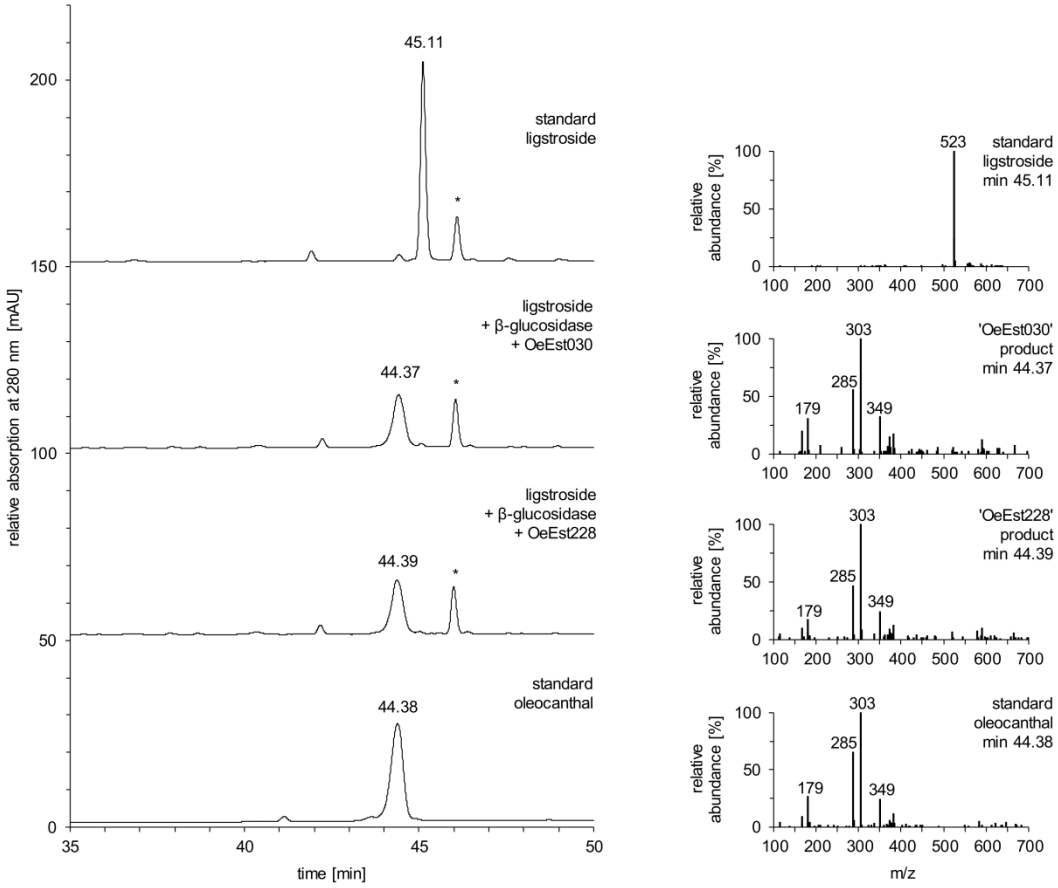

Figure 11: LC-MS analysis of assays for esterase activity of OeEst030 and OeEst228 towards ligstroside aglycone. The conversion of ligstroside (Rt of 45.11 min; m/z of 523) through β-glucosidase from almonds and either OeEst030 or OeEst228 yielded a compound with a highly similar retention time and mass spectrum compared to an oleocanthal standard (Rt of 44.38 min; major ion featuring an m/z of 303). The peak marked with an asterisk represents an impurity within the substrate preparation, which was not converted in any of the analyzed reaction approaches.

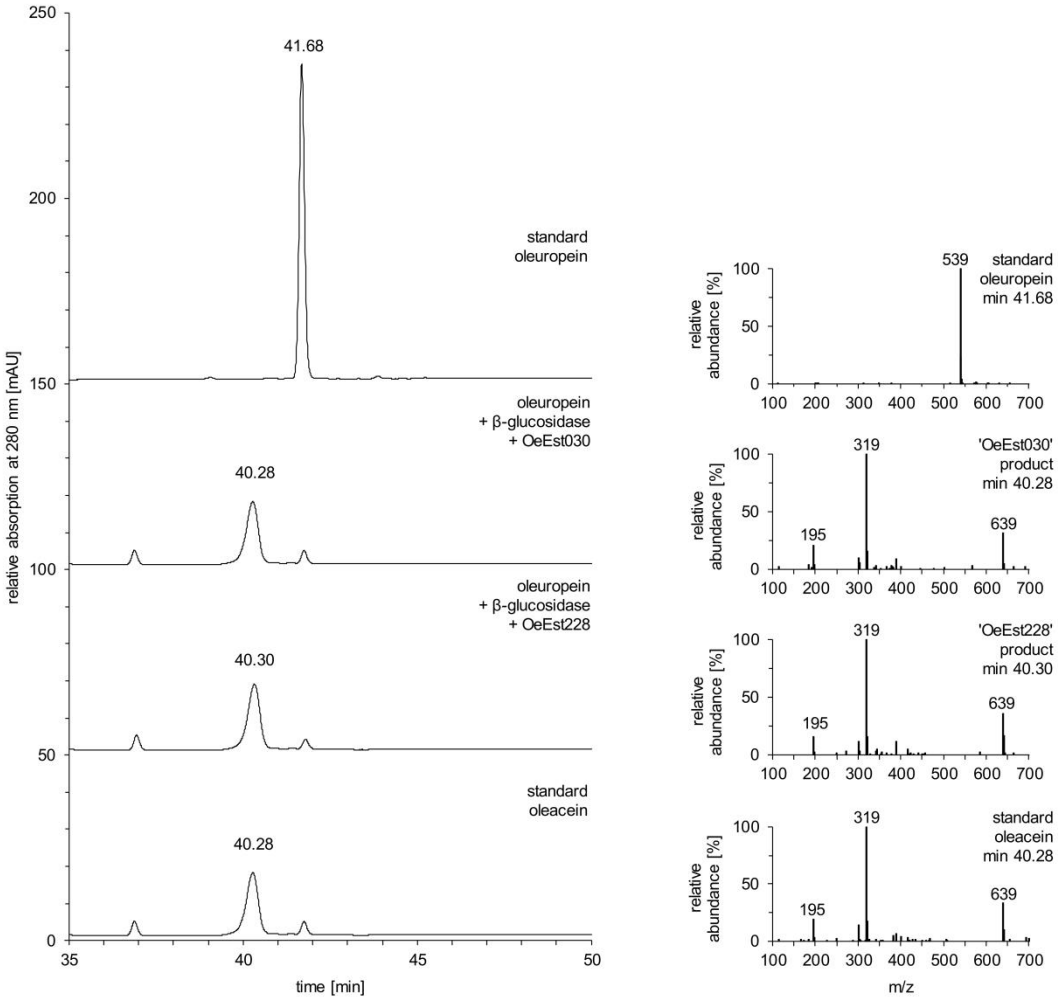

Figure 12: LC-MS analysis of assays for esterase activity of OeEst030 and OeEst228 towards oleuropein aglycone. The conversion of oleuropein (Rt of 41.68 min; m/z of 539) through β-glucosidase from almonds and either OeEst030 or OeEst228 yielded a compound featuring a highly similar retention time and mass spectrum compared to an oleacein standard (Rt of 40.28 min; major ion featuring an m/z of 319).

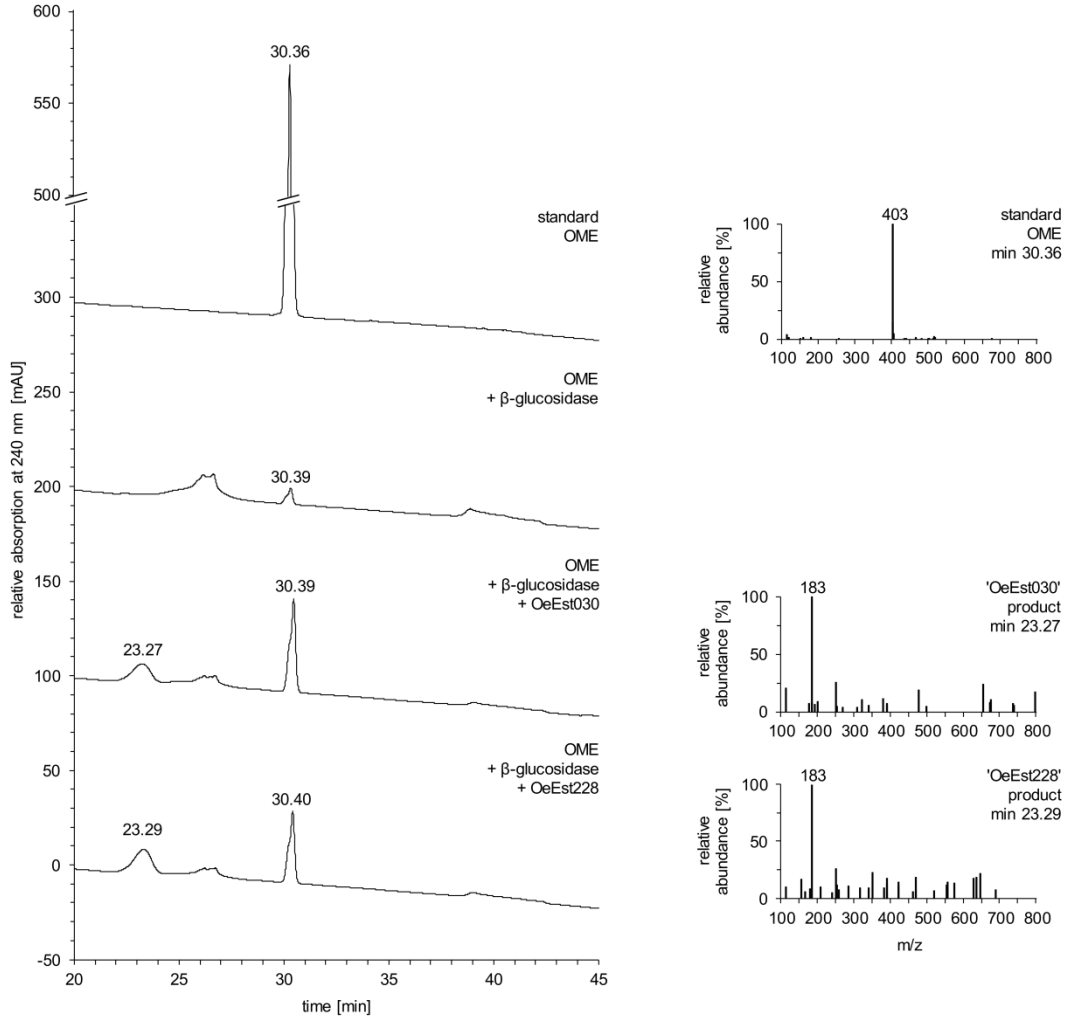

Figure 13: LC-MS analysis of assays for esterase activity of OeEst030 and OeEst228 towards elenolic acid. The conversion of OME (Rt of 30.36 min; m/z of 403) through β-glucosidase from almonds and either OeEst030 or OeEst228 yielded a compound with a retention time of 23.27 and 23.29 min, respectively. Corresponding mass spectrum showed an m/z of 183 as major ion measured in negative ion mode.

3.5.3. Screening for further substrates

3.5.3.1. Verification of substrate specificity

After the successful identification of deglycosylated oleoside derivatives as substrates for OeEst030 and OeEst228, first verification of substrate specificity was accomplished using two structurally similar compounds, namely strictosidine and strictosidine aglycone. Appropriate activity assays consisted of 0.15 mM strictosidine and 100 µg/mL of recombinant enzyme buffered either in sodium phosphate (pH 7.4) or sodium citrate (pH 5.0). For the generation of corresponding aglycone, strictosidine glucosidase (SG) was applied to the assay composition. After one hour of incubation at 30°C, samples were analyzed by LC-MS (2.6.1.3.).

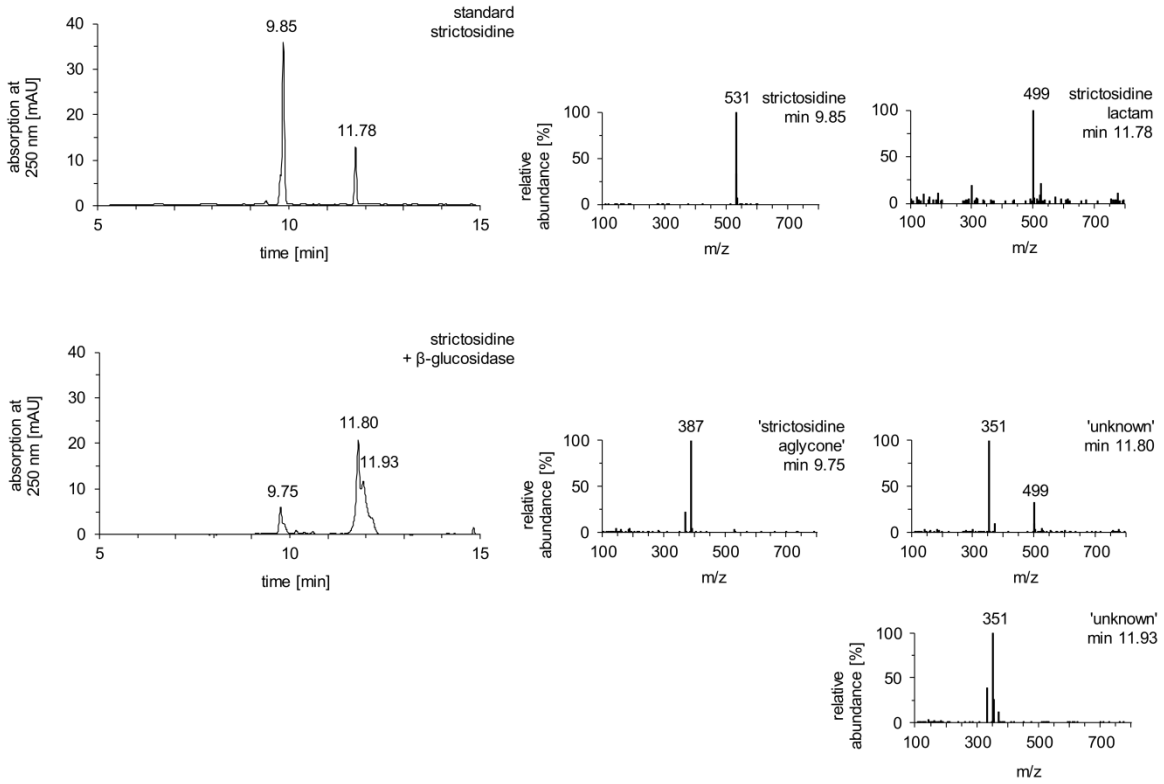

Figure 14: LC-MS of strictosidine and its deglycosylation product. A standard preparation of strictosidine was treated according to the reaction conditions and subsequently analyzed. Resulting peaks corresponded to strictosidine (Rt of 9.85 min and m/z of 531 $(M+H)^+$) and its degradation product strictosidine lactam (Rt of 11.78 min and m/z of 499 $(M+H)^+$). In a second reaction, the same strictosidine preparation was incubated together with a protein preparation of SG leading, amongst others, to the formation of strictosidine aglycone (Rt of 9.75 min and m/z of 387 $(M+H)^+$).

Under the applied conditions no enzymatic conversion of strictosidine (530.57 g/mol) through the examined esterases could be observed. Accordingly, only strictosidine (Rt of 9.85 min; m/z of 531) and its degradation product strictosidine lactam (Rt of 11.78 min; m/z of 499), which was already present in the substrate preparation, were detected (Figure 14). Deglycosylation of strictosidine resulted in the formation of three peaks detectable at a wavelength of 250 nm. The first peak featured an elution time of 9.75 min and an m/z value of 387 indicating successful generation of strictosidine aglycone (368.43 g/mol). The other two peaks detectable at min 11.80 and 11.93 did not show any baseline separation. The former peak seemed to result from at least two substances with highly similar elution times. While the corresponding m/z value of 351 could not be identified, the co-eluting compound featuring an m/z value of 499 could be associated with strictosidine lactam (498.53 g/mol). Also the peak at min 11.93 represented a substance with an m/z value of 351.

Further conversion of strictosidine aglycone by esterase activity, however, could not be observed in any of the analyzed samples.

3.5.3.2. Plant hormones

Due to remarkable sequence homology of the newly identified esterases with MJE and SABP2, it was assumed that they may also possess activity towards similar substrates. Therefore, in another set of enzyme activity assays, the plant hormones methyl jasmonate (MeJA), methyl salicylate (MeSA) and methyl indole-3-acetate (MeIAA) were tested as substrates for the recombinant enzymes (2.5.4.). At first instance, 100 µg/mL of protein were incubated with 2 mM of substrate in sodium phosphate buffered reaction mixture. After 1 h at 30°C reactions were stopped and extracted with diethyl ether. The organic layer was then concentrated and analyzed by thin-layer chromatography on a silica gel plate (2.6.3.). Reference compounds were treated the same way. As depictured in Figure 15, all assay approaches with MeJA as substrate, except for the one containing the TRX fusion protein, resulted in the formation of a compound with the same retention factor (Rf) compared to a jasmonic acid (JA) standard. Furthermore, all four esterases from *O. europaea* produced a second compound showing an Rf value even higher than the one of MeJA. MeIAA was also clearly converted by the newly identified esterases, but only barely by PNAE. Especially OeEst030 and OeEst228 showed significant activity resulting in the complete conversion of the substrate into indole acetic acid (IAA). The reaction mixtures containing OeEst391 and OeEst905 resulted also here in the formation of two products: one with the same Rf compared to IAA and one substance with an Rf value higher than the one of MeIAA. PNAE, in contrast, generated only traces of product as indicated by a weak spot corresponding to IAA. MeSA, on the other hand, was only converted by OeEst905 into a significant concentration of a substance featuring the same Rf like a salicylic acid (SA) standard.

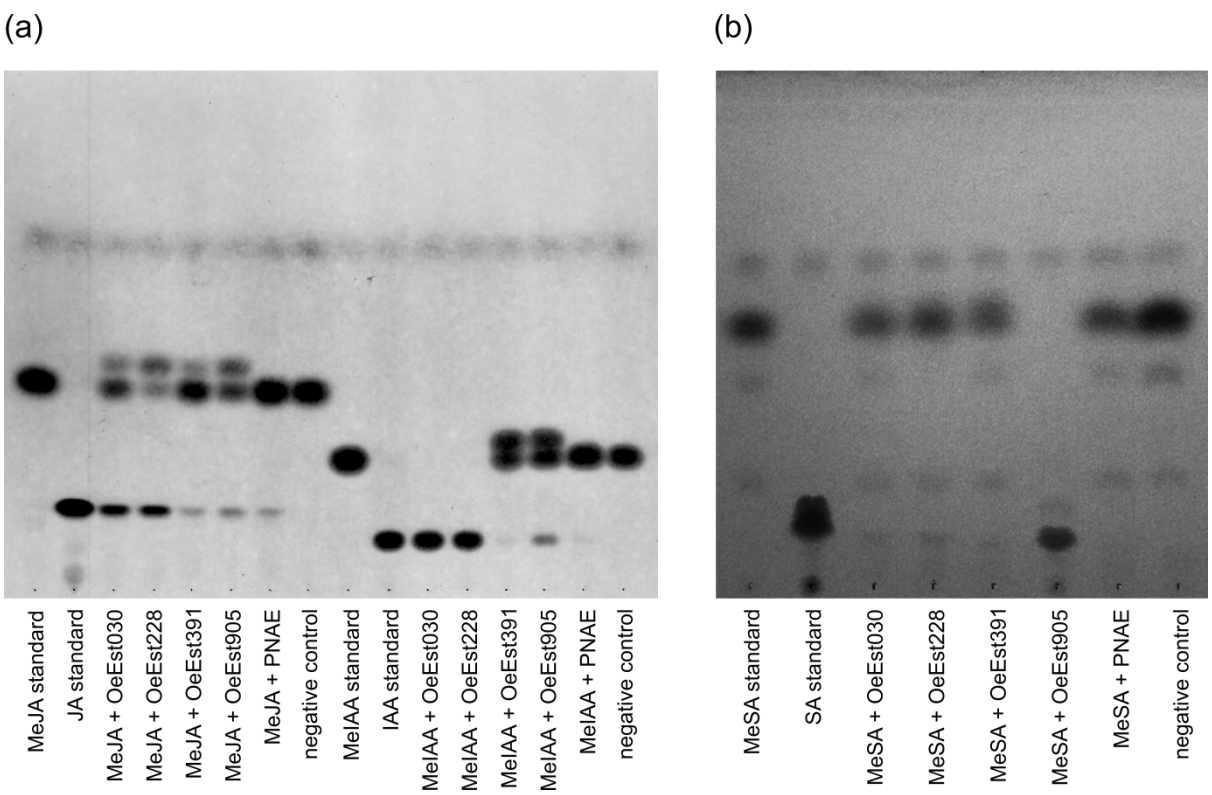

Figure 15: TLC analysis of the reaction products derived from the incubation of recombinant esterases with MeJA, MeIAA and MeSA. Reaction mixtures consisted of 2 mM of substrate and 100 µg/mL of either recombinant esterases or TRX fusion protein ('negative control'). After incubation, samples were first extracted with diethyl ether and then applied to a silica gel. Development of the TLC was performed using a solvent system consisting of n-hexane, ethyl acetate and acetic acid. (a) TLC plates harboring MeJA, MeIAA and derivatives were sprayed with p-anisaldehyde coloration solution and subsequently 'burned'. (b) Visualization of MeSA and its derivatives on TLC plates, in contrast, was accomplished under UV light.

Following up on those first assays visualized by TLC, further reactions were performed for subsequent analysis by GC-MS and LC-MS. In this way, the identity of generated products, especially those lacking appropriate reference compounds, could be verified on basis of corresponding mass data. Therefore, reaction mixtures containing MeJA as substrate were processed as described before, but additionally treated with a silylation reagent right before analysis by GC-MS (2.6.2.).

As depicted in Figure 16, enzymatic conversion of MeJA by the tested esterases led to the production of a compound with the same retention time (10.63 min) and mass fragmentation pattern compared to the JA standard. Furthermore, all esterases from *O. europaea* generated a second product with a retention time of 10.32 min. The ratio between the two produced compounds varied significantly depending on the enzyme used. In case of OeEst905, the unidentified product was generated in amounts even higher than those observed for JA as indicated by the signal intensity. A comparison of corresponding mass spectrum with data of available standards showed a high similarity to the fragmentation pattern of MeJA. However, both differed in the ion with the highest detected m/z

value: 224 for MeJA and 238 in case of the unidentified compound. A comparison of the mass fragmentation pattern with those of published JA derivatives led to the assumption that this additional product could be ethyl jasmonate (EtJA) [101]. Due to the lack of an appropriate standard, however, this assumption could not be finally proven.

Liquid chromatography analysis of assays with MeIAA (2.6.1.2.), on the other hand, required a modification of the inactivation procedure. Reactions were stopped by addition of one volume of ice-cold acetonitrile. Samples were then centrifuged and subsequently analyzed by LC-MS.

As already indicated by TLC, the esterases OeEst030 and OeEst228 both completely converted MeIAA (Rt of 7.40 min) into a compound featuring the same retention time (Rt of 3.00 min) and mass-to-charge ratio (m/z of 176) compared to the IAA standard (Figure 17). The recombinant enzymes OeEst391 and OeEst905, in contrast, generated two products: one compound with the aforementioned characteristics and another compound showing a retention time of 8.76 min. Mass spectrometry analysis of this product revealed an m/z value of 204 measured in positive ion mode. Hence, the unknown MeIAA derivative featured, similar to the unidentified product detected in the MeJA assays, an m/z value increase of + 14 compared to the substrate. Also here, a comparison with published mass spectra of IAA derivatives revealed a high similarity with its ethylated form, namely ethyl indole-3-acetate (EtIAA). LC-MS analysis of an appropriate standard confirmed this assumption. Interestingly, assays containing MeIAA and OeEst030 or OeEst228 were lacking this additional product, even though two products were observed when MeJA was used as substrate. Therefore, their activity towards MeIAA was further investigated in assays with modified reaction conditions. A reduction of enzyme concentration from 100 to 10 µg/mL in combination with a decrease of incubation time from 1 h to 20 min, for example, led to the production of the same substances as observed with OeEst391 and OeEst905 (see Appendix, Supporting Figure 5).

Since the reaction mixtures consisted of 0.5 % (v/v) ethanol derived from the substrate stock solution, it was suggested that EtIAA was produced either by ethylation of IAA or by transesterification of MeIAA with ethanol. Therefore, all assays were repeated using a substrate preparation dissolved in methanol or DMSO instead of ethanol. Subsequent analysis of corresponding reactions confirmed the presence of IAA as the only conversion product. In a next step, recombinant olive esterases were incubated together with IAA in the presence of 0.5 % (v/v) ethanol in order to check if esterification could be observed. LC-MS analysis of those reactions, however, did not result in the detection of any conversion products. Thus, it was concluded that EtIAA is generated from MeIAA through enzymatic conversion in the presence of ethanol.

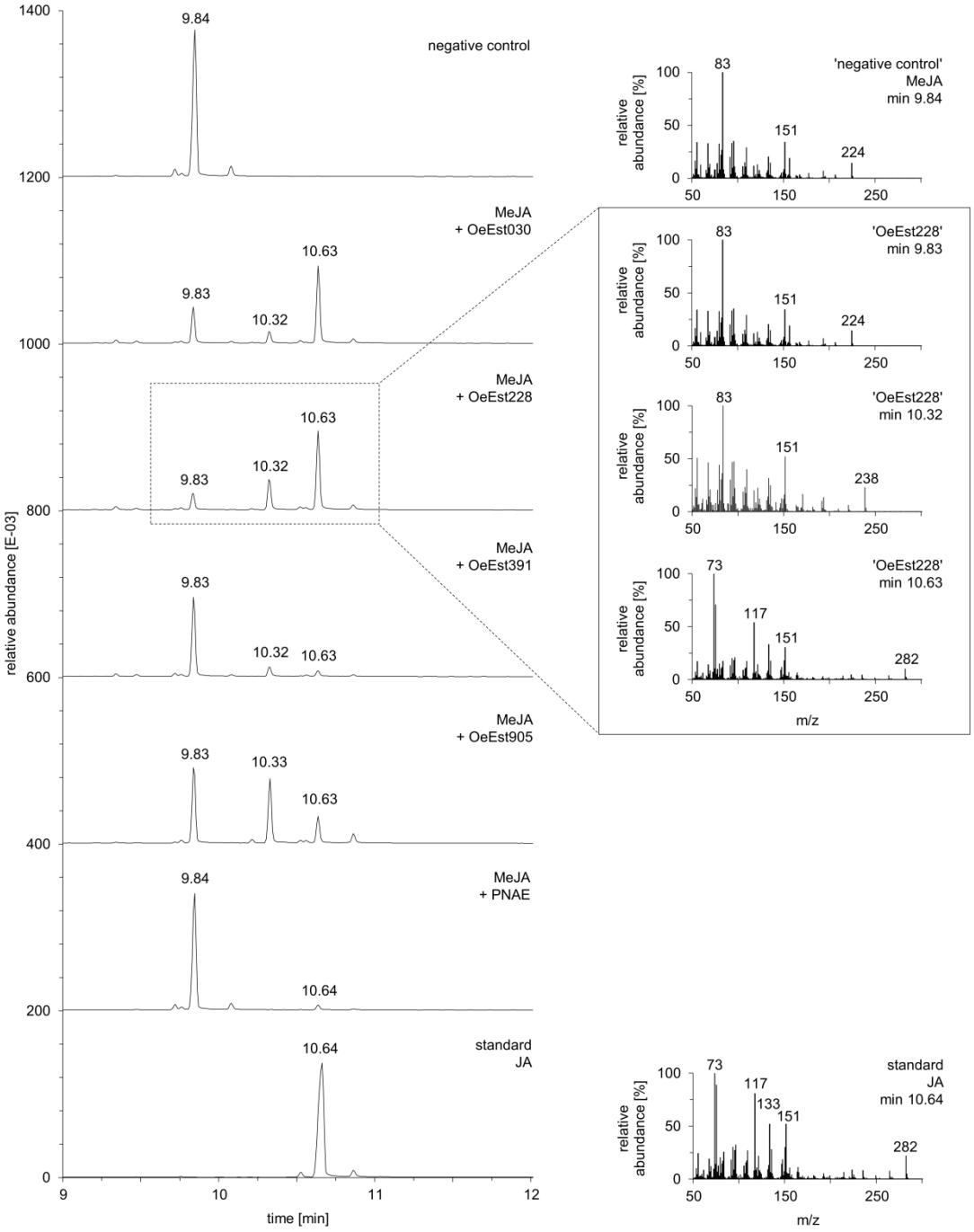

Figure 16: GC-MS analysis of the reaction products generated during the incubation of recombinant esterases with MeJA. TRX fusion protein was also incubated with substrate in order to serve as a negative control. Reaction mixtures consisted of 2 mM of substrate and 100 µg/mL of protein preparation. After incubation, samples were first extracted with diethyl ether and then treated with silylation reagent. Subsequently, analysis of MeJA and its derivatives was performed by GC-MS.

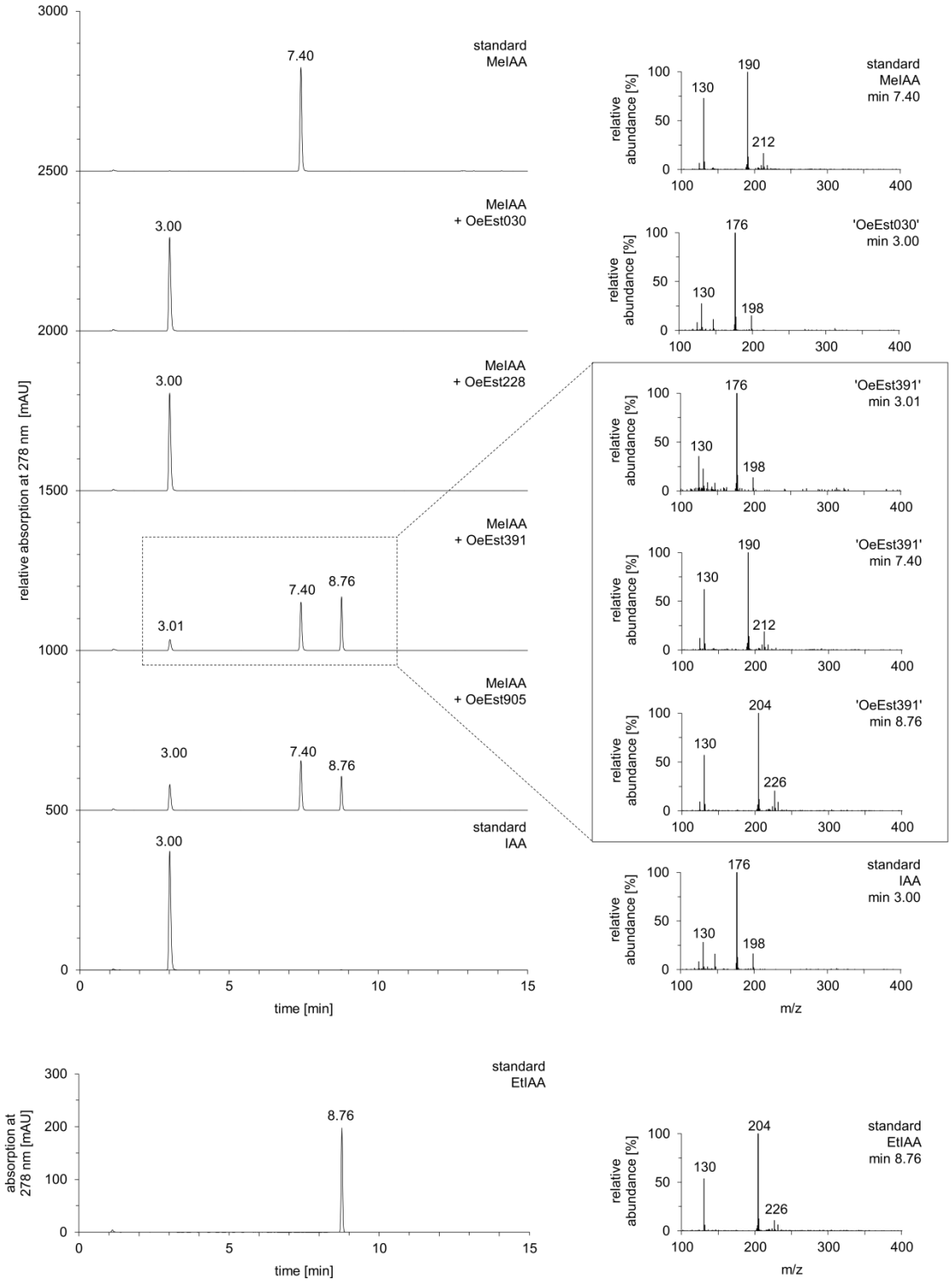

Figure 17: LC-MS analysis of reaction products generated during the incubation of recombinant esterases with MeIAA. Reaction mixtures consisted of 2 mM of substrate and 100 µg/mL of protein preparation. Detection of MeIAA and derivatives was performed at a wavelength of 278 nm, while corresponding mass-to-charge values were determined using the negative ionization mode.

Following up on this, a next set of assays was focused on the fate of EtIAA during the incubation time. Therefore, MeIAA, initially dissolved in ethanol, was incubated together with OeEst030 or OeEst288 for 2 h at 30°C. In intervals of 10 min, samples were taken and subsequently analyzed by LC. Peaks corresponding to MeIAA, IAA and EtIAA were integrated and resulting peak areas were plotted against the incubation time.

Incubation of MeIAA with OeEst030 resulted in increasing concentrations of IAA and EtIAA during the first 40 min (Figure 18). While IAA still continued to accumulate afterwards, levels of EtIAA declined continuously. A similar trend could be observed for reactions containing esterase OeEst228. Conversion rates, however, seemed to be higher in comparison to those of OeEst030. Thus, accumulation of EtIAA stopped already after 20 min of incubation showing slightly higher absorption intensity and thus concentration as described for the assays with OeEst030. Furthermore, after 100 min of incubation no remaining amounts of MeIAA could be detected. Nevertheless, concentration of IAA kept increasing during the complete incubation time. Thus, it can be concluded that MeIAA seemed to be converted first into both, IAA and EtIAA. When MeIAA concentrations significantly dropped until a total decline was reached, however, also EtIAA levels started to decrease in correlation with increasing IAA concentrations.

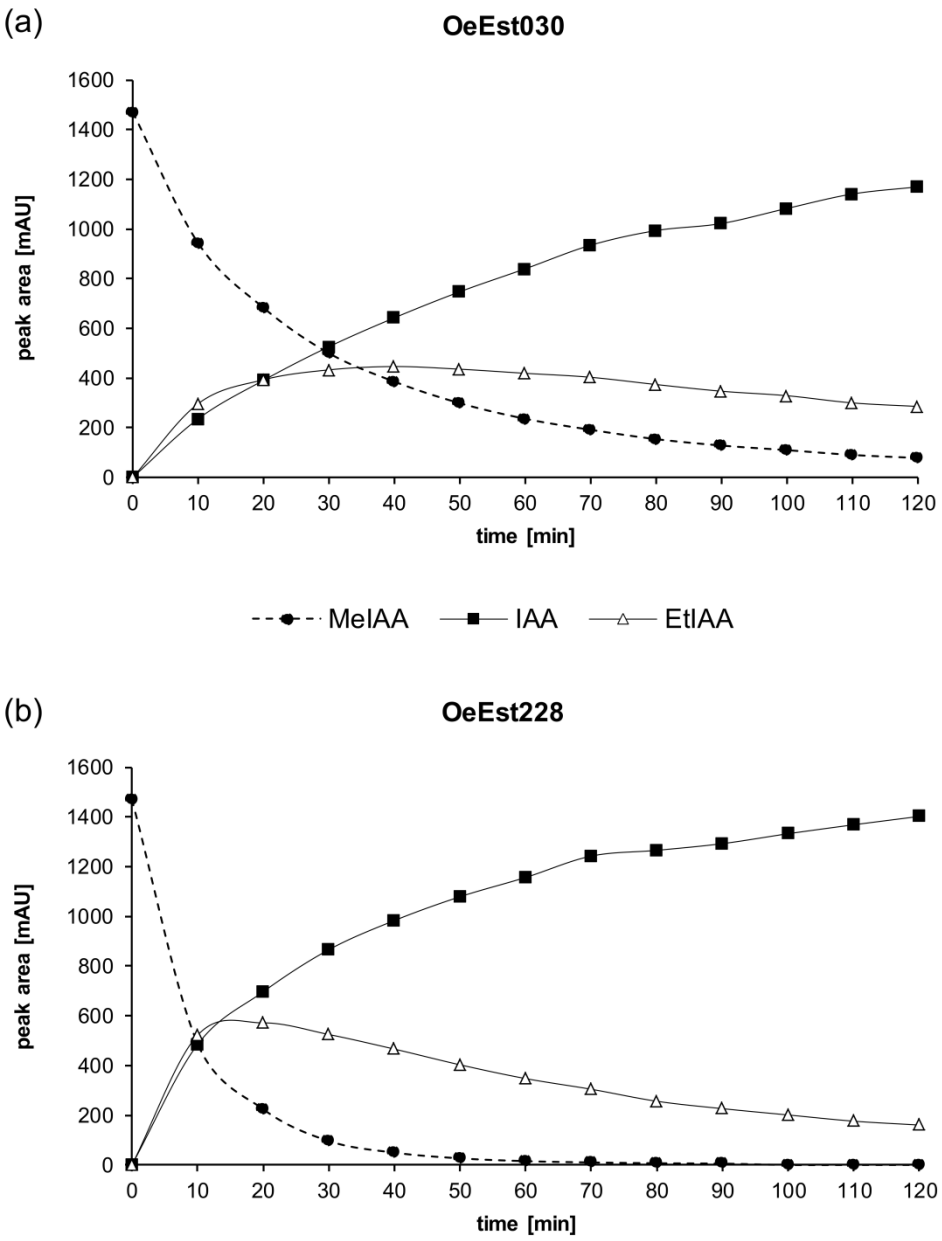

Figure 18: Generation of IAA and EtIAA during the incubation of MeIAA with (a) OeEst030 or (b) OeEst228. Samples were taken in intervals of 10 min during a total incubation time of 120 min and subsequently analyzed by LC. Relative quantities of the three compounds were determined by respective absorption intensity at 278 nm.

3.6. Homology modeling of OeEst030 and OeEst228

While all tested olive esterases showed activity towards several methyl esters, only OeEst030 and OeEst228 accepted deglycosylated oleoside-type secoiridoid derivatives as substrates. Based on previous MSA analysis (3.1.) the predicted catalytic amino acids serine and histidine could be identified in both proteins (OeEst030: Ser83 and His240; OeEst228: Ser83 and His241). The position of the acidic member of the catalytic triad typical for α/β hydrolase fold enzymes, on the other hand,

could not be located so far. Interestingly, the sequence segment around the expected position is highly conserved in both proteins. Thus, OeEst030 and OeEst228 share an identical amino acid composition between position 186-233 and 187-234, respectively, with the only different amino acid being Ser212 in OeEst030 and Thr213 in OeEst228. In order to identify acidic residues which could represent a potential member of the catalytic triad, the 3D structure of both proteins was simulated.

Homology modeling was performed by means of the SWISS-MODEL server using the crystal structure of the PNAE from *R. serpentina* (PDB accession code: 2WFL.1.A) as a template. To evaluate the quality of resulting models, GMQE (Global Model Quality Estimation) and QMEAN were determined. Respective calculations resulted in a GMQE of 0.73 and a QMEAN of -2.73 for OeEst030, while the model of OeEs288 featured a GMQE value of 0.74 and a QMEAN value of -2.06. Analysis of the amino acid torsion angles within the models of OeEst030 and OeEst228 resulted in Ramachandran plots showing 94.8 % and 95.7 %, respectively, of the amino acids in the favored regions. Therefore, generated models were considered reliable. When compared to the sequence of PNAE, however, both OeEst030 as well as OeEst228 showed variations in the amino acid sequence segment in close proximity to the expected position of the acidic member of the catalytic triad. This lack of homology in respective region led to a low local quality estimates for the position 212 for the model of OeEst030 and in position 213 for the model of OeEst228 (Figure 20).

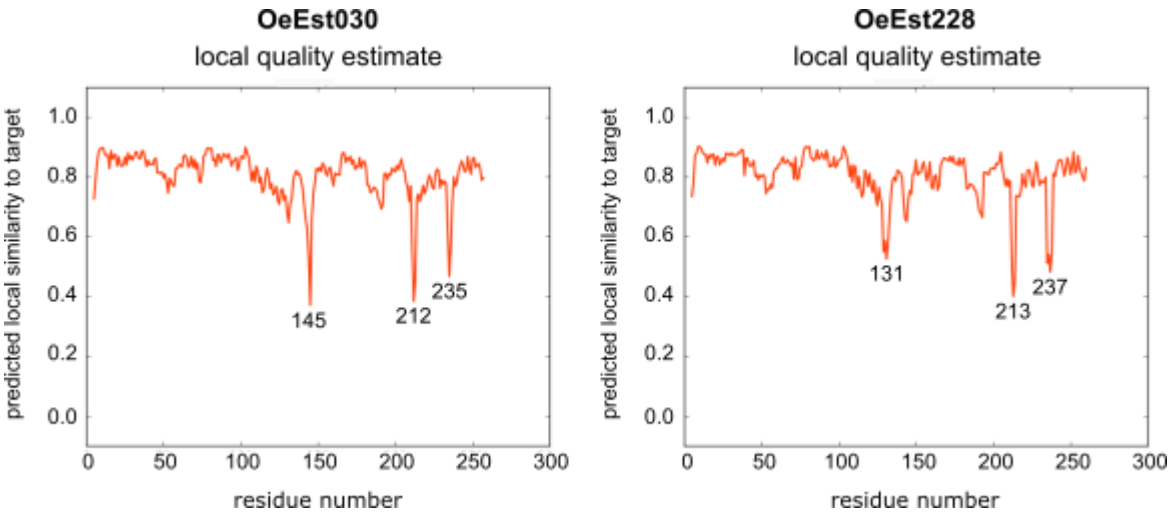

Figure 19: Local quality estimate for the amino acids within the generated 3D models of OeEst030 and OeEst228. Calculations are based on the QMEAN-score analysis implemented into the SWISS-MODEL server.

First, the protein model of OeEst030 was superimposed with the model obtained for OeEst228 revealing highly similar 3D structures (Figure 20a). Explicit differences could be only observed in the

region at the C-terminal site of helix αA and between β8 sheet and helix αH. Regions expected to form the active binding site, however, did not show any deviations. Therefore, all further analyses of the 3D structures were illustrated in Figure 20 using the example of OeEst030. Comparison of the structure of OeEst030 with PNAE revealed a siginificant difference in the region between β7 and αG (Figure 20b, 20c). Thus, according to the generated model, OeEst030 as well as OeEst228 both showed an extra turn of helix αG (Figure 20c), while the corresponding region of the PNAE is forming a loop towards the catalytic center. However, this structural feature of the reference protein represents a crucial element as it places the catalytic aspartate into the spatial proximity of His244 (Figure 20e). Since the models of OeEst030 and OeEst228 both featured a low local quality estimate for the region of this 'extra turn' of helix αG, the lack of aforementioned loop towards the catalytic histidine in the generated 3D structures could be due to inaccuracy of the models. Despite the aforementioned deviation, a high similarity between PNAE crystal structure and the generated models of OeEst030 and OeEst228 could be noted. Thus, the 'cap domain' which has been described for the PNAE [77] seems to be present in both olive proteins (Figure 20d). Based on the superimposed models it can be suggested that also in case of OeEst030 and OeEst228 this domain is formed by three α helices (αD, αE, αF) and two β-sheets (β5, β6).

As shown in the MSA (3.1.), OeEst030 as well as OeEst228 both possess several acidic amino acids (OeEst030: Glu213, Glu215 and Aps217; OeEst228: Glu214, Glu216 and Asp218) in close proximity to the expected position of the catalytic acidic residue. On basis of the 3D models, however, only Glu214 and Glu215 of OeEst030 and OeEst228, respectively, seem to be positioned in a way that could enable molecular interactions with the proposed catalytic histidine (Figure 20f).

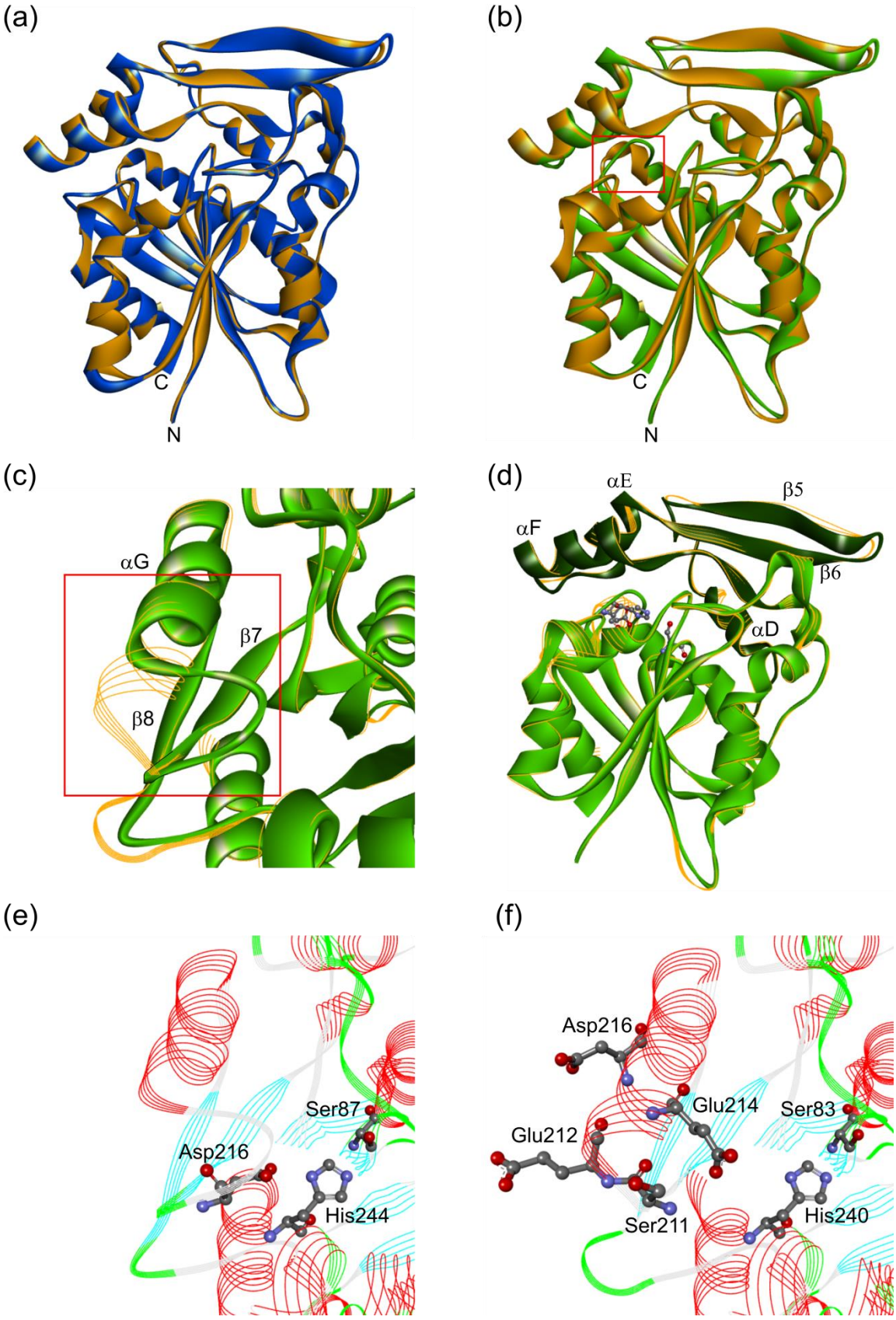

Figure 20: The predicted 3D structures of OeEst030 and OeEst228 in comparison with the crystal structure of PNAE. The generated model of OeEst030 (orange) was superimposed with (a) the one of OeEst228 (blue) and (b) the available crystal structure of PNAE (green). (c) The red frame highlights an area within the 3D structure of OeEst030 that differs significantly

from the reference model and therefore, is shown again from another perspective. (d) The structural element of the cap-domain (dark green) described for the PNAE is also present in a highly similar arrangement in the model of OeEst030. The catalytic amino acids of PNAE are highlighted as ball and stick models. (e) A more detailed illustration of the catalytic triad using a line ribbon model format for the PNAE structure. (f) Presentation of the OeEst030 model in the same way as described for (e), highlighting acidic amino acids within the seventh α helix structure (αG). As indicated by MSA of the protein sequences, the amino acid position of Ser211 is corresponding to the position of the catalytic aspartate in PNAE and therefore, is also highlighted.

3.7. Site directed mutagenesis for identification of catalytic amino acids

As indicated by the *in silico* studies, glutamic acid in position 214 and 215 within the amino acid sequence of OeEst030 and OeEst228, respectively, is expected to represent the acidic member of the catalytic triad. This assumption should be confirmed in the following experiments by means of mutagenesis studies using the example of OeEst030. Therefore, the nucleotide in position 641 (thymine) was substituted by cytosine resulting in an amino acid exchange at position 215 from glutamic acid (G) to alanine (A) in corresponding protein. Additionally, two acidic amino acids located in close proximity, glutamic acid 212 and aspartic acid 216, were also investigated for their impact on the enzyme activity. The fourth mutation approach, however, was focused on amino acid position 211, which was initially assumed to harbor the acidic member of the catalytic triad as indicated by MSA (3.1.). Since the amino acid sequence of OeEst030 featured a serine at this position, it was of interest to verify if replacement with aspartic acid would somehow result in modified esterase activity. Thus, a total of four muteins were generated featuring the amino acid exchanges S211D, E212A, E214A and D216A. All mutations were performed by site-directed mutagenesis (2.3.11.) of the coding sequence OeEst030 within the pCR-Blunt vector using the oligonucleotides no 23-30 (2.1.2.). Subsequent introduction into a bacterial expression system and the following generation of corresponding protein preparations was performed as described before (3.4.). Analysis of the quantity (Table 5) and the quality (Figure 21) of the protein samples revealed results comparable to those of the wild-type protein preparation (see Table 3 and Figure 8). It has to be noted, however, that the protein preparation of OeEst030-E212A showed the presence of smear below the band of around 46 kDA. This could be an indicator for starting protein degradation. Furthermore, in sample OeEst030-E214A the intensity of the band corresponding to the protein of interest was weaker compared to the other samples analyzed. This observation was accompanied by slightly more visible background proteins of various sizes.

Table 5: Concentration of recombinant protein preparations of OeEst030 muteins. Calculations were done on basis of three dilutions with three technical replicates each. SD, standard deviation

protein sample	concentration [µg/mL]	SD [%]
OeEst030-S211D	1,193	± 4.7
OeEst030-E212A	1,104	± 4.7
OeEst030-E214A	973	± 5.9
OeEst030-D216A	1,295	± 3.8

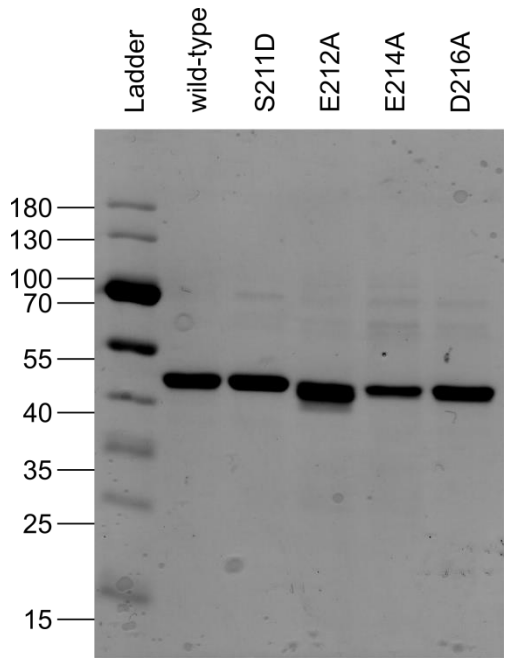

Figure 21: SDS-PAGE analysis of the protein preparations generated in course of mutagenesis studies. Visualization was accomplished by subsequent staining of the gel with silver nitrate. Approximately 1-1.2 µg of each protein sample was applied to the gel. Sample 'wild-type' refers to the protein preparation OeEst030 described in chapter 3.4, while 'S211D', 'E212A', 'E214A' and 'D216A' refer to protein preparations of corresponding muteins. Numbers to the left indicate molecular mass of marker proteins in kDa.

In order to compare the muteins with the wild-type enzyme regarding their esterase activity, conversion rates were determined by means of enzyme activity assays with pNPA, pNPB and MeIAA. Assays with the artificial substrates pNPA and pNPB were performed the same ways as described before (2.5.1.). The procedure for enzyme activity analysis towards MeIAA (2.5.4.), in contrast, was modified: 10 µg/mL of protein preparation were incubated with 0.5 mM of MeIAA buffered in 50 mM sodium phosphate (pH 7.4) for 10 min. Assays were stopped and immediately analyzed by

LC (2.6.1.2.). On basis of resulting chromatograms, product quantity generated by the muteins was set in relation to the amount of IAA produced by wild-type OeEst030. All assays were performed in three independent approaches each including three technical replicates per sample.

As presented in Figure 22, the protein preparation OeEst030-E214A generated comparable low concentrations of product when incubated with the aforementioned substrates. While conversion of pNPA was decreased to around 56 %, the substances pNPB and MeIAA were demethylated at even lower rates. Mutations introduced at amino acid positions 212 and 216, in contrast, did not result in proteins with significantly different activities. Thus, protein sample OeEs030-E213A showed 70.6 %, 87.9 % and 98.1 % activity compared to the wild-type when tested with the substrates pNPA, pNPB and MeIAA, respectively. Similarly, conversion by OeEst030-D216A resulted in efficiencies between 71.2 % and 85.8 % when compared to the reference preparation. Assays containing OeEst030-S211D, on the other hand, yielded a higher product concentration than those containing the wild-type protein preparation.

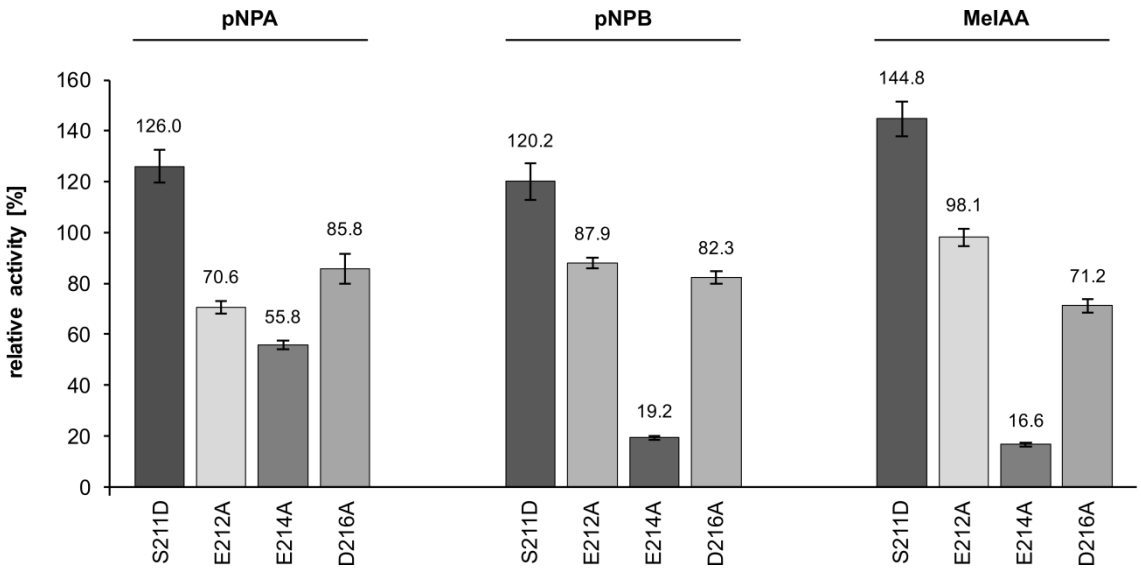

Figure 22: Enzymatic activity of OeEst030 muteins towards pNPA, pNPB and MeIAA. The amount of product generated by OeEst030-S211D, OeEst030-E212A, OeEst030-E214A and OeEst030-D216A was determined and set in relation to the results obtained with the wild-type protein. Assays were repeated three times with each measurement relying on three technical replicates per sample. Error bars represent the determined standard deviation.

3.8. Relative gene expression of OeEst030, OeEst228 and OeEst905 in tissues of *O. europaea*

For a more in-depth understanding of the potential role of OeEst030, OeEst228 and OeEst905 in the metabolism of *O. europaea*, relative gene expression levels in different types of tissue were analyzed

by qPCR. Therefore, young and mature leaves as well as green-black fruits were harvested from the same three trees of *O. europaea* L. cv. Canino and ground in liquid nitrogen. Sterile olive plantlets were grown from the remaining olive stones and subsequently used for the initiation of callus cultures. During subcultivation for 45 cycles in intervals of 14-16 days, two callus lines with different morphological characteristics were obtained: one generating intensive green cells with minimal contact to each other (Figure 23a) and another generating yellowish, more compact cell clusters (Figure 23b). From both lines, cultures grown on three different plates were harvested and treated as described before.

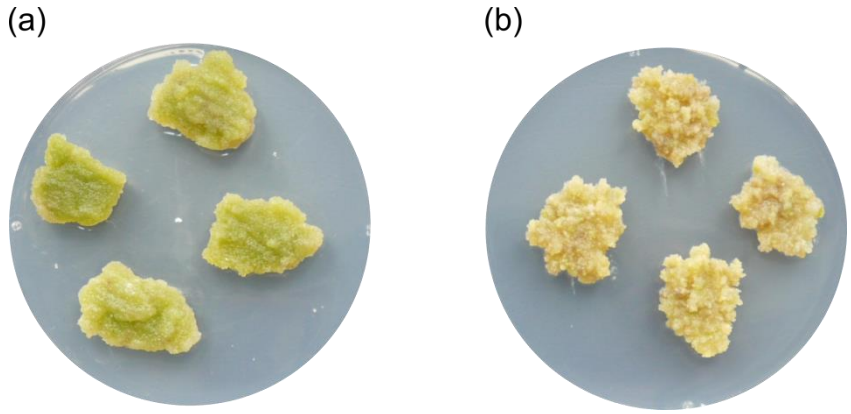

Figure 23: Callus cultures generated from tissue of *O. europaea* L. cv. Canino. Although both culture lines originate from the leaf tissue, they developed differently during subcultivation. (a) Callus line 'G' grew as friable cell clusters featuring a higher concentration of chlorophyll as indicated by its intense green color. (b) Callus line 'Y', in contrast, produced more compact cell clusters showing a more yellowish-brown color.

3.8.1.1. Isolation of total RNA and cDNA synthesis

Total RNA was isolated from the aforementioned tissue and quantified by means of a NanoDrop device. Only samples exhibiting a nucleic acid concentration of more than 150 ng/µL while featuring low protein and salt contaminations as indicated by 260 to 280 nm and 260 to 230 nm ratios higher than 1.8 and 1.5, respectively, were used for further procedures.

RNA integrity was then analyzed by agarose gel electrophoresis. The quality was considered sufficient for downstream experiments when both plastid-derived ribosomal sub units were represented by two compact and clearly visible bands of 1.5 and 2.9 kb size. Cloudy bands or the lack of evidence for the presence of the large ribosomal sub unit, however, were considered as indicators for a higher degree in nucleic acid degradation. As depicted in Figure 24, total RNA samples derived from leaf tissue and callus material passed those quality parameters. Although gel electrophoresis analysis of the RNA samples isolated from fruit tissue could proof the presence of the small ribosomal subunit,

no band corresponding to the large subunit could be detected. Several repetitions of the RNA isolation procedure, however, did not lead to improved results. Hence, taking the possible degradation into account, the fruit derived total RNA was also used for downstream processes, but the generated results were critically examined.

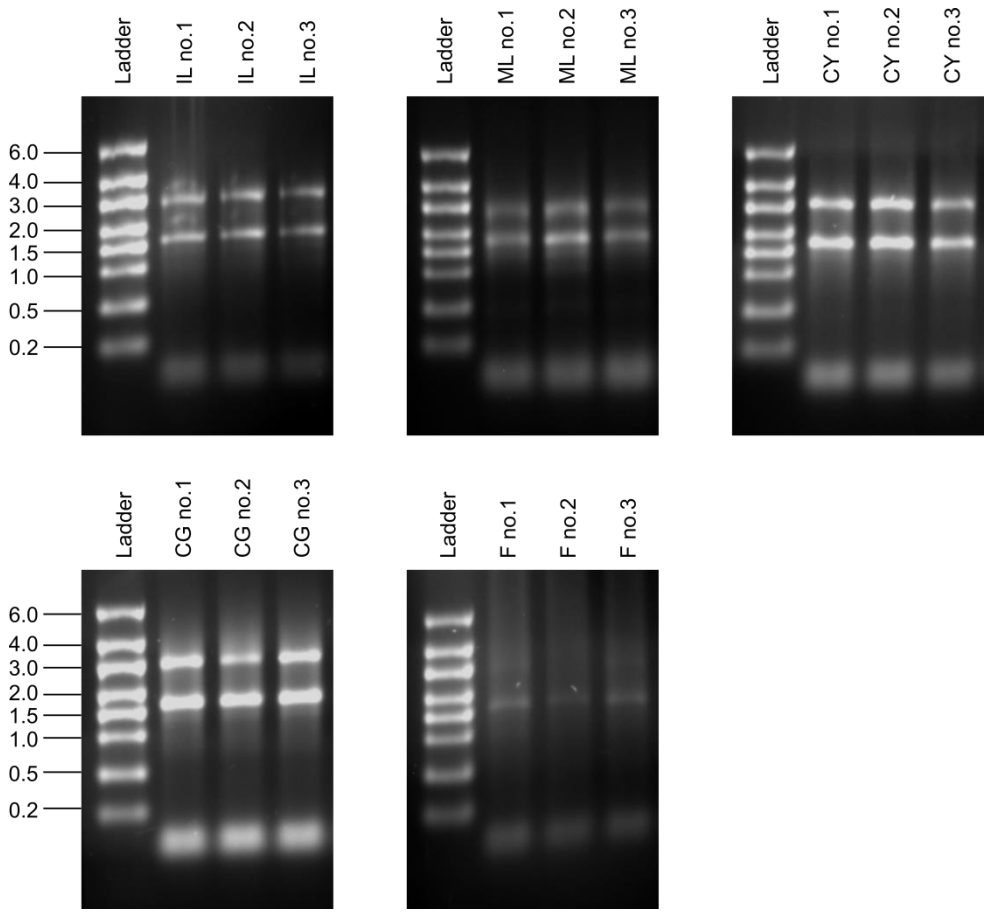

Figure 24: Agarose gel electrophoresis of total RNA isolated from different tissues of *O. europaea* L. cv. Canino. Total RNA was isolated from three biological replicates per tissue. Numbers following the sample name indicate the biological replicate. Numbers to the left indicate the size (kbp) of marker RNA fragments (Ladder). IL, immature leaves; ML, mature leaves; CY, callus 'yellow'; CG, callus 'green'; F, fruits.

In a next step, samples of total RNA were treated with DNase and subsequently used for cDNA synthesis *via* reverse transcription using oligo(dT) primers and the SuperScript IV Reverse Transcriptase (Thermo Fisher Scientific Inc., Waltham, MA, USA), an enzyme that is optimized for difficult plant RNA samples ('Super Script IV RT' application note). Afterwards, remaining total RNA was removed by treatment with RNAse H (2.3.5.). In order to minimize inhibitory effects of components derived from previous reactions on the following RT-PCR, resulting cDNA samples were

diluted 1 to 25 using nuclease-free water. Thus, the final concentration of cDNA was corresponding to 1 ng/µL of initially inserted total RNA.

3.8.1.2. Selection of reference genes and primer design

For determination of relative expression levels of the genes of interest *via* qPCR, it was necessary to co-analyze expression levels of reference genes (formerly referred to as housekeeping genes). In that way, target sequences could be normalized for variations in expression levels introduced due to various factors such as RNA stability, reaction efficiencies or the amount of cDNA inserted into each reaction. Selection of appropriate endogenous control sequences was based on the reference gene validation studies by Nonis *et al.* [102] and L Ray *et al.* [103]. While both could demonstrate a highly stable expression of *elongation factor 1 alpha* (*EF1-α*) and *serine/threonine protein phosphatase 2A* (*PP2A*) in mesocarp tissue of *O. europaea*, Nonis *et al.* were also able to show similar results for leaf tissue. The nucleic acid sequences described in both publications, however, were provided as contigs and thus, represented only a part of the specific mRNA. Therefore, the initial step was to screen the previously described transcriptome data base [91] for the corresponding full-length sequence. In this way, the data base entries OE6A028067P1 (length of 1,350 bp) and OE6A014464P1 (length of 921 bp) were identified as the putative coding sequences of *EF1-α* and *PP2A*, respectively, and used for the design of the primers no 31-34 (2.1.2.).

Since the design of oligonucleotides for qPCR requires the most accurate sequence information on the genes to be investigated, the coding sequences of *OeEst030*, *OeEst228* and *OeEst905* as well as *EF1-α* and *PP2A* were isolated from cDNA of the specific varitety Canino and sequenced. The isolation procedure was accomplished according to the previously described methods (2.3.1.1.) using the cDNA sample ‘mature leaves 3’ (biological replicate no. 3) and the oligonucleotides no 1-4, 7,8 and 31-34 (2.1.2.). Sequencing results were then used for the design of qPCR primers (2.1.2.; no. 35-44) by means of the Primer3web software (2.7.2.). Both the specificity and the optimal annealing temperature of each primer set were evaluated experimentally *via* qPCR (template: cDNA sample ‘mature leaves 3’) with subsequent melting curve analysis. By applying the annealing temperatures shown in Table 6, each reaction resulted in the presence of a single amplicon as indicated by one specific melting temperature of the product, while featuring comparable low Cq values.

Table 6: Targets analyzed for corresponding expression level in tissue of *O. europaea* by means of qPCR.

target	oligonucleotides	T_a (°C)	amplicon length (bp)	amplicon T_m (°C)
EF1-α	no. 35, 36	63	200	82.4
PP2A	no. 37, 38	63	81	79.8
OeEst030	no. 39, 40	60	56	76.5
OeEst228	no. 41, 42	60	147	82.0
OeEst905	no. 43, 44	60	196	79.1

3.8.1.3. Determination of relative expression levels

In summary, expression levels of three genes of interest and two reference genes were analyzed in five different tissues with three biological replicates per target/tissue combination. Obtained fluorescence data were analyzed for Cq values and target specific amplification efficiencies by means of the LinRegPCR software. Further data analysis was then performed using the extended delta-delta-Cq model for relative quantification described by Hellemans *et al.* [94]. Resulting normalized relative quantities (NRQs) of the same target within different tissues were set in relation to the lowest calculated value. Biological replicates were then combined and presented in bar charts (Figure 25).

The highest expression levels of *OeEst030* could be measured in samples derived from young leaves of *O. europaea* L. cv. Canino. The amount of this specific mRNA in older leaves, in contrast, seemed to be around 13 times lower. Even lower expression levels were detected in both callus samples as well as in the fruit tissue. While the calculated NRQ value corresponding to the latter tissue was significantly lower compared to the values obtained for immature and mature leaves, no significant difference could be detected when compared to the NRQ values of the samples ‘callus yellow’ and ‘callus green’ (p-value of 0.118 and 0.083, respectively).

Relative expression analysis of *OeEst228*, on the other hand, revealed a 6-fold increased abundance of corresponding mRNA in ‘mature leaves’ compared to ‘immature leaves’. Also in case of *OeEst228*, no significant differences between the NRQ values of both callus samples could be verified. However, it should be emphasized that both biological groups exhibit the highest expression levels detected. Measured mRNA levels of *OeEst228* in fruit tissue were distinctly lower than in all other tissues. Furthermore, it has to be noted that a large heterogeneity could be observed in the results of the biological replicates of the samples ‘mature leaves’, ‘callus yellow’ and ‘callus green’.

Analysis of the *OeEst905* expression levels revealed the highest abundance in callus tissue of the sample ‘callus green’, followed by the samples ‘callus yellow’ and ‘mature leaves’. As observed for

OeEst288, also *OeEs905* seemed to be expressed in immature leaves and fruit tissue in smaller amounts as indicated by a 5.6-fold and 31.5-fold smaller NRQ value, respectively.

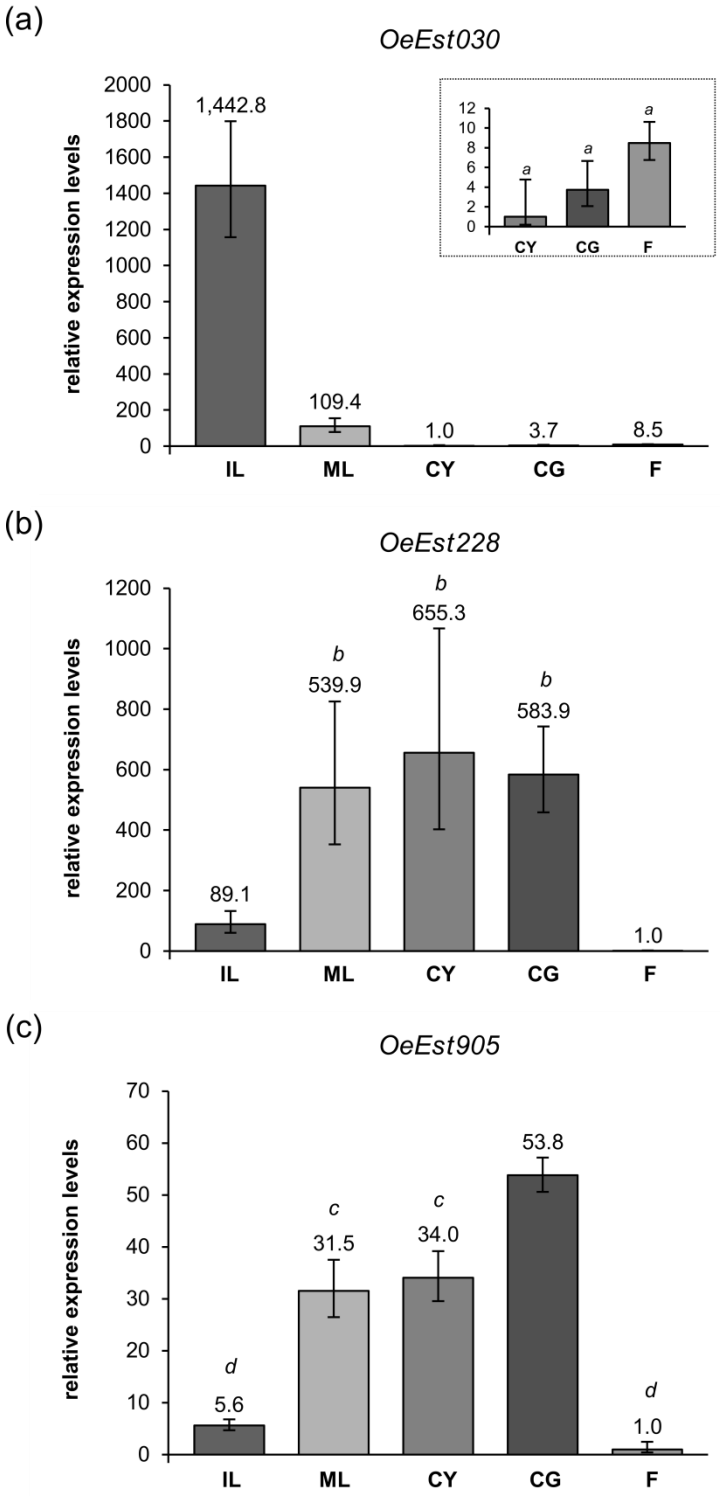

Figure 25: Relative expression levels of (a) *OeEst030*, (b) *OeEst228* and (c) *OeEst905* in different tissues of *O. europaea* L. cv. Canino. Relative gene expression was analyzed by qPCR using cDNA samples derived from three different biological replicates per tissue. Results obtained for samples of the same biological group were combined and related to the averaged

results of the group showing the lowest NRQ values. Error bars indicate the standard deviation within each biological group. Results marked with the same letter do not differ significantly from each other as indicated by a p-value ≥ 0.05. IL, immature leaves; ML, mature leaves; CY, callus 'yellow'; CG, callus 'green'; F, fruits.

3.9. Identification and characterization of further esterase candidates

The last part of this study was dedicated to the identification of further esterases in *O. europaea* that possess the same shift in the acidic member of the catalytic triad as present in OeEst030 and OeEst228. Amongst all *O. europaea* transcriptome data base entries [91] showing a sequence similarity of more than 50 % compared to the PNAE, only sequence OE6A068679P2 showed the lack of an acidic amino acid at the position expected to harbor the acidic member of the catalytic triad (Figure 26). An MSA against OeEst030 and OeEst228 revealed an identity of 76.4 % and 71.4 % and a similarity of 86.5 % and 83.8 %, respectively. Based on the corresponding DNA coding sequence, primers (2.1.2., oligonucleotides no 45, 46) were designed and used for the isolation procedure applying the previously described procedure (3.2.). Subsequent DNA sequencing of the isolated candidate, hereinafter referred to as OeEst679, could verify an identity of 99.6 % towards the reference data base entry. Following gene expression and protein purification was accomplished by means of the already established methods (3.3 & 3.4.). Quantification of the recombinant protein preparation of OeEst679 resulted in a concentration of 1,255.4 mg/mL (± 9.4 %). Analysis *via* SDS-PAGE with subsequent silver nitrate staining (see Appendix, Supporting Figure 6) revealed the presence of the protein of interest as indicated by a band of approximately 46-47 kDA. Significant contaminations by proteins of differing sizes could not be detected.

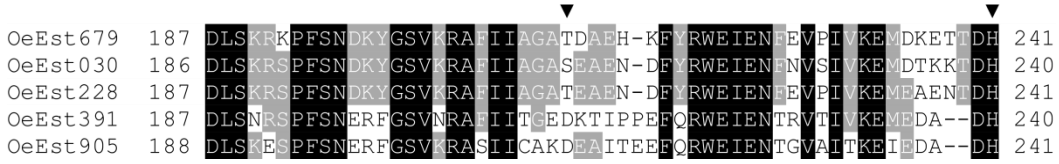

Figure 26: Section of an MSA of amino acid sequences of the putative esterases OeEst679 with already characterized olive esterases. Amino acids identical in all or at least three sequences are shown in white letters on black background or shaded in grey, respectively. The positions expected to harbor the catalytic histidine (H) as well as the aspartate (D) are marked with black arrows. The new candidate shows remarkably high sequence identity compared to the methyl esterases OeEst030 and OeEst228.

Initial enzyme activity assays were performed using the substrates pNPA and pNPB (2.5.1.). Both substances were converted by OeEst679 into pNP at a specific activity of 42.4 ± 2.2 U/g and 370.3 ± 16.3 U/g, respectively.

Following up on this, ligstroside, oleuropein and oleoside 11-methyl ester were tested as substrates (2.5.2.). Under the applied conditions, however, no enzymatic activity could be proven. Thus, LC-MS analysis of potential reaction products could only confirm the presence of the substrates. In a subsequent set of experiments, β-glucosidase from almonds was applied to the assay compositions, thus providing corresponding aglycones as substrates. As shown in Figures 27-29, deglycosylation products of ligstroside, oleuropein and oleoside 11-methylester were successfully converted by OeEst679 resulting in compounds with the retention times 44.08 min, 40.23 min and 23.11 min, respectively. A comparison with assays containing aforementioned substrates as well as β-glucosidase and OeEst228 revealed that the generated products were the same with both esterases. Thus, it can be concluded that also OeEst679 features similar activity towards the aglycones of ligstroside, oleuropein and oleoside 11-methyl ester as observed with OeEst030 and OeEst228.

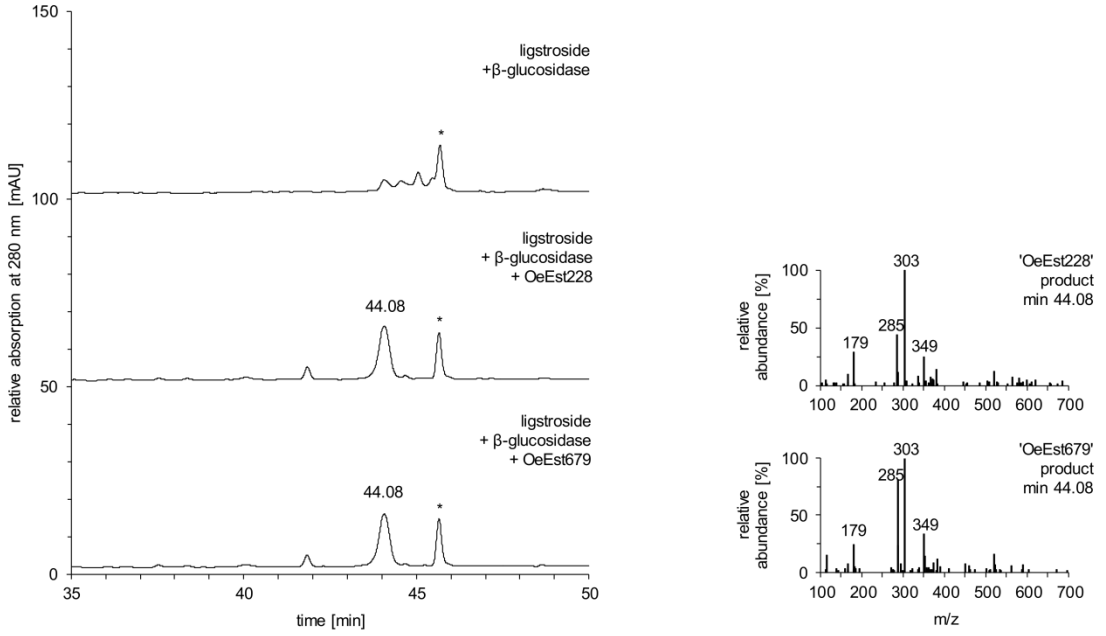

Figure 27: LC-MS analysis of assays verifying esterase activity of OeEst679 towards ligstroside aglycone. The conversion of ligstroside through β-glucosidase from almonds and OeEst679 yielded the same product as observed for assays containing β-glucosidase and OeEst228. The peak marked with an asterisk represents an impurity within the substrate preparation, which was not converted in any of the tested reaction approaches.

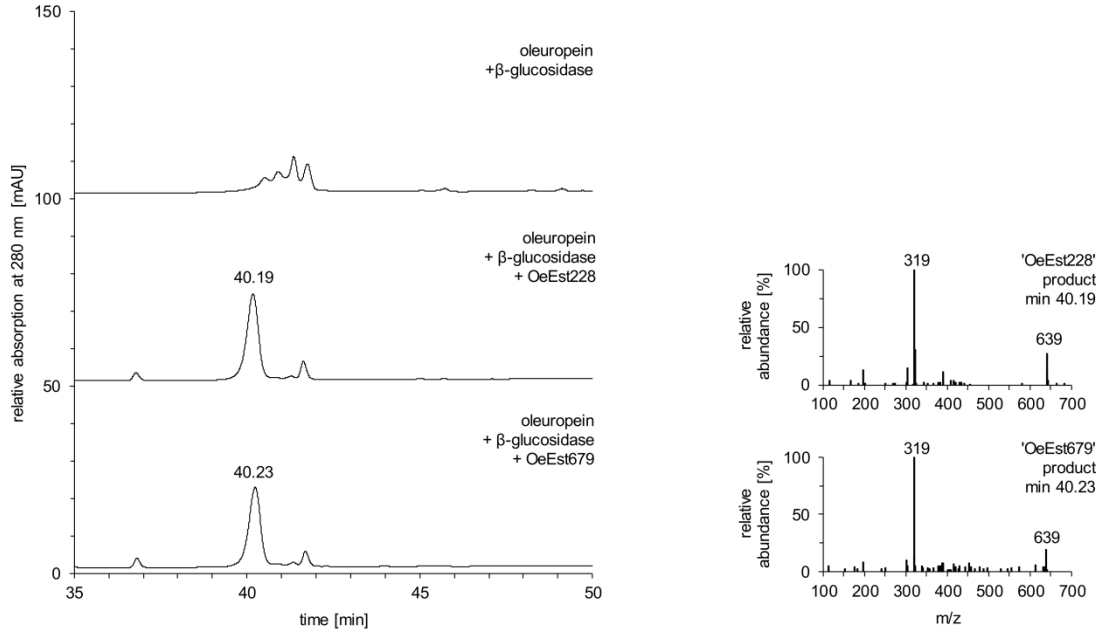

Figure 28: LC-MS analysis of assays verifying esterase activity of OeEst679 towards oleuropein aglycone. The conversion of oleuropein through β-glucosidase from almonds and OeEst679 yielded the same product as observed for assays containing β-glucosidase and OeEst228.

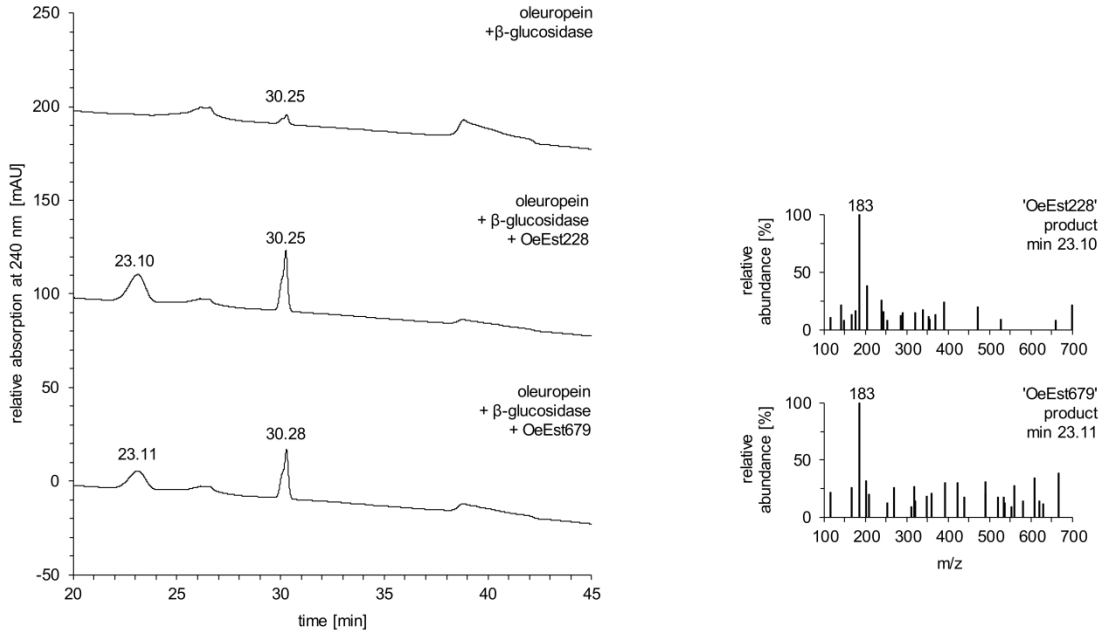

Figure 29: LC-MS analysis of assays verifying esterase activity of OeEst679 towards elenolic acid. The conversion of elenolic acid through β-glucosidase from almonds and OeEst679 yielded the same product as observed for assays containing β-glucosidase and OeEst228.

4. Discussion

4.1. Degradation of oleuropein and derivatives

The degradation of ligstroside and oleuropein is expected to result in a variety of different compounds, most of them being unstable intermediates. Various studies have shown that the underlying mechanisms are mainly oxidation and hydrolysis processes catalyzed by enzymes from the classes of polyphenol oxidases (PPO), peroxidases (POD), β-glucosidases and esterases [56, 57]. With the exception of a β-glucosidase [64], however, none of the specific enzymes involved have been discovered.

In this study, five methyl esterases from *O. europaea* have been identified. Three of those, namely OeEst030, OeEst228 and OeEst679, are capable of cleaving the methyl ester within the structure of ligstroside aglycone, oleuropein agylcone and elenolic acid. Thus, in accordance with the studies of Koudounas *et al.* on the oleuorpein specific glucosidase OeGLU [64], one of the possible oleoside-type secoiridoid degradation routes was revealed (Figure 30).

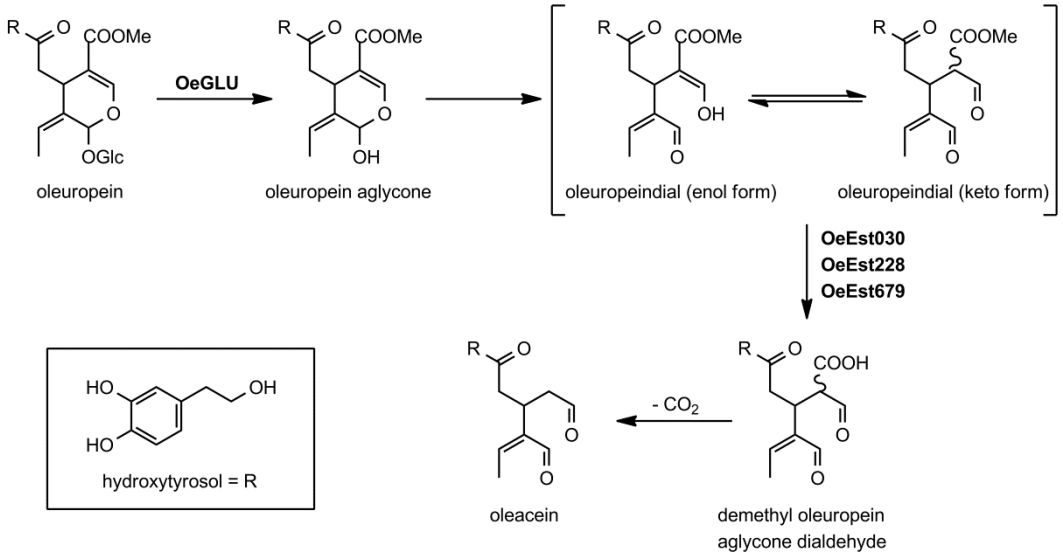

Figure 30: Transformation of oleuropein into oleacein by olive endogenous enzymes. Based on studies by Koudounas *et al.* [64] as well as the here described study, it can be assumed that oleuropein is first deglycosylated by OeGLU followed by demethylation of resulting aglycone by the newly identified esterases OeEst030, OeEst228 and OeEst679. Demethyl oleuropein aglycone dialdehyde then immediately undergoes spontaneous decarboxylation leading to oleacein. A similar route of degradation can be expected for ligstroside as well as oleoside 11-methyl ester as indicated by successful conversion of corresponding aglycones by the aforementioned esterases.

Oleuropein, the most abundant secoiridoid in *O. europaea*, is localized in the cytosol or vacuole of the cells [104], while its specific β-glucosidase is targeted to the nucleus. This compartmentalization ensures the stability of oleuropein aglycone in intact plant cells, thus avoiding cytotoxicity. Only upon cell disruption, for example by herbivore attack, both components can get in physical proximity enabling the activation of oleuropein *via* enzymatic deglycosylation by OeGLU. As observed for other iridoid aglycones, also the deglycosylation product of oleuropein is unstable and highly reactive. Detachment of the stabilizing glucose molecule leads to opening of the elenolic ring. The resulting keto-enol tautomeric equilibrium is then generating further isomers of corresponding aglycone [65, 67, 105]. Additionally, the formation of the cyclic mono aldehyde form has been observed as a consequence of hydration followed by structural rearrangement [58, 106]. Oleuropein aglycone is then further degraded through demethylation by the here described esterases, namely OeEst030, OeEst228 and OeEst679, leading to demethyl oleuropein aglycone, which immediately undergoes non-enzymatic decarboxylation yielding oleacein. However, it is not known whether one of the generated oleuropein aglycone isomers represents the preferred substrate for the esterases or is even not accepted at all.

4.2. Demethylation of oleuropein aglycone as a plant defense mechanism

The generation of oleuropein aglycone upon cell disruption is an extensively described plant defense mechanism present in several members of the Oleaceae family, such as *Ligustrum obtusifolium* [67] and *O. europaea* [64]. This system is compromising of two physically separated components: the non-active glycosylated precursor oleuropein and the corresponding β-glucosidase and therefore, is also referred to as 'two component defense system' [64]. Despite the wide metabolic diversity within the plant kingdom, such mechanisms seem to be a conserved strategy for plant chemical defense against herbivores and pathogens. Well studied examples of constitutive defense compounds that are activated by deglycosylation can be found within the classes of cyanogenic glucosides, avenacosides, glucosinolates, benzoxazinoid glucosides and iridoid glucosides [107].

Up to now, most studies on the oleoside-mediated defense mechanism were focused on the protein-crosslinking and denaturing activities of oleuropein aglycone. And yet, this substance does not represent the single most abundant oleoside aglycone present in intact and processed olive fruits [57, 70, 108, 109]. Its decarboxymethyl derivative, namely oleacein, was detected in concentrations up to 227.97 and 258.32 µmol/g in immature fruits of *O. europaea* L. cv. Hojiblanca and Arbequina, respectively, while corresponding concentrations of oleuropein aglycone were 201.06 and 196.41 µmol/g [57]. Also quantitative measurements of secoiridoid derivatives in various EVOO

samples derived from fruits of *O. europaea* L. cv. Koroneiki revealed significantly higher concentrations for oleacein compared to oleuropein aglycone [70]. Even though this supports the assumption that a similar trend may occur as a result of herbivor or pathogen attack, the specific impact of oleacein on plant defense has not yet been investigated.

The outstanding protein-crosslinking activity of oleuropein aglycone has been mainly associated with the keto form of its dialdehyde, which features structural similarities with glutaraldehyde. In contrast to the latter, this isomer of oleuropein aglycone could undergo up to three alkylation reactions with nucleophilic side chains of proteins, preferably with those of lysine and cysteine. Due to the unstable nature of oleuropein after deglycosylation, however, specific reactivity of the individual isomers could not be determined experimentally. Instead it can be assumed that the deglycosylation product tested in the experiments of Konno *et al.* was composed of the isomers described in the chapter before [67]. Given the fact that the keto form of oleuropeindial may indeed possess the strongest protein-crosslinking properties, it could be beneficial in context of the plant defense mechanism to stabilize this form. And this might be the physiological role of subsequent demethylation of oleuropein aglycone by OeEst030, OeEst228 and OeEst679. Upon cleavage by methyl esterase activity and subsequent decarboxylation, the dialdehyde oleacein is formed as a single product [110]. Neither in experiments presented in the course of this study, nor in other reports, there is evidence for the presence of naturally occurring isomers of this compound. Although, there is no published study investigating the protein-crosslinking activity of oleacein, based on its chemical structure a similar reactivity compared to the keto form of oleuropein aglycone can be expected. It is possible that an even higher protein-crosslinking activity could be attained by the loss of the sterically hindering carboxymethyl group. This would mean that it could be rather a three instead of a two component defense system involving the methyl esterases OeEst030, OeEst228 and OeEst679 in addition to oleuropein and its β-glucosidase OeGLU. A similar mechanism based on the activation of a non-toxic compound *via* β-glucosidase and subsequent α/β hydrolase activity has been described in context of cyanogenesis. Here, cyanogenic glycosides are deglycosylated and further hydrolyzed by HNL releasing highly toxic hydrogen cyanide (HCN) [111]. Strikingly, an alignment of OeEst030, OeEst228 and OeEst228 with HNL of *H. brasilienses* revealed around 60 % homology.

4.3. Potential role in plant hormone metabolism

In addition to the deglycosylated oleosides, also methylated plant hormones represent accepted substrates of the esterases OeEst030, OeEst228, OeEst391 and OeEst905. MeJA and MeIAA were successfully converted by all four esterases into JA and IAA, respectively. Interestingly, also PNAE

showed activity towards both plant hormones. In contrast, only OeEst905 converted MeSA into significant amounts of SA. Since those plant hormones possess a broad range of regulatory functions, those activities might indicate an essential role of the corresponding esterases in plant hormone signaling.

Jasmonates, for example, possess regulatory functions in plant development processes, like seed germination and root growth [112], as well as in response to abiotic and biotic stresses. Especially the role of jasmonates in wounding [113] and plant defense response to herbivores and necrotrophic pathogens has been extensively investigated [114]. While it was initially assumed that jasmonic acid or even methyl jasmonate represent active compounds, recent studies indicate that both compounds do not feature direct bioactivity. In fact, the conjugate (+)-7-iso-jasmonoyl-L-isoleucine (JA-Ile) has been revealed as the most bioactive jasmonate [115]. JA-Ile is formed *via* adenylation of JA by jasmonyl-isoleucine synthetase (JAR1 in *Arabidopsis thaliana*) making JA an important mediator in associated signaling pathways. Since this conjugation requires a free carboxy-group, however, MeJA is not an accepted substrate [116]. Therefore, modification of JA by carboxyl methyl transferase (AtJMT in *A. thaliana*; [117]) and, conversely, the demethylation of MeJA by corresponding methyl jasmonate esterase (LeMJE in *S. lycopersicum*; [99]) represent mechanisms to adjust the pool of active jasmonates [118]. Similar to jasmonates, also salicylic acid covers a broad range of signaling functions in plants. It is involved in processes like seed germination, cell growth, respiration, basal thermogenesis and diseases resistance. Some of its effects, however, are due to alteration of synthesis and signaling of other plant hormones. Especially between SA and JA extensive cross-talk was demonstrated. Even though those interactions can be bidirectional, mainly antagonistic effects of SA towards JA signaling were documented [119]. In contrast to JA, the SA-mediated plant defense is triggered upon biotrophic pathogen attack resulting in programmed cell death (PCD). This hypersensitive response (HR) is leading to local acquired resistance (LAR) followed by systemic acquired resistance (SAR) [120]. Due to its cell toxicity, SA levels are tightly regulated by modification reactions like glycosylation, methylation and conjugation with amino acids. Resulting derivatives are generally thought to be inactive serving as rapidly accessible sources for SA generation [121]. Due to its volatility, MeSA furthermore functions as long-distance signal molecule for the transport of SA from infected cells to the systemic tissue [122]. Finally, the plant hormone IAA represents the main auxin in most plants and controls processes such as cell division, elongation and differentiation [123]. Since its regulatory function takes place in a concentration-dependent manner, adjustment of IAA levels is essential for plant growth and development. This involves not only the biosynthesis of IAA, but also the conjugation into inactive storage forms like IAA-glucose or MeIAA [124]. In *A. thaliana*,

the latter is generated from IAA by IAMT1 [125], while the reverse reaction is catalyzed by MES17 [126].

In conclusion, methylation represents a mechanism for the temporary inactivation of the aforementioned plant hormones as well as for the long-distance transport in case of JA and SA, enabling not only intra-plant signaling but also inter-plant communication. This mechanism does require both a carboxyl methyl transferase for the generation of the derivative and an esterase present in the target location that is cleaving the methyl ester again. As indicated by *in vitro* experiments, demethylation of respective plant hormones in *O. europaea* could be accomplished by the here described esterases. This would extend the role of OeEst030 and OeEst228 in plant defense from solely generating oleacein and oleocanthal to a more divers function by additionally participating in the activation of jasmonate-mediated defense mechanisms. Although both functions would be in accordance with each other or even result in a synergistic effect, it remains unclear whether the activity towards plant hormones possesses a physiological role in plant metabolism. A common approach to verify such assumptions would be a knock-out, silencing or overexpression of respective gene within the target organism. Based on studies using T-DNA insertional mutants of *A. thaliana*, for example, it was possible to associate the activity of methyl esterase AtMES17 with auxin homeostasis by significantly enhanced root growth of corresponding knock-out line [126]. Therefore, it would be beneficial for our understanding of the *in vivo* function of the here described genes, particularly OeEst030 and OeEst228, to perform similar experiments in *O. europaea*. Appropriate protocols for agrobacterium-mediated genetic transformation of olive have already been developed [127-129].

4.4. Transesterification reaction catalyzed by olive esterases

Beside the demethylation an additional reaction was observed when MeJA and MeIAA were incubated with OeEst030, OeEst228, OeEst391 and OeEst905: all four enzymes generated remarkable amounts of the ethyl esters of JA and IAA. Conversion of MeJA and MeIAA by PNAE, in contrast, yielded only demethylation products. Based on the results generated in several control reactions it was concluded that both EtIAA and the supposed EtJA were generated from MeIAA and MeJA, respectively, by transesterification in the presence of ethanol. Analysis of the reaction kinetics of OeEst030 and OeEst228 with MeIAA revealed that transesterification and demethylation rates of MeIAA were comparable during the beginning of the reaction. Moreover, both enzymes showed significant lower demethylation activity towards EtIAA indicating the preference towards MeIAA as substrate.

A similar transesterification reaction catalyzed by a plant esterase has not yet been described. Interestingly, an indication for the presence of this activity in some already characterized plant esterases can be found in results published by Koo *et al.* [87, 130]. Even though not explained by the authors, an illustrated TLC analysis of the reaction products generated by AtMES8, a methyl esterase from *A. thaliana*, clearly shows the conversion of MeJA into two products with similar retention behavior compared to those described here. Moreover, corresponding GC-MS analysis also revealed the presence of a second product as indicated by a mass peak featuring a retention time between the one of MeJA and JA. Since both TLC and GC-MS analysis generated in course of the here presented study, were performed using parameters highly similar to those applied by Koo and co-authors, it seems reasonable to compare the obtained results [87]. Therefore, one could argue that also AtMES8 might be capable of performing a reaction similar to the transesterification observed for the olive esterases. However, it remains unclear whether such a reaction towards phytohormones take place *in planta* and if so, what physiological role it has.

Transesterification reactions have been extensively described for lipases from different fungal and bacteria species. Lopéz Giraldo and co-authors, for example, successfully showed the transesterification of a methyl derivative of the naturally occurring phenol chlorogenic aicd with fatty alcohols of various chain lengths by *Candida antarctica* B lipase [131]. Other studies investigated the transesterification synthesis of geranyl acetate from geraniol and vinyl acetate catalyzed by lipases, amongst others, from *Rhizopus oliosporus* [132], *Pseudomonas fluorescens* [133] and *Thermomyces lanuginosus* [134]. The majority of demonstrated transesterification reactions, however, require an anhydrous or low-water solvent system in order to outperform the competing hydrolytic activity [135]. The transesterification catalyzed by the here described olive esterases, in contrast, was accomplished in a medium consisting of sodium phosphate buffered water containing only 0.5 % (v/v) ethanol. Thus, these enzymes not only represent the first plant derived esterases for which such an activity has been reported, but also belong to a minority of enzymes that are capable of performing this reaction in aqueous medium. However, this also raises the question of whether a reduction of the water content by replacement with ethanol or even another organic solvent could enhance the synthesis of EtIAA or rather would lead to a significant loss in general enzyme activity instead.

4.5. Modelling an mutagenesis studies

Based on the protein models generated by *in silico* homology studies, it was predicted that both oleoside aglycone converting esterases, OeEst030 and OeEst228, feature a remarkable high similarity towards the crystal structure of PNAE and thus, also towards each other. As it was described for the PNAE, also those olive esterases seem to consist of a core domain including six β sheets flanked by five α helices (Figure 31). Additional two β sheets and three α helices are predicted to form the cap-domain which features the highest deviation in corresponding amino acid sequence in all three proteins. Concerning the active site, the models of OeEst030 and OeEst228 superimposed with the crystal structure of PNAE revealed a nearly identical positioning of serine and histidine putatively forming the catalytic triad. The lowest local quality estimate for the generated 3D structures, however, was obtained for the region around the predicted position of the acidic member of the triad. Nevertheless, the calculated model strongly implied an involvement of Glu214 in the formation of the catalytic triad in OeEst030 (OeEst228: Glu215) as indicated by its location proximal to His240 (OeEst228: His241). Mutagenesis studies, however, could not confirm this assumption. Thus, the amino acid exchange E214A did not result in a total loss of activity as it would have been expected in case of a catalytic function.

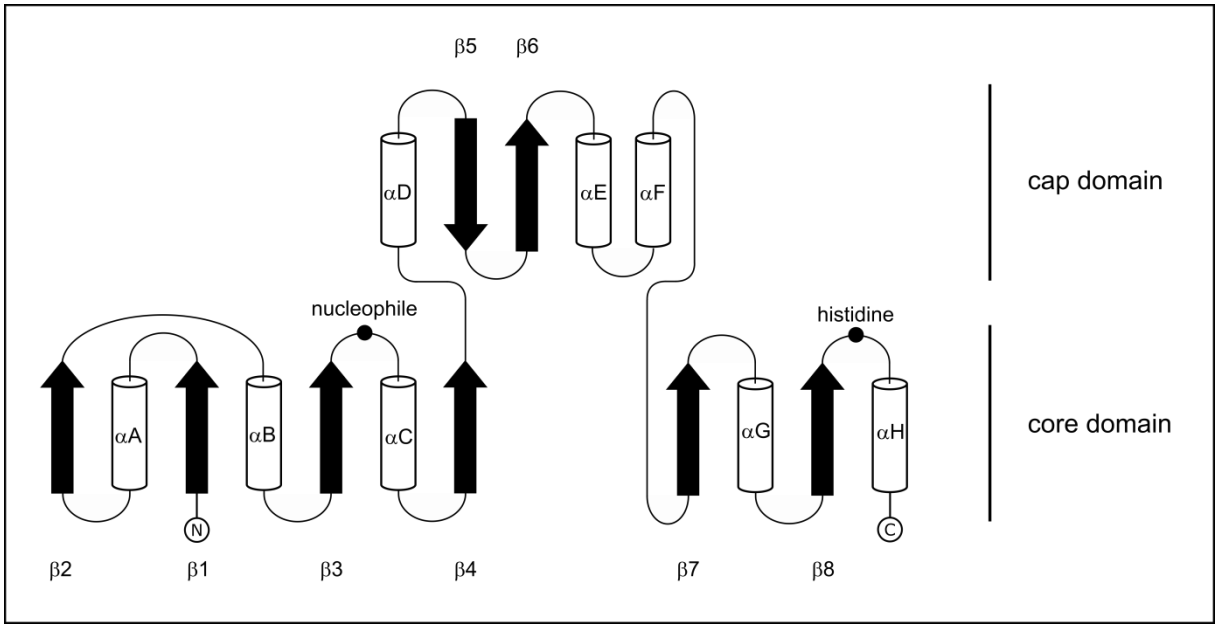

Figure 31: Scheme representing the fold of OeEst030 and OeEst228 as predicted by *in silico* modelling of corresponding three dimensional structures.

The acidic member of the catalytic triad, in most cases aspartic acid, possesses a bifunctional character in the formation of the active site. One oxygen of the negatively charged carboxyl group orients the imidazole of the catalytic histidine [136] and assists in the charge relay system [137]. The second oxygen forms hydrogen bonds to the backbone nitrogen of a residue few amino acids towards the C-terminus of the protein, thus stabilizing the region around the catalytic triad [71, 136]. The impact of this amino acid on the enzyme activity has been demonstrated in several studies. Mutagenesis of corresponding position in PNAE, for example, yielded an esterase (mutein D216A) inactive towards its natural substrate [80]. Similar results were generated in studies on carboxylesterases of different origins such as AChE from *Torpedo californica* [138] and cocE from a *Rhodococcal* strain [139].

Although mutant OeEst030 E214A showed activity, conversion rates towards the artificial substrate pNPB and the plant hormone MeIAA were five and 6-fold decreased, respectively. Even though its participation in the formation of the catalytic triad seems unlikely, those results indicate a certain structure stabilizing function of Glu214 on corresponding region. Further acidic residues in close proximity to the catalytic histidine, however, have not been identified on basis of the generated 3D structures of OeEst030 and OeEst228. Therefore, it might be concluded that such 3D models are more inaccurate than implied by corresponding GMQE and QMEAN values. In order to finally determine the exact position of the catalytic aspartic or glutamic acid it is necessary to determine the X-ray crystal structure of one of both olive esterases.

An interesting additional observation was the enhanced activity of OeEst030 after introduction of an aspartic acid at position 211 (mutein S211D). The resulting 45 % increase in MeIAA conversion rates might be attributed either to structural changes or to stabilization of the structure which supports substrate binding or the catalytic activity of the triad.

4.6. Substrate specificity of olive esterases

For the olive esterases OeEst030, OeEst228 and OeEst679 significant activity towards all three tested oleoside aglycones could be proven. Thus, the phenolic moiety is neither a structural feature required for substrate binding nor representing a steric hindrance. Corresponding glycosides, in contrast, were not accepted as substrate at all, meaning that the presence of the bulky and polar glucose molecule represents an exclusion criterion. This glucose dependent substrate discrimination is very likely caused by the cap-domain which consists of a high percentage of hydrophobic residues. Based on homology models superimposed with the crystal structure of PNAE [140], it can be assumed that this region consists of the sequence segment Asp112-Phe184 and Asp112-Phe185 in

OeEst030 and OeEst228, respectively. Analysis of the corresponding amino acid composition revealed a content of around 47 % and 41 % of hydrophobic residues. In most members of the α/β-hydrolase fold superfamily, this highly variable domain covers the active site of the enzyme and thus, contributes to substrate selectivity and binding [72].

In context of a plant defense mechanism with oleuropein as a central compound, it seems reasonable that the glucoside does not represent a substrate for enzymes other than the physically separated β-glucosidases. This enables the accumulation of oleuropein leading to high concentrations in the vacuole or cytoplasm as extensively described [104]. However, there is evidence for the existence of a methyl esterase acting on oleuropein in intact cells of *O. europaea*. In fruits of the variety Cailletier [60] and Frantoio [58] high concentrations of demethyloleuropein have been detected, while other cultivars, e.g. Picholine [60] and Picual [141], contained not even traces of this substance in fruit tissue. Nevertheless, identification of corresponding methyl esterase could improve our understanding of the exact mechanisms behind the substrate discrimination observed for OeEst030, OeEst228 and OeEst679.

Further substrates tested for their conversion by the aforementioned esterases included the secologanin-like secoiridoid strictosidine and its aglycone. Strictosidine is the key intermediate in the biosynthesis of indole alkaloids. It is produced by condensation of tryptamine and secologanin and thus, features a secoiridoid moiety that is highly similar to the oleoside structure. This is also reflected in the structural changes that strictosidine undergoes after deglycosylation. As documented for oleuropein and its derivatives, detachment of its stabilizing glucose molecule exposes the labile hemiacetal resulting in opening of corresponding ring. Therefore, strictosidine aglycone is converted into its dialdehydic form [142].

Based on the results observed for enzyme activity assays with oleosides, it seems logical that also for the glycoside strictosidine no conversion product was generated. Interestingly, also its deglycosylation product was not accepted as substrate, even though it features high structural similarities to the tested deglycosylation products of oleosides (Figure 32). Here, the tryptamine moiety might cause steric hinderance. Nevertheless, all three esterases as well as OeEst391 and OeEst905 do not seem to be highly substrate specific. Thus, for all tested olive enzymes activity towards the plant hormones MeJA and MeIAA was shown, while OeEst905 additionally was able to cleave the methylester of MeSA.

Also for the PNAE activity towards MeJA, MeSA and the artificial substrates pNPA and pNPB was demonstrated for the first time. This is of special interest since it has been described to be highly substrate specific [78]. The corresponding study investigated the esterase activity of PNAE towards

15 structurally different esters most of them being metabolites derived from strictosidine. Only polyneuridine aldehyde and its 16-epimer, akuammidine aldehyde, were successfully tested for their demethylation by PNAE. The artificial substrate pNPA, in contrast, was not converted in experiments performed by the authors. In course of this study, however, esterase activity towards pNPA was clearly proven.

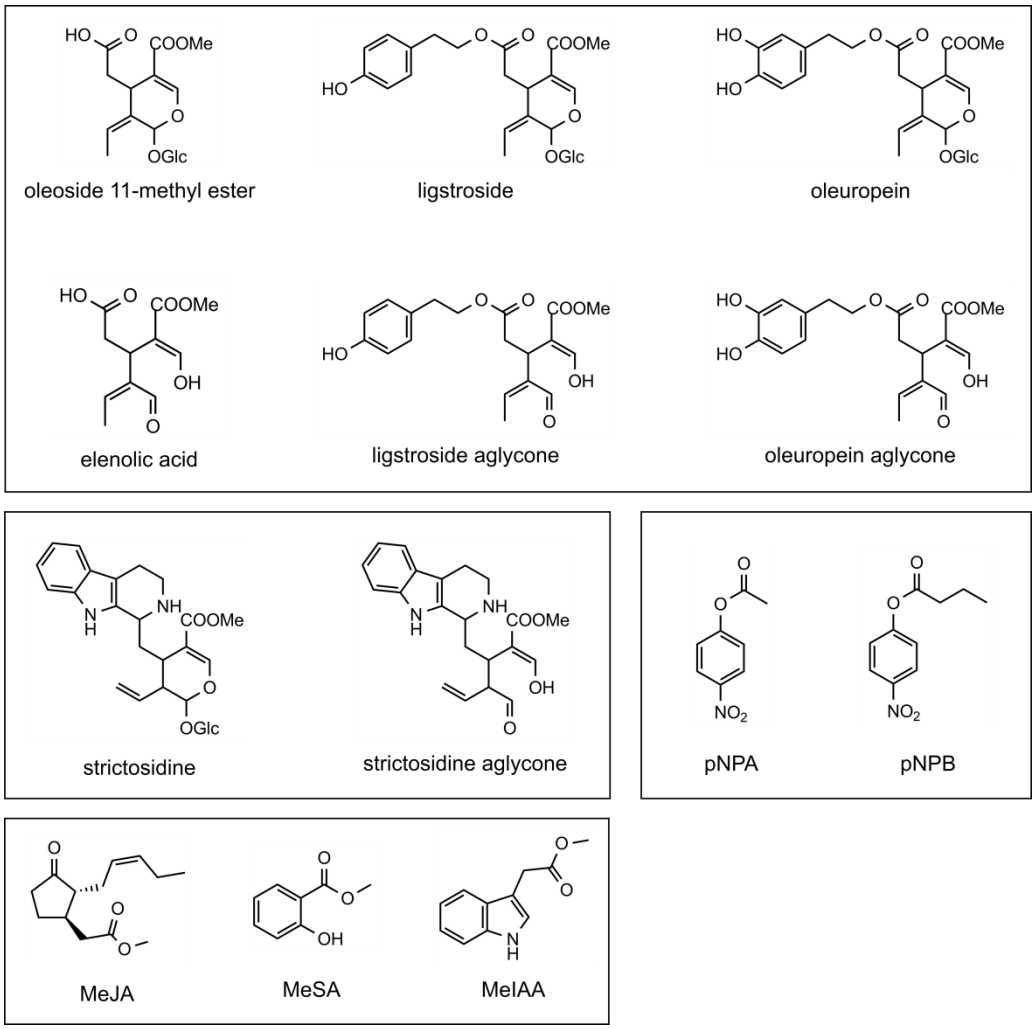

Figure 32: Overview of the chemical structure of all compounds tested as substrates for the olive esterases and PNAE. The aglycones of ligstroside and oleuropein and strictosidine as well as elenolic acid are depicted in the open-ring enol form which is expected to represent the predominant isomer of deglycosylation products [110]. Similarly, also strictosidine aglycone is represented as the dialdehyde generated after opening of the ring system [142].

4.7. Expression levels of *OeEst030*, *OeEst228* and *OeEst905*

Since enzymes of the classes β-glucosidases and esterases play an important role in the degradation of oleuropein and its derivatives in *O. europaeae*, there has been an increasing interest in

investigating their activity during fruit maturation. It has been observed in fruits of various cultivars that general esterase activity is increasing during ripening reaching its highest value during black maturation. Oleuropein levels, in contrast, have been observed to decrease continuously during the same period of time [60, 61, 63]. In fruits of some varieties, such as the Italian cultivar Canino, this decline is accompanied by a significant accumulation of demethyloleuropein indicating a direct correlation with the rising esterase activity. Equivalent analysis of esterase activity and oleoside profile changes in maturing leaf tissue, however, has yet not been investigated.

Metabolite analysis performed by N-Zyme BioTec GmbH revealed that oleuropein concentrations in young leaves of *O. europaea* L. cv. Canino were higher compared to those measured in mature leaves (see Appendix, Supporting Table 1), thus, following a similar trend as observed for olive fruits. For this reason, also a comparable increase in abundance of oleuropein degrading enzymes was assumed. As revealed by relative expression analysis, changes in OeEst030 and OeEst228 transcript abundance followed an opposite trend when compared to each other. While transcription of OeEst030 seemed to be 13.2-fold downregulated in course of leaf maturation, transcript abundance of OeEst228 showed with a 6-fold increase results comparable to expression level changes of OeEst905, which does not seem to be involved in oleoside degradation. This strongly suggests a differing mechanism regulating the gene expression of OeEst030 and OeEst228. Concerning the fact that corresponding enzymes showed highly similar activities in the conducted assays, both esterases could represent isoenzymes possibly featuring different subcellular localization. Moreover, the remarkable high expression levels of OeEst030 exclusively in young leaves could be an indicator for a regulatory role in leaf development.

Interestingly, neither OeEst030 nor OeEst228 could be associated with high expression levels in olive fruits tissue. In fact, corresponding transcript abundance in fruits harvested in October (green-black color, maturity index of 2-3) was significantly lower compared to the values obtained for the leaf samples. At this point, however, it cannot be excluded that the poor quality of total RNA isolated from this tissue had a considerable impact on the qPCR results.

5. References

1. **Velzquez-Palmero, D., *et al.***, An oleuropein β-Glucosidase from olive fruit is involved in determining the phenolic composition of virgin olive oil. Frontiers in Plant Science, 2017. **8**.
2. **Besnard, G., *et al.***, The complex history of the olive tree: from Late Quaternary diversification of Mediterranean lineages to primary domestication in the northern Levant. Proceedings of the Royal Society B-Biological Sciences, 2013. **280**(1756).
3. **Diez, C.M., *et al.***, Olive domestication and diversification in the Mediterranean Basin. New Phytologist, 2015. **206**(1): p. 436-447.
4. **Besnard, G. and R.R. de Casas**, Single vs multiple independent olive domestications: the jury is (still) out. New Phytologist, 2016. **209**(2): p. 466-470.
5. **Bracci, T., *et al.***, Molecular studies in olive (*Olea europaea* L.): overview on DNA markers applications and recent advances in genome analysis. Plant Cell Reports, 2011. **30**(4): p. 449-462.
6. **Obaid, R., H. Abu-Qaoud, and R. Arafeh**, Molecular characterization of three common olive (*Olea europaea* L.) cultivars in Palestine, using simple sequence repeat (SSR) markers. Biotechnology & Biotechnological Equipment, 2014. **28**(5): p. 813-817.
7. **Cantini, C., A. Cimato, and G. Sani**, Morphological evaluation of olive germplasm present in Tuscany region. Euphytica, 1999. **109**(3): p. 173-181.
8. **Vossen, P.**, Olive oil: History, production, and characteristics of the world's classic oils. Hortscience, 2007. **42**(5): p. 1093-1100.
9. **Tardi, A.**, The culinary uses of extra-virgin olive oil. Extra-Virgin Olive Oil Handbook, 2014: p. 321-337.
10. **International Olive Council**. World Olive Oil Figures. 2018 [cited 2018 20 April]; Available from: http://www.internationaloliveoil.org/estaticos/view/131-world-olive-oil-figures.
11. **The Online Scientists**. About the Seven Country Study. [cited 2018 20 April]; Available from: https://www.sevencountriesstudy.com/about-the-study/.
12. **Keys, A.B.**, Seven countries: a multivariate analysis of death and coronary heart disease. 1980, Cambridge, Mass.: Harvard University Press. xi, 381 p.
13. **Menotti, A., *et al.***, Cardiovascular risk factors as determinants of 25-year all-cause mortality in the seven countries study. European Journal of Epidemiology, 2001. **17**(4): p. 337-46.
14. **Alonso, A., *et al.***, Cardiovascular risk factors and dementia mortality: 40 years of follow-up in the Seven Countries Study. Journal of the Neurological Sciences, 2009. **280**(1-2): p. 79-83.
15. **Menotti, A. and P.E. Puddu**, Coronary heart disease differences across Europe: a contribution from the Seven Countries Study. Journal of Cardiovascular Medicine, 2013. **14**(11): p. 767-72.
16. **Verschuren, W.M.M.**, Serum cholesterol and coronary heart disease - A public health perspective. Netherlands Journal of Medicine, 1997. **51**(1): p. 1-9.
17. **Widmer, R.J., *et al.***, The Mediterranean diet, its components, and cardiovascular disease. The American Journal of Medicine, 2015. **128**(3): p. 229-38.
18. **Keys, A., *et al.***, The diet and 15-year death rate in the seven countries study. American Journal of Epidemiology, 1986. **124**(6): p. 903-15.
19. **Rossell, J.B.**, Frying: improving quality. Woodhead Publishing in food science and technology. 2001, Boca Raton, FL Cambridge, England: CRC Press ; Woodhead Pub. xii, 369 p.

20. **Fito, M., et al.**, Antioxidant effect of virgin olive oil in patients with stable coronary heart disease: a randomized, crossover, controlled, clinical trial. Atherosclerosis, 2005. **181**(1): p. 149-58.

21. **Harper, C.R., M.C. Edwards, and T.A. Jacobson**, Flaxseed oil supplementation does not affect plasma lipoprotein concentration or particle size in human subjects. The Journal of Nutrition, 2006. **136**(11): p. 2844-8.

22. **Aguilera, C.M., *et al.***, Sunflower oil does not protect against LDL oxidation as virgin olive oil does in patients with peripheral vascular disease. Clinical Nutrition, 2004. **23**(4): p. 673-81.

23. **Servili, M. and G. Montedoro**, Contribution of phenolic compounds to virgin olive oil quality. European Journal of Lipid Science and Technology, 2002. **104**(9-10): p. 602-613.

24. **Cicerale, S., L. Lucas, and R. Keast**, Biological activities of phenolic compounds present in virgin olive oil. International Journal of Molecular Sciences, 2010. **11**(2): p. 458-79.

25. **Covas, M.I., *et al.***, Minor components of olive oil: Evidence to date of health benefits in humans. Nutrition Reviews, 2006. **64**(10): p. S20-S30.

26. **Marrugat, J., *et al.***, Effects of differing phenolic content in dietary olive oils on lipids and LDL oxidation-a randomized controlled trial. European Journal of Nutrition, 2004. **43**(3): p. 140-7.

27. **Weinbrenner, T., *et al.***, Olive oils high in phenolic compounds modulate oxidative/antioxidative status in men. Journal of Nutrition, 2004. **134**(9): p. 2314-2321.

28. **Gao, S., *et al.***, Association between circulating oxidized low-density lipoprotein and atherosclerotic cardiovascular disease: a meta-analysis of prospective observational studies. Journal of the American College of Cardiology, 2017. **70**(16): p. C79-C80.

29. **Gordon, D.J., *et al.***, High-density lipoprotein cholesterol and cardiovascular disease. Four prospective american studies. Circulation, 1989. **79**(1): p. 8-15.

30. **Olafiranye, O., *et al.***, Management of hypertension among patients with coronary heart disease. International Journal of Hypertension, 2011. **2011**: p. 653903.

31. **Hashim, Y.Z., *et al.***, Virgin olive oil phenolics extract inhibit invasion of HT115 human colon cancer cells in vitro and in vivo. Food & Function, 2014. **5**(7): p. 1513-9.

32. **Hamdi, H.K. and R. Castellon**, Oleuropein, a non-toxic olive iridoid, is an anti-tumor agent and cytoskeleton disruptor. Biochemical and Biophysical Research Communications, 2005. **334**(3): p. 769-78.

33. **Salvini, S., *et al.***, Daily consumption of a high-phenol extra-virgin olive oil reduces oxidative DNA damage in postmenopausal women. British Journal of Nutrition, 2006. **95**(4): p. 742-51.

34. **Peng, Y., *et al.***, Hydroxytyrosol mildly improve cognitive function independent of APP processing in APP/PS1 mice. Molecular Nutrition & Food Research, 2016. **60**(11): p. 2331-2342.

35. **Grossi, C., *et al.***, The polyphenol oleuropein aglycone protects TgCRND8 mice against Ass plaque pathology. PLOS ONE, 2013. **8**(8): p. e71702.

36. **Abuznait, A.H., *et al.***, Olive-oil-derived oleocanthal enhances β-amyloid clearance as a potential neuroprotective mechanism against Alzheimer's disease: in vitro and in vivo studies. ACS Chemical Neuroscience, 2013. **4**(6): p. 973-82.

37. **Lattanzio, V.**, Phenolic compounds: introduction, in natural products: Phytochemistry, botany and metabolism of alkaloids, phenolics and terpenes, K.G. Ramawat and J.-M. Mérillon, Editors. 2013, Springer Berlin Heidelberg: Berlin, Heidelberg. p. 1543-1580.

38. **Rigacci, S. and M. Stefani**, Nutraceutical properties of olive oil polyphenols. An itinerary from cultured cells through animal models to humans. International Journal of Molecular Sciences, 2016. **17**(6).

39. **Bendini, A., *et al.***, Phenolic molecules in virgin olive oils: a survey of their sensory properties, health effects, antioxidant activity and analytical methods. An overview of the last decade. Molecules, 2007. **12**(8): p. 1679-719.

40. **Damtoft, S., H. Franzyk, and S.R. Jensen**, Biosynthesis of secoiridoid glucosides in oleaceae. Phytochemistry, 1993. **34**(5): p. 1291-1299.

41. **Miettinen, K., *et al.***, The seco-iridoid pathway from *Catharanthus roseus*. Nature Communications, 2014. **5**: p. 3606.

42. **Simkin, A.J., *et al.***, Characterization of the plastidial geraniol synthase from Madagascar periwinkle which initiates the monoterpenoid branch of the alkaloid pathway in internal phloem associated parenchyma. Phytochemistry, 2013. **85**: p. 36-43.

43. **Collu, G., *et al.***, Geraniol 10-hydroxylase, a cytochrome P450 enzyme involved in terpenoid indole alkaloid biosynthesis. FEBS Letters, 2001. **508**(2): p. 215-20.

44. **Geu-Flores, F., *et al.***, An alternative route to cyclic terpenes by reductive cyclization in iridoid biosynthesis. Nature, 2012. **492**(7427): p. 138-42.

45. **Salim, V., *et al.***, 7-deoxyloganetic acid synthase catalyzes a key 3 step oxidation to form 7-deoxyloganetic acid in *Catharanthus roseus* iridoid biosynthesis. Phytochemistry, 2014. **101**: p. 23-31.

46. **Asada, K., *et al.***, A 7-deoxyloganetic acid glucosyltransferase contributes a key step in secologanin biosynthesis in Madagascar periwinkle. The Plant Cell, 2013. **25**(10): p. 4123-34.

47. **Vezzaro, A., *et al.***, Isolation and characterization of terpene synthases potentially involved in flavor development of ripening olive (*Olea europaea*) fruits. Journal of Plant Physiology, 2012. **169**(9): p. 908-14.

48. **Alagna, F., *et al.***, Identification and Characterization of the Iridoid Synthase Involved in Oleuropein Biosynthesis in Olive (*Olea europaea*) Fruits. The Journal of Biological Chemistry, 2016. **291**(11): p. 5542-54.

49. **Alagna, F., *et al.***, Olive phenolic compounds: metabolic and transcriptional profiling during fruit development. BMC Plant Biology, 2012. **12**: p. 162.

50. **Damtoft, S., H. Franzyk, and S.R. Jensen**, Biosynthesis of Iridoids in *Syringa* and *Fraxinus* - Secoiridoid Precursors. Phytochemistry, 1995. **40**(3): p. 773-784.

51. **Amiot, M.J., A. Fleuriet, and J.J. Macheix**, Importance and evolution of phenolic-compounds in olive during growth and maturation. Journal of Agricultural and Food Chemistry, 1986. **34**(5): p. 823-826.

52. **Savournin, C., *et al.***, Rapid high-performance liquid chromatography analysis for the quantitative determination of oleuropein in *Olea europaea* leaves. Journal of Agricultural Food Chemistry, 2001. **49**(2): p. 618-21.

53. **Letutour, B. and D. Guedon**, Antioxidative activities of *Olea europaea* leaves and related phenolic compounds. Phytochemistry, 1992. **31**(4): p. 1173-1178.

54. **Ortega-Garcia, F. and J. Peragon**, HPLC analysis of oleuropein, hydroxytyrosol, and tyrosol in stems and roots of *Olea europaea* L. cv. Picual during ripening. Journal of Science of Food and Agriculture, 2010. **90**(13): p. 2295-300.

55. **Sivakumar, G., C.B. Bati, and N. Uccella**, HPLC-MS screening of the antioxidant profile of Italian olive cultivars. Chemistry of Natural Compounds, 2005. **41**(5): p. 588-591.

56. **Ramirez, E., *et al.***, Endogenous enzymes involved in the transformation of oleuropein in Spanish table olive varieties. Journal of Agricultural and Food Chemistry, 2014. **62**(39): p. 9569-75.

57. **Gutierrez-Rosales, F., *et al.***, Metabolites involved in oleuropein accumulation and degradation in fruits of *Olea europaea* L.: Hojiblanca and Arbequina varieties. Journal of Agricultural and Food Chemistry, 2010. **58**(24): p. 12924-12933.

58. **Obied, H.K., *et al.***, Chemical screening of olive biophenol extracts by hyphenated liquid chromatography. Analytical Chimica Acta, 2007. **603**(2): p. 176-89.

59. **Obied, H.K., *et al.***, Biosynthesis and biotransformations of phenol-conjugated oleosidic secoiridoids from *Olea europaea* L. Natural Product Reports, 2008. **25**(6): p. 1167-79.

60. **Amiot, M.J., A. Fleuriet, and J.J. Macheix**, Accumulation of oleuropein derivatives during olive maturation. Phytochemistry, 1989. **28**(1): p. 67-69.

61. **Briante, R., *et al.***, Changes in phenolic and enzymatic activities content during fruit ripening in two Italian cultivars of *Olea europaea* L. Plant Science, 2002. **162**(5): p. 791-798.

62. **Gutierrez-Rosales, F., *et al.***, β-Glucosidase Involvement in the formation and transformation of oleuropein during the growth and development of olive fruits (*Olea europaea* L. cv. Arbequina) grown under different farming practices. Journal of Agricultural and Food Chemistry, 2012. **60**(17): p. 4348-4358.

63. **Jemai, H., M. Bouaziz, and S. Sayadi**, Phenolic composition, sugar contents and antioxidant activity of Tunisian sweet olive cultivar with regard to fruit ripening. Journal of Agricultural and Food Chemistry, 2009. **57**(7): p. 2961-8.

64. **Koudounas, K., *et al.***, A defence-related *Olea europaea* β-glucosidase hydrolyses and activates oleuropein into a potent protein cross-linking agent. Journal of Experimental Botany, 2015. **66**(7): p. 2093-106.

65. **Limiroli, R., *et al.***, ^{1}H and ^{13}C NMR characterization of new oleuropein aglycones. Journal of the Chemical Society-Perkin Transactions 1, 1995(12): p. 1519-1523.

66. **Uccella, N.**, Olive biophenols: biomolecular characterization, distribution and phytoalexin histochemical localization in the drupes. Trends in Food Science & Technology, 2000. **11**(9-10): p. 315-327.

67. **Konno, K., *et al.***, Enzymatic activation of oleuropein: a protein crosslinker used as a chemical defense in the privet tree. Proceedings of the National Academy of Sciences, 1999. **96**(16): p. 9159-64.

68. **Visioli, F., A. Poli, and C. Gall**, Antioxidant and other biological activities of phenols from olives and olive oil. Medicinal Research Reviews, 2002. **22**(1): p. 65-75.

69. **Sabatini, N. and V. Marsilio**, Volatile compounds in table olives (*Olea Europaea* L., Nocellara del Belice cultivar). Food Chemistry, 2008. **107**(4): p. 1522-1528.

70. **Karkoula, E., *et al.***, Quantitative measurement of major secoiridoid derivatives in olive oil using qNMR. Proof of the artificial formation of aldehydic oleuropein and ligstroside aglycon isomers. Journal of Agricultural and Food Chemistry, 2014. **62**(3): p. 600-7.

71. **Ollis, D.L., *et al.***, The alpha/beta hydrolase fold. Protein Engineering Design and Selection, 1992. **5**(3): p. 197-211.

72. **Carr, P.D. and D.L. Ollis**, Alpha/beta hydrolase fold: an update. Protein and Peptide Letters, 2009. **16**(10): p. 1137-48.

73. **Nardini, M. and B.W. Dijkstra**, Alpha/beta hydrolase fold enzymes: the family keeps growing. Current Opinion in Structural Biology, 1999. **9**(6): p. 732-7.

74. **Copley, S.D.**, Microbial dehalogenases: enzymes recruited to convert xenobiotic substrates. Current Opinion in Chemical Biology, 1998. **2**(5): p. 613-7.

75. **Hynkova, K., *et al.***, Identification of the catalytic triad in the haloalkane dehalogenase from Sphingomonas paucimobilis UT26. FEBS Letters, 1999. **446**(1): p. 177-81.

76. **Liu, J.Q., et al.**, Reaction mechanism of fluoroacetate dehalogenase from *Moraxella* sp. B. The Journal of Biological Chemistry, 1998. **273**(47): p. 30897-902.

77. **Stockigt, J. and S. Panjikar**, Structural biology in plant natural product biosynthesis-architecture of enzymes from monoterpenoid indole and tropane alkaloid biosynthesis. Natural Product Reports, 2007. **24**(6): p. 1382-400.

78. **Pfitzner, A. and J. Stockigt**, Characterization of polyneuridine aldehyde esterase, a key enzyme in the biosynthesis of sarpagine/ajmaline type alkaloids. Planta Medica, 1983. **48**(8): p. 221-7.

79. **Yang, L., *et al.***, Structural basis and enzymatic mechanism of the biosynthesis of C9- from C10-monoterpenoid indole alkaloids. Angewandte Chemie International Edition, 2009. **48**(28): p. 5211-3.

80. **Mattern-Dogru, E., *et al.***, Potential active-site residues in polyneuridine aldehyde esterase, a central enzyme of indole alkaloid biosynthesis, by modelling and site-directed mutagenesis. European Journal of Biochemistry, 2002. **269**(12): p. 2889-96.

81. **Qosa, H., *et al.***, Oleocanthal enhances amyloid-β clearance from the brains of TgSwDI mice and in vitro across a human blood-brain barrier model. ACS Chemical Neuroscience, 2015. **6**(11): p. 1849-59.

82. **Valvekens, D., M. Van Montagu, and M. Van Lijsebettens**, *Agrobacterium tumefaciens*-mediated transformation of *Arabidopsis thaliana* root explants by using kanamycin selection. Proceedings of the National Acaddemy of Sciences, 1988. **85**(15): p. 5536-40.

83. **Bertani, G.**, Studies on lysogenesis. I. The mode of phage liberation by lysogenic *Escherichia coli*. Journal of Bacteriology, 1951. **62**(3): p. 293-300.

84. **Higuchi, R., *et al.***, Kinetic PCR analysis: real-time monitoring of DNA amplification reactions. Biotechnology (N Y), 1993. **11**(9): p. 1026-30.

85. **Ginzinger, D.G.**, Gene quantification using real-time quantitative PCR: an emerging technology hits the mainstream. Experimental Hematology, 2002. **30**(6): p. 503-12.

86. **Simpson, R.J.**, Staining proteins in gels with silver nitrate. Cold Spring Harbor Protocols, 2007. **2007**: p. pdb prot4727.

87. **Koo, Y.J., *et al.***, An advanced method for the determination of carboxyl methyl esterase activity using gas chromatography-chemical ionization-mass spectrometry. Journal of Chromatography B, 2008. **863**(1): p. 80-7.

88. **Altschul, S.F., *et al.***, Basic local alignment search tool. Journal of Molecular Biology, 1990. **215**(3): p. 403-10.

89. **McWilliam, H., *et al.***, Analysis Tool Web Services from the EMBL-EBI. Nucleic Acids Research, 2013. **41**(Web Server issue): p. W597-600.

90. **Untergasser, A., *et al.***, Primer3-new capabilities and interfaces. Nucleic Acids Research, 2012. **40**(15).

91. **Cruz, F., *et al.***, Genome sequence of the olive tree, *Olea europaea*. Gigascience, 2016. **5**: p. 29.

92. **Ramakers, C., *et al.***, Assumption-free analysis of quantitative real-time polymerase chain reaction (PCR) data. Neuroscience Letters, 2003. **339**(1): p. 62-6.

93. **Ruijter, J.M., *et al.***, Amplification efficiency: linking baseline and bias in the analysis of quantitative PCR data. Nucleic Acids Research, 2009. **37**(6): p. e45.

94. **Hellemans, J., *et al.***, qBase relative quantification framework and software for management and automated analysis of real-time quantitative PCR data. Genome Biology, 2007. **8**(2): p. R19.

95. **Waterhouse, A., *et al.***, SWISS-MODEL: homology modelling of protein structures and complexes. Nucleic Acids Research, 2018. **46**(W1): p. W296-W303.

96. **Benkert, P., M. Biasini, and T. Schwede**, Toward the estimation of the absolute quality of individual protein structure models. Bioinformatics, 2011. **27**(3): p. 343-50.

97. **Dogru, E., *et al.***, The gene encoding polyneuridine aldehyde esterase of monoterpenoid indole alkaloid biosynthesis in plants is an ortholog of the α/β hydrolase super family. European Journal of Biochemistry, 2000. **267**(5): p. 1397-406.

98. **Hasslacher, M., *et al.***, Molecular cloning of the full-length cDNA of (S)-hydroxynitrile lyase from *Hevea brasiliensis*. Functional expression in *Escherichia coli* and *Saccharomyces cerevisiae* and identification of an active site residue. Journal of Biological Chemistry, 1996. **271**(10): p. 5884-91.

99. **Stuhlfelder, C., M.J. Mueller, and H. Warzecha**, Cloning and expression of a tomato cDNA encoding a methyl jasmonate cleaving esterase. European Journal of Biochemistry, 2004. **271**(14): p. 2976-83.

100. **Kumar, D. and D.F. Klessig**, High-affinity salicylic acid-binding protein 2 is required for plant innate immunity and has salicylic acid-stimulated lipase activity. Proceedings in the National Academy of Science, 2003. **100**(26): p. 16101-6.

101. **Gundlach, H., *et al.***, Jasmonic acid is a signal transducer in elicitor-induced plant cell cultures. Proceedings in the National Academy of Science, 1992. **89**(6): p. 2389-93.

102. **Nonis, A., A. Vezzaro, and B. Ruperti**, Evaluation of RNA extraction methods and identification of putative reference genes for real-time quantitative polymerase chain reaction expression studies on olive (*Olea europaea* L.) fruits. Journal of Agricultural and Food Chemistry, 2012. **60**(27): p. 6855-6865.

103. **Ray, D.L. and J.C. Johnson**, Validation of reference genes for gene expression analysis in olive (*Olea europaea*) mesocarp tissue by quantitative real-time RT-PCR. BMC Research Notes, 2014. **7**: p. 304.

104. **Konno, K., *et al.***, Glycine protects against strong protein-denaturing activity of oleuropein. A phenolic compound in privet leaves. Journal of Chemical Ecology, 1998. **24**(4): p. 735-751.

105. **Bianco, A.D., *et al.***, Bioactive derivatives of oleuropein from olive fruits. Journal of Agricultural and Food Chemistry, 1999. **47**(9): p. 3531-4.

106. **Guiso, M. and C. Marra**, Highlights in oleuropein aglycone structure. Natural Product Research, 2005. **19**(2): p. 105-109.

107. **Morant, A.V., *et al.***, β-Glucosidases as detonators of plant chemical defense. Phytochemistry, 2008. **69**(9): p. 1795-813.

108. **Romero-Segura, C.**, ***et al.***, The role of olive beta-glucosidase in shaping the phenolic profile of virgin olive oil. Food Research International, 2012. **45**(1): p. 191-196.

109. **Ammar, S.**, ***et al.,*** LC-DAD/ESI-MS/MS characterization of phenolic constituents in Tunisian extra-virgin olive oils: Effect of olive leaves addition on chemical composition. Food Research International, 2017. **100**: p. 477-485.

110. **Sivakumar, G., C. Briccoli Bati, and N. Uccella**, Demethyloleuropein and β-glucosidase activity in olive fruits. Biotechnology Journal, 2007. **2**(3): p. 381-5.

111. **Poulton, J.E.**, Cyanogenesis in Plants. Plant Physiology, 1990. **94**(2): p. 401-405.

112. **Huang, H., *et al.***, Jasmonate action in plant growth and development. Journal of Experimental Botany, 2017. **68**(6): p. 1349-1359.

113. **Koo, A.J. and G.A. Howe**, The wound hormone jasmonate. Phytochemistry, 2009. **70**(13-14): p. 1571-80.

114. **Yan, C. and D.X. Xie**, Jasmonate in plant defence: sentinel or double agent? Plant Biotechnology Journal, 2015. **13**(9): p. 1233-1240.

115. **Fonseca, S., *et al.***, (+)-7-iso-Jasmonoyl-L-isoleucine is the endogenous bioactive jasmonate. Nature Chemical Biology, 2009. **5**(5): p. 344-50.

116. **Staswick, P.E., I. Tiryaki, and M.L. Rowe**, Jasmonate response locus JAR1 and several related Arabidopsis genes encode enzymes of the firefly luciferase superfamily that show activity on jasmonic, salicylic, and indole-3-acetic acids in an assay for adenylation. The Plant Cell, 2002. **14**(6): p. 1405-15.

117. **Seo, H.S., *et al.***, Jasmonic acid carboxyl methyltransferase: a key enzyme for jasmonate-regulated plant responses. Proceedings in the National Academy of Sciences, 2001. **98**(8): p. 4788-93.

118. **Stitz, M., *et al.***, Ectopic expression of AtJMT in *Nicotiana attenuata*: creating a metabolic sink has tissue-specific consequences for the jasmonate metabolic network and silences downstream gene expression. Plant Physiology, 2011. **157**(1): p. 341-354.

119. **Vlot, A.C., D.A. Dempsey, and D.F. Klessig**, Salicylic acid, a multifaceted hormone to combat disease. Annual Review of Phytopathology, 2009. **47**: p. 177-206.

120. **Durrant, W.E. and X. Dong**, Systemic acquired resistance. Annual Review of Phytopathology, 2004. **42**: p. 185-209.

121. **Dempsey, D.A. and D.F. Klessig**, How does the multifaceted plant hormone salicylic acid combat disease in plants and are similar mechanisms utilized in humans? BMC Biology, 2017. **15**.

122. **Shulaev, V., P. Silverman, and I. Raskin**, Airborne signalling by methyl salicylate in plant pathogen resistance. Nature, 1997. **385**(6618): p. 718-721.

123. **Davies, P.J., P.J. Davies, and P.J. Davies**, Plant hormones: biosynthesis, signal transduction, action! 3rd ed. 2004, Dordrecht ; Boston: Kluwer Academic Publishers.

124. **Korasick, D.A., T.A. Enders, and L.C. Strader**, Auxin biosynthesis and storage forms. Journal of Experimental Botany, 2013. **64**(9): p. 2541-2555.

125. **Zubieta, C., *et al.***, Structural basis for substrate recognition in the salicylic acid carboxyl methyltransferase family. The Plant Cell, 2003. **15**(8): p. 1704-1716.

126. **Yang, Y., *et al.***, Inactive methyl indole-3-acetic acid ester can be hydrolyzed and activated by several esterases belonging to the AtMES esterase family of *Arabidopsis*. Plant Physiology, 2008. **147**(3): p. 1034-45.

127. **Jafarzadeh-Bajestani, M., *et al.***, Genetic transformation of olive somatic embryos through *Agrobacterium tumefaciens* and regeneration of transgenic plants. African Journal of Biotechnology, 2011. **10**(28): p. 5468-5474.

128. **Perez-Barranco, G., *et al.***, Studies on genetic transformation of olive (*Olea europaea* L.) somatic embryos: I. Evaluation of different aminoglycoside antibiotics for nptII selection; II. Transient transformation via particle bombardment. Plant Cell Tissue and Organ Culture, 2009. **97**(3): p. 243-251.

129. **Torreblanca, R., *et al.***, Development of a high throughput system for genetic transformation of olive (*Olea europaea* L.) plants. Plant Cell Tissue and Organ Culture, 2010. **103**(1): p. 61-69.

130. **Koo, Y.J., *et al.***, Characterization of a Methyl Jasmonate Specific Esterase in *Arabidopsis*. Journal of the Korean Society for Applied Biological Chemistry, 2013. **56**(1): p. 27-33.

131. **Giraldo, L.J.L., *et al.***, Lipase-catalyzed synthesis of chlorogenate fatty esters in solvent-free medium. Enzyme and Microbial Technology, 2007. **41**(6-7): p. 721-726.

132. **Mahapatra, P., *et al.***, Kinetics of solvent-free geranyl acetate synthesis by *Rhizopus oligosporus* NRRL 5905 lipase immobilized on to cross-linked silica. Biocatalysis and Biotransformation, 2009. **27**(2): p. 124-130.

133. **Xiong, J., *et al.***, Lipase-catalyzed transesterification synthesis of geranyl acetate in organic solvents and its kinetics. Food Science and Technology Research, 2014. **20**(2): p. 207-216.

134. **Gupta, A., *et al.***, Geranyl acetate synthesis catalyzed by *Thermomyces lanuginosus* lipase immobilized on electrospun polyacrylonitrile nanofiber membrane. Process Biochemistry, 2013. **48**(1): p. 124-132.

135. **Yang, K. and Y. Wang**, Lipase-catalyzed transesterification in aqueous medium under thermodynamic and kinetic control using carboxymethyl cellulose acetylation as the model reaction. Enzyme and Microbial Technology, 2004. **35**(2-3): p. 223-231.

136. **Lau, E.Y. and T.C. Bruice**, Consequences of breaking the Asp-His hydrogen bond of the catalytic triad: Effects on the structure and dynamics of the serine esterase cutinase. Biophysical Journal, 1999. **77**(1): p. 85-98.

137. **Hasslacher, M., *et al.***, Hydroxynitrile lyase from *Hevea brasiliensis*: Molecular characterization and mechanism of enzyme catalysis. Proteins-Structure Function and Genetics, 1997. **27**(3): p. 438-449.

138. **Duval, N., *et al.***, Site-directed mutagenesis of active-site-related residues in *Torpedo* acetylcholinesterase - presence of a glutamic-acid in the catalytic triad. FEBS Letters, 1992. **309**(3): p. 421-423.

139. **Turner, J.M., *et al.***, Biochemical characterization and structural analysis of a highly proficient cocaine esterase. Biochemistry, 2002. **41**(41): p. 12297-12307.

140. **Stockigt, J. and S. Panjikar**, Structural biology in plant natural product biosynthesis - architecture of enzymes from monoterpenoid indole and tropane alkaloid biosynthesis. Natural Product Reports, 2007. **24**(6): p. 1382-1400.

141. **Gomez-Rico, A., G. Fregapane, and M.D. Salvador**, Effect of cultivar and ripening on minor components in Spanish olive fruits and their corresponding virgin olive oils. Food Research International, 2008. **41**(4): p. 433-440.

142. **Guirimand, G., *et al.***, Strictosidine activation in Apocynaceae: towards a "nuclear time bomb"? BMC Plant Biology, 2010. **10**: p. 182.

6. Appendix

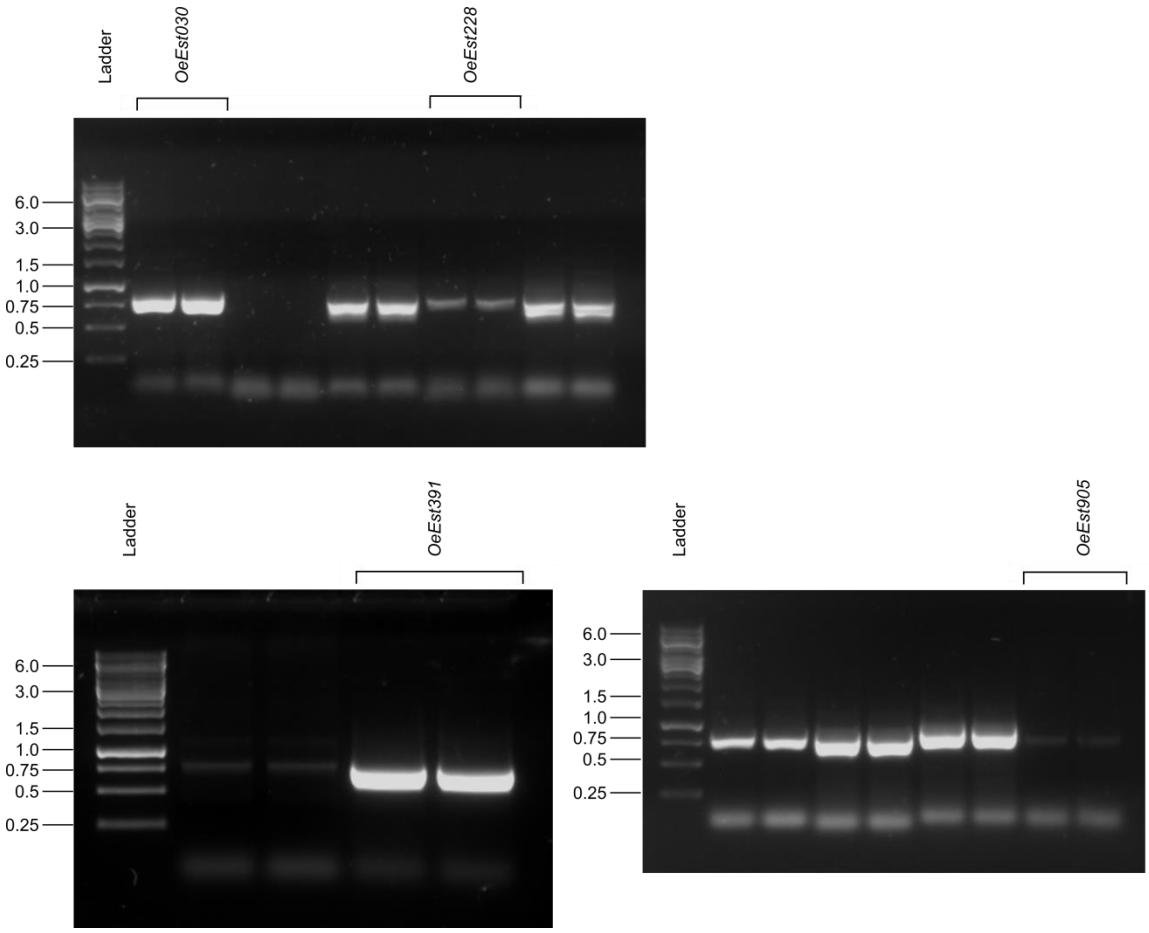

Supporting Figure 1: Agarose gel electrophoresis of DNA fragments generated in course of the CDS isolation procedure. Candidate sequences OeEst030, OeEst228, OeEst391 and OeEst905 were amplified from cDNA of O. europaea using gene-specific primers. Each sample was analyzed on two lanes. Numbers to the left indicate the size (kbp) of marker DNA fragments (Ladder).

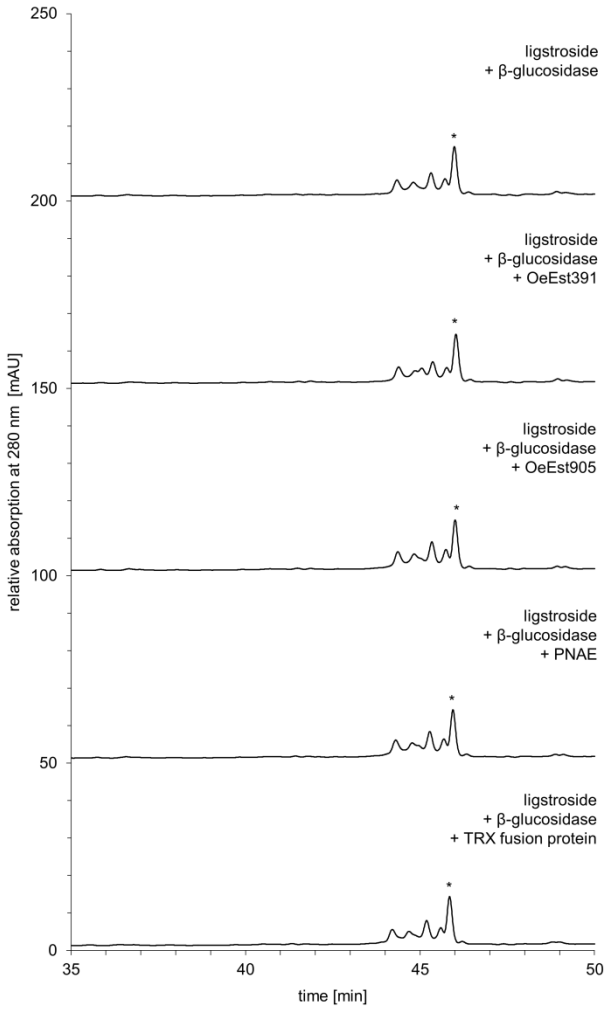

Supporting Figure 2: LC-MS analysis of assays for esterase activity of OeEst391, OeEst905 and PNAE towards ligstroside aglycone. Except for isomers of ligstroside aglycone (Rt of 44.27, 44.74, 45.25 and 46.66 min), no further reaction products could be observed. The peak marked with an asterisk represents an impurity within the substrate preparation, which was not converted in any of the analyzed reaction approaches.

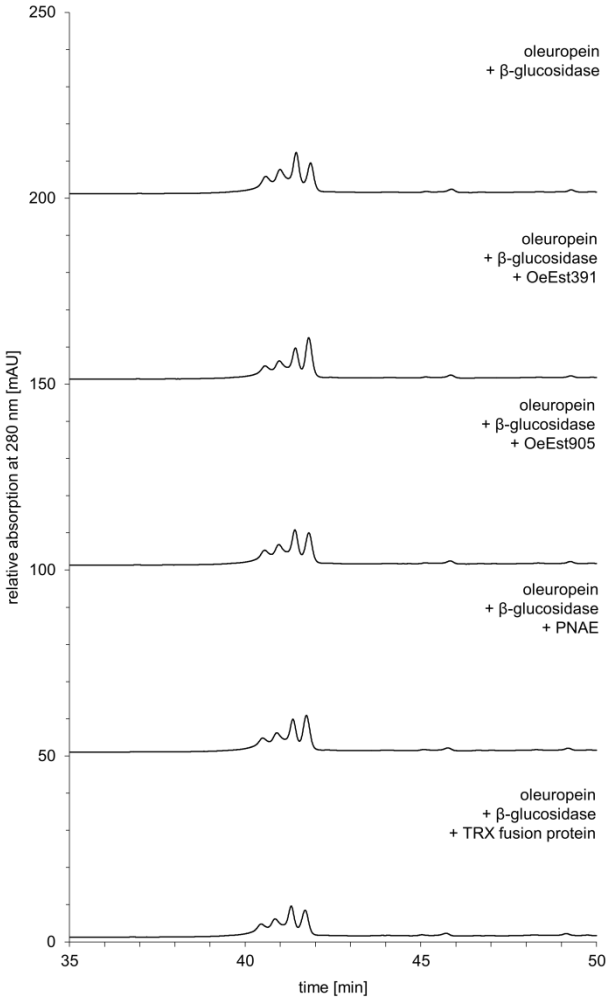

Supporting Figure 3: LC-MS analysis of assays for esterase activity of OeEst391, OeEst905 and PNAE towards oleuropein aglycone. Except for isomers of oleuropein aglycone (Rt of 40.59, 41.00, 41.45 and 41.86 min), no further reaction products could be observed.

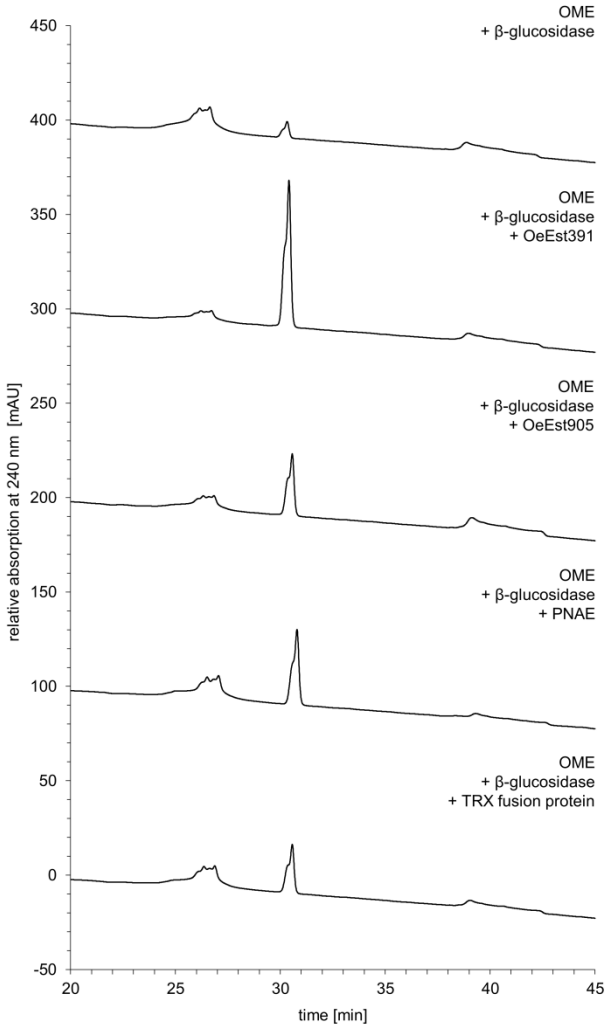

Supporting Figure 4: LC-MS analysis of assays for esterase activity of OeEst391, OeEst905 and PNAE towards elenolic acid. Except for isomers of elenolic acid (Rt of 26.15, 26.63 and 38.87 min) and oleoside 11-methyl ester (Rt of 30.33), no further reaction products could be observed.

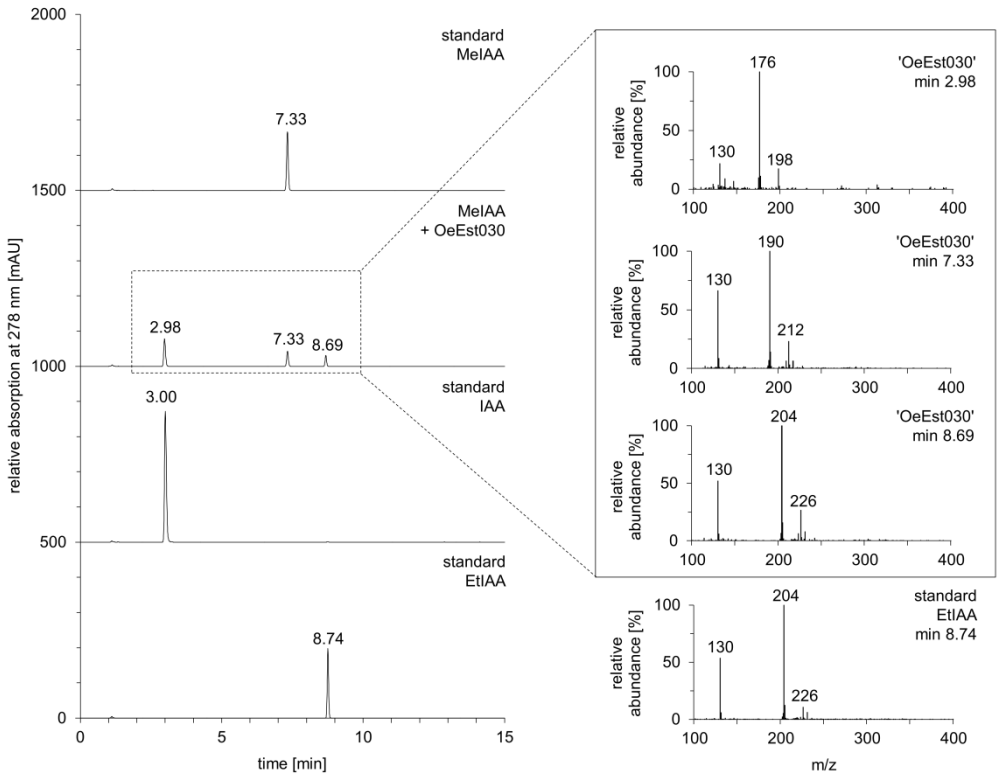

Supporting Figure 5: LC-MS analysis of products generated during the incubation of OeEst030 with MeIAA under modified reaction parameters. Reaction mixtures consisted of 2 mM of substrate and 10 µg/mL of protein preparation and were incubated for 20 min. Detection of MeIAA and derivatives was performed at a wavelength of 278 nm, while corresponding mass-to-charge values were determined using the negative ionization mode.

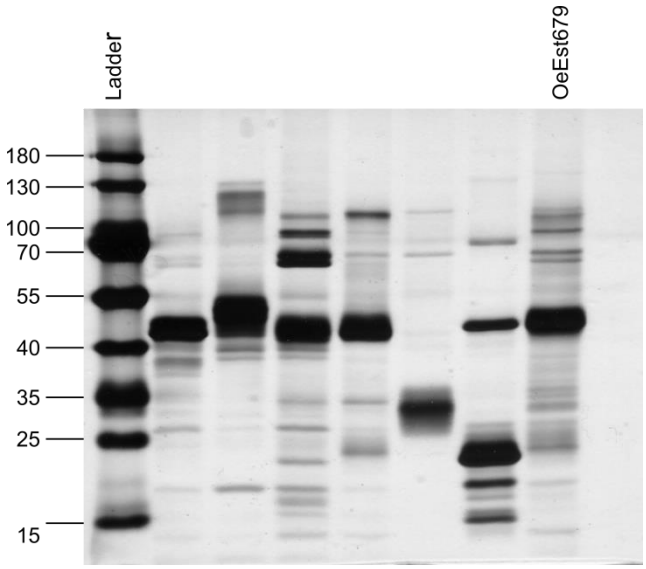

Supporting Figure 6: SDS-PAGE analysis of recombinant protein preparations 'OeEst679'. Visualization was accomplished by subsequent staining of the gel with silver nitrate. Approximately 1.0-1.5 µg were applied to the gel. Numbers to the left indicate molecular mass of marker proteins in kDa (Ladder).

Supporting Table 1: Quantification of specific oleosides in leaf tissue of *O. europaea* L. cv. Canino. Plant material was pulverized in liquid nitrogen using mortar and pestle. Methanol extraction procedure as well as following quantification by HPLC were carried out by N-Zyme BioTec GmbH. Samples were additionally analyzed by qPCR in order to determine relative expression levels of *OeEst030*, *OeEst228* and *OeEst905*. n.d., not detected.

tissue	biological replicate	concentration (mg/g)		
		ligstroside	oleuropein	oleacein
young leaves	1	8.38	8.38	n.d.
young leaves	2	9.29	9.29	n.d.
young leaves	3	6.91	6.91	n.d.
mature leaves	1	2.34	2.34	n.d.
mature leaves	2	1.53	1.53	n.d.
mature leaves	3	3.51	3.51	n.d.

7. Declaration of own work

Experiments, data analysis, data representation and writing of the thesis were exclusively performed by myself with exception of:

- Subcloning of the CDSs *OeEst030 and OeEst391* from the pCR-Blunt vector into the expression vector pET-32a(+) (3.3.), subsequent bacterial expression and purification of resulting recombinant protein as well as final quantification *via* BCA-assay (3.4.) were performed by Jonas Düring (Bachelor Thesis) under my supervision.
- Bacterial expression of *OeEst905* and subsequent purification *via* IMAC (3.4.) were performed by Levin Hafa (Bachelor Student) under my supervision.
- Subcloning of the CDS *OeEst679* from the pCR-Blunt vector into the expression vector pET-32a(+), subsequent bacterial expression and purification of resulting recombinant protein (3.9.) were performed by Marius Münch (Master Thesis) under my supervision. SDS-PAGE analysis, protein quantification as well as enzyme activity assays described or illustrated in chapter 3.9 were performed by myself.

8. Acknowledgments - Danksagung

An erster Stelle möchte ich mich bei Herrn Prof. Dr. Heribert Warzecha dafür bedanken, dass er mir nicht nur die Möglichkeit einer Doktorarbeit gegeben hat, sondern auch für das Vertrauen sehr frei und selbststrukturiert neben dem Hauptprojekt NeurOliv auch an weiteren Nebenprojekten arbeiten zu dürfen. Bei Fragestellungen oder auch Ideen traf ich stets auf ein offenes Ohr. Sowohl auf fachlicher als auch menschlicher Ebene hätte ich mir keinen besseren Doktorvater wünschen können.

Mein herzlicher Dank gilt auch Herrn Prof. Dr. Thiel für das Übernehmen der Rolle als Zweitgutachter.

Weitergehend möchte ich mich beim gesamten NeurOliv-Team bedanken. Es war eine außerordentlich interessante und angenehme Zusammenarbeit. Daher möchte ich auf diesem Wege nochmal die Gelegenheit ergreifen den Kollegen der Arbeitsgruppe um Prof. Dr. Gunter Eckert sowie den Kollegen von N-Zyme BioTec bzw. Döhler GmbH alles Gute für ihre weiteren Projekte zu wünschen.

Bei Dr. Michael Heethoff und Dr. Adrian Brückner möchte ich mich für das Ermöglichen der GC-MS Messungen bedanken.

Ein riesen Dankeschön geht natürlich auch an all meine Kollegen aus der Arbeitsgruppe Warzecha. Auch wenn ich viel Zeit im Labor verbracht habe und mancher Tag bzw. Versuch nie zu enden schien, haben sich die Arbeitstage durch euch dann doch eher nach Freizeit angefühlt. Wir haben gemeinsam nicht nur Gene kloniert, Pflanzen und Bakterien kultiviert, Substanzen und Proteine isoliert, Geräte repariert und Versuche geplant, sondern auch in unseren Pausen oder nach Feierabend gemeinsam gegessen, getrunken, gefeiert, gespielt und AG-Events organisiert. Es war eine wundervolle Doktoranden-Zeit, welche alleine deswegen schon jegliche investierte Mühe wert war. Hierbei möchte ich vor allem nochmal explizit die Personen hervorgreifen, die mich am längsten und engsten während dieser Zeit begleitet haben und somit auch zu wirklich guten Freunden geworden sind. Daher einen ganz besonderen Dank an Simone Bartl-Zimmermann, Sabine und meinen Bürogenossen Marcus.

Abschließend möchte ich mich bei meiner Familie für die Unterstützung während meiner gesamten akademischen Laufbahn bedanken! Besonders Alessa war eine große Unterstützung für mich. Daher sollen meine abschließenden Worte auch an dich gehen: Danke für deine geduldige und konstante Unterstützung während meiner Zeit als Doktorand. Allein durch deine außerordentlich motivierende und positive Art hast du dazu beigetragen, dass ich so viel Energie in die Forschungsprojekte stecken konnte.

9. Curriculum Vitae

Personal information

Name	Jascha Volk
Address	Schützenstraße 3, 65824 Schwalbach am Taunus, Germany
Date of Birth	24/04/1989
Place of Birth	Frankfurt am Main
Nationality	German

Academic career

09/2014 –11/2018	**PhD Student** at the Department of Biology Technische Universität Darmstadt, Darmstadt (Germany) Plant Biotechnology and Metabolic Engineering **Title:** 'Identification and characterization of esterases involved in the conversion of oleosides in *Olea europaea*'
10/2012 – 08/2014	**Master of Science**, Technische Biologie Technische Universität Darmstadt, Darmstadt (Germany) Plant Biotechnology and Metabolic Engineering **Title:** 'Conversion of the monoterpenoid indole alkaloid vinorine by recombinant P450 3A4 – potential for plant metabolic engineering'
10/2009 – 09/2012	**Bachelor of Science**, Biologie Technische Universität Darmstadt, Darmstadt (Germany) Plant Biotechnology and Metabolic Engineering **Title:** 'Application of a modular cloning system for the engineering of monoterpenoid indole alkaloid biosynthesis'
08/1999 – 06/2008	**Allgemeine Hochschulreife** Albert-Einstein-Gymnasium, Schwalbach am Taunus (Germany)

Publications

06/2018 Geissler M., **Volk J.**, Stehle F., Kayser O., Warzecha H.; Subcellular localization defines modification and production of Δ^9- tetrahydrocannabinolic acid synthase in transiently transformed *Nicotiana benthamiana*, Biotechnology Letters (2018) 40: 981.

06/2017 European Patent Application EP 17 17 4221.6

Dr. Alla Sarafidennov, Dr. Jens Zotzel, Dr. Stefan Marx, Prof. Dr. Heribert Warzecha, **M. Sc. Jascha Volk**; 'An esterase that is capable of converting iridoids and seco-iridoids',

03/2016 Geissler M., Burghard M., **Volk J.**, Staniek A., Warzecha H.; A novel cinnamyl alcohol dehydrogenase (CAD)-like reductase contributes to the structural diversity of monoterpenoid indole alkaloids in *Rauvolfia*, Planta (2016) 243: 813.

10. Ehrenwörtliche Erklärung

Ich erkläre hiermit ehrenwörtlich, dass ich die vorliegende Arbeit entsprechend den Regeln guter wissenschaftlicher Praxis selbstständig und ohne unzulässige Hilfe Dritter angefertigt habe.

Sämtliche aus fremden Quellen direkt oder indirekt übernommenen Gedanken sowie sämtliche von Anderen direkt oder indirekt übernommenen Daten, Techniken und Materialien sind als solche kenntlich gemacht. Die Arbeit wurde bisher bei keiner anderen Hochschule zu Prüfungszwecken eingereicht.

Darmstadt, den 06.11.2018